The influence of sediment texture on the mobility of mixed beds

Annular flume experiments and numerical modelling

DISSERTATION

zur Erlangung des Doktorgrades der Naturwissenschaften
am Fachbereich Geowissenschaften der Universität Bremen

submitted in fulfilment of the requirements for the doctoral degree in natural sciences at the Faculty of Geosciences of the University of Bremen

Vorgelegt von / By:
Franziska Staudt

Bremen, Januar / January 2016

Gutachter:

Prof. Dr. Katrin Huhn-Frehers, Universität Bremen

Dr. Julia C. Mullarney, University of Waikato

Datum des Dissertationskolloquiums:

24. Juni 2016

Prüfungsausschuss:

Prof. Dr. Katrin Huhn-Frehers

Dr. Julia C. Mullarney

Prof. Dr. Tobias Mörz

PD Dr. Christian Winter

Dr. Stefan Kreiter

Robert Büssing

Abstract

Knowledge about sediment transport dynamics and sediment stability is a key component to understand the geomorphology of fluvial and coastal systems. However, many processes and factors influencing the transport dynamics of mixed sediment remain obscure. The research objectives in this dissertation were inspired by studies investigating the influence of fine sediment on the mobility of a mixed sediment bed on different grain scales and in different flow environments. While studies investigating fluvial sediment transport have concluded that the addition of fine material mobilizes the riverbed, other studies investigating mainly estuarine and marine sediment transport have found that the addition of fine material can lead to bed stabilization. In both cases, the changes in bed stability are attributed to small-scale processes at the bed surface. Based on this contrast, two series of laboratory flume experiments and a numerical model were used to analyse the influences of the sediment texture and the particle shape on the near-bed flow field and the mobility of a mixed bed, and to find a possible transition between the different modes of behaviour. The sediment texture was characterized by the fine-grained fraction and the grain-size ratio $RD = D_{coarse}/D_{fine}$ between the diameters of the coarse and the fine particles.

In laboratory experiments with spherical glass beads ($D_{50} \leq 367$ µm) and various grain-size ratios (RD = 3.9; 5.8; 9.4) and fine fractions (10; 20; 40 % dry weight), the mobility of the bed and the near-bed flow velocities were investigated. In an annular flume, one unimodal bed and three glass-bead mixtures were subjected to increasing flow velocities (U = 0.01–0.19 m s^{-1}). The bed "mobility" was derived from changes in suspended particulate matter, as well as from changes of the bed level over time, using a new approach to analyse the data collected by an acoustic Doppler velocimeter. A transition between mobilizing and stabilizing behaviour was found at $3.9 < RD_{cr} < 5.8$: Relative to a unimodal reference bed, the bimodal beds with a low grain-size ratio (RD = 3.9) became more mobile with an increase in fine content (from 10 to 40 %), whereas beds with a high grain-size ratio (RD = 5.8; 9.4) became more stable. With the addition of fine material, the bed roughness decreased, as the fine particles filled the surface gaps between the coarser particles, and the near-bed flow accelerated. In the mixed experiments, the flow velocities at the bed surface increased with a decrease of the grain-size ratio. It is hypothesized that due to differences in particle packing (which are induced by the different grain-size ratios), the inflow into the bed is higher if RD is low. The high inflow can subsequently lead to more particle entrainment.

Based on these findings, a numerical micro-scale model was used to investigate the differences in the 3D flow field at the sediment-fluid interface. Different combinations of spherical particles ($D \leq 600$ µm, one unimodal reference model, three mixed beds with RD = 4; 4.8; 6, and 14–18 % fines) were generated and laminar flow (U = 0.08–0.31 m s^{-1}) was simulated above and through the particle matrix. The model showed that the flow velocities in the upper layers of the sediment bed increase with a decrease of the grain-size ratio. The velocities were highest in the bed with RD = 4 and lowest in the bed with RD = 6. In addition, the flow direction changed to cross-stream and vertical flow, as the streamwise flow through the bed was deflected around the particles. The results

suggest that high cross-stream and vertical flow velocities inside a bed with a low grain-size ratio could facilitate particle entrainment at the bed surface.

In a second series of laboratory flume experiments (U = 0.02–0.23 m s^{-1}), the findings from the glass-bead experiments and the numerical model could be validated with natural sediment. For sand-sand and sand-silt mixtures (D_{50} ≤ 410 µm) with various grain-size ratios (RD = 2; 3.5; 7.7) and large fine fractions (40 % dry weight), a transition between the mobilizing and stabilizing behaviour was found at 3.5 < RD_{cr} < 7.7. The mixed bed with a low grain-size ratio of RD = 2 behaved similar to the unimodal reference bed. The flow velocities at the surface of the different beds could be related to the erosion and mobility during different stages of the experiment. In direct comparison with the glass-bead experiments, the natural sediment was more stable, implying the stabilizing effect of the particle complexity. In addition, the near-bed flow profiles above the natural beds were slightly different from the flow profiles above the glass beads, indicating dissimilarities in bed roughness resulting from the different particle shapes.

This dissertation presents an important, novel contribution to the question how the sediment texture and the grain shape influence sediment stability. The presented studies show that in the tested sand-silt range (D_{50} ≤ 600 µm) the grain-size ratio is of greater importance for the mobility of a mixed bed than the amount of fines. As observed in gravel-bedded rivers, the addition of fines to a unimodal sand bed can lead to bed mobilization if RD of the bed is about 2–4. At a higher grain-size ratio however, the bed will stabilize with the addition of small amounts of fines. The presence of the fine particles influences micro-scale flow processes at the bed surface that subsequently control particle entrainment and bed mobility.

Zusammenfassung

Das Transportverhalten von Sedimenten unterschiedlicher Korngrößen ist maßgeblich für die Entstehung und morphologische Veränderung von Flussläufen und Küstensystemen. Um die komplexen Sedimentbewegungen in fließenden Gewässern genauer verstehen und prognostizieren zu können, müssen zunächst die Erosions- und Transportprozesse gemischter Sedimente untersucht werden. Die Fragestellung dieser Arbeit wurde durch Forschungsergebnisse aus dem fluvialen als auch aus dem Ästuar- bzw. Küstenbereich inspiriert. In Flüssen führt der Eintrag von feinem, sandigem Material zu erhöhtem Geschiebetransport an der Gewässersohle. Im Ästuar- und Küstenbereich verbindet man mit der Beimischung von feinem Material jedoch allgemeinhin eine Stabilisierung der Sohle. In beiden Forschungsbereichen haben Studien den (mobilisierenden bzw. stabilisierenden) Einfluss des feinkörnigen Materials mit kleinskaligen Prozessen an der Gewässersohle in Verbindung gebracht. Basierend auf diesem Gegensatz untersucht die vorliegende Arbeit den Einfluss der Korngrößenverteilung und der Kornform auf das sohlennahe Strömungsprofil und die Stabilität der Gewässersohle. Dazu wurden Laborversuche in einem Kreisgerinne mit einem mikroskaligen, numerischen Modell der Sedimentoberfläche kombiniert. Als charakteristische Größe für die Korngrößenverteilung wird das Korngrößenverhältnis $RD = D_{coarse}/D_{fine}$ zwischen grobkörnigem und feinkörnigem Sohlenmaterial eingeführt.

In Laborversuchen im Kreisgerinne wurde zunächst die Mobilität von Glaskugeln ($D_{50} \leq 367$ µm) und die damit zusammenhängenden sohlnahen Strömungsprozesse untersucht. Das Erosionsverhalten von einer homogenen Sohle und drei Gemischen mit unterschiedlichen Korngrößenverhältnissen (RD = 3.9; 5.8; 9.4) und verschiedenen Feinanteilen (10; 20; 40 % Trockengewicht) wurde bei ansteigender Strömungsgeschwindigkeit (U = 0.01–0.19 m s^{-1}) analysiert. Die „Mobilität“ wurde dabei einerseits durch die Änderung der Schwebstoffkonzentration bestimmt, andererseits mit Hilfe eines neuentwickelten Ansatzes von der zeitlichen Variabilität der Sohle abgeleitet. In den Versuchen wurde bei einem Korngrößenverhältnis von $3.9 < RD_{cr} < 5.8$ der Übergang zwischen Mobilisierung und Stabilisierung gefunden. Im Verhältnis zum homogenen Referenzversuch ohne Feinanteil wurden die Gemische mit niedrigem Korngrößenverhältnis (3.9) mit einem Anstieg des Feinanteils (von 10 auf 40 %) mobiler, während die Gemische mit hohem Korngrößenverhältnis (5.8; 9.4) stabiler wurden. Die Zugabe von feinen Glaskugeln führte zur Verringerung der Sohlrauheit, indem die feineren Kugeln die Lücken zwischen den groben Kugeln auffüllen. Des Weiteren konnten die Strömungsgeschwindigkeiten direkt an der Oberfläche der Sohle mit der Mobilität des jeweiligen Sohlenmaterials in Zusammenhang gebracht werden: Während an der Oberfläche der instabilen Sohle (RD niedrig) relative hohe Strömungsgeschwindigkeiten gemessen wurden, waren die an der Oberfläche der stabilen Sohle (RD hoch) gemessenen Geschwindigkeiten niedriger. Basierend auf dieser Datenlage wird angenommen, dass sich die Kugelpackung je nach Korngrößenverhältnis unterscheidet, und dass es durch die Unterschiede in Packung und Porenraum zu unterschiedlich starkem Wassereinstrom ins Sohlenmaterial kommt.

Im Anschluss wurden in einem mikroskaligen, numerischen Modell die dreidimensionalen Strömungsgeschwindigkeiten an der Grenze zwischen Sediment und Wassersäule untersucht. Verschiedene Sedimente wurden durch unterschiedliche Kugelpackungen dargestellt ($D \leq 600$ µm, ein homogener Referenzversuch, drei Mischungen mit RD = 4; 4.8; 6 und 14–18 % Feinanteil). In dem Modell wurde simuliert, wie sich eine laminare Strömung (U = 0.08–0.31 m s^{-1}) in den oberen Schichten der Kugelpackung ausbreitet. Die Ergebnisse zeigen eine Abhängigkeit der Strömungsgeschwindigkeiten innerhalb der Kugelpackungen vom Korngrößenverhältnis RD. Zudem wird die Strömung in der Kugelpackung durch die unterschiedliche Korngrößen unterschiedlich stark in horizontale und vertikale Richtung abgelenkt. Besonders die vertikalen Strömungskomponenten im Modell mit RD = 4 war um ein Vielfaches höher als in den anderen Modellen (RD = 4.8; 6). Dieses Ergebnis lässt darauf schließen, dass die Kugeln an der Oberfläche durch die hohen Strömungsgeschwindigkeiten im Sediment leicht destabilisiert werden könnten. Da die Strömungsgeschwindigkeiten in der Kugelpackung mit RD = 4 am höchsten waren, unterstützt dies die Ergebnisse aus den Laborversuchen, bei denen die Mischung mit RD = 3.9 die höchste Mobilität aufwies.

In einer zweiten Serie von Laborversuchen (U = 0.02–0.23 m s^{-1}) konnten die Ergebnisse aus den bisherigen Versuchen auf natürliches Sediment übertragen werden. Für Sand-Sand und Sand-Schluff-Gemische ($D_{50} \leq 410$ µm) wurde die maximale Mobilität bei einem Korngrößenverhältnis von RD = 3.5, die höchste Stabilität bei RD = 7.7 gefunden. Dieser Trend ist vergleichbar mit den Ergebnissen für die Glaskugelgemische. Zwischen dem Sand-Sand-Gemisch mit RD = 2 und dem homogenen Referenzversuch waren nur geringfügige Unterschiede in der Stabilität erkennbar. Insgesamt war das natürliche Sediment stabiler als die Glaskugeln derselben mittleren Korngröße, was darauf schließen lässt, dass die Kornform eine weitere wichtige Rolle für die Sohlenstabilität spielt. Des Weiteren liefern die Strömungsprofile Hinweise darauf, dass die Kornform die sohlnahen Strömungsgeschwindigkeiten beeinflussen.

Die Versuche im Kreisgerinne und die kleinskaligen, numerischen Simulationen konnten beweisen, dass dem Korngrößenverhältnis RD eine Schlüsselrolle für die Stabilität gemischter Sedimente ($D_{50} \leq 600$ µm) zukommt. Die Rolle des Feinanteils ist dieser unterzuordnen. Ähnlich dem Erosionsverhalten von groben Kies-Sand-Gemischen in Flussläufen, kann eine Erhöhung des Feinanteils ebenfalls in einem feinkörnigen, sandigen Sediment mit RD = 2–4 zur Destabilisierung führen. Im Gegensatz dazu führt der Feinanteil bei einem höheren Korngrößenverhältnis zur Stabilisierung der Sohle. Die numerischen Simulationen haben gezeigt, dass sich das Geschwindigkeitsfeld an der Sedimentoberfläche bzw. in den oberen Sedimentschichten in Abhängigkeit vom Korngrößenverhältnis gravierend ändern kann, was in der Folge die Stabilität der Sohle beeinflusst.

List of abbreviations

ADV	Acoustic Doppler velocimetry
DEM	Discrete element method
FDM	Finite difference method
OBS	Optical backscatter sensor
PIV	Particle image velocimetry
PSD	Particle-size distribution
SPM	Suspended particulate matter concentration
SSC	Suspended sediment concentration

List of symbols

Symbol	Units	Meaning
A	m^2	Cross-sectional area of a grain
BS	dB	Acoustic backscatter intensity
C_D	-	Drag coefficient
D	m	Grain diameter
D_{50}	m	Mean grain diameter
D_*	-	Dimensionless grain size
d_b	m	Distance between ADV and bottom
$\overline{d_b}$	m	Average distance between ADV and bottom
F_D	N	Drag force
F_G	N	Immersed weight of sediment grain
F_L	N	Lift force
F_R	N	Frictional/resisting force
g	$m\ s^{-2}$	Gravitational constant
m	kg	Mass
N	-	Number of measurements
n_{Int}	-	Number of flow speed intervals
q_s	$m\ s^{-1}$	Specific discharge
RD	-	Grain-size ratio
Re	-	Reynolds number
r	m	Particle radius
SPM	$mg\ l^{-1}$	Suspended particulate matter concentration
TKE	$N\ m^{-2}$	Turbulent kinetic energy
Δt	s	Time span

U	m s^{-1}	Free flow velocity
U_{cr}	m s^{-1}	Critical free flow velocity
$\overline{U}$	m s^{-1}	Depth-averaged flow velocity
u	m s^{-1}	Flow velocity
u_x	m s^{-1}	Streamwise flow component
u_y	m s^{-1}	Cross-stream flow component
u_z	m s^{-1}	Vertical flow component
u'	m s^{-1}	Flow velocity fluctuation
u_*	m s^{-1}	Friction velocity, shear velocity
$\overline{u_y}$	m s^{-1}	Average cross-stream velocity component
$\overline{u_z}$	m s^{-1}	Average vertical velocity component
z	m	Distance from the bed surface (flume)
z	m	Model depth (numerical model)
z_0	m	Bed roughness length
ε	Pa s	Eddy viscosity
θ_{cr}	-	Critical Shields parameter
κ	-	Von Karman's constant
μ	Pa s	Dynamic viscosity
μ	-	Friction coefficient
ν	m^2 s^{-1}	Kinematic viscosity
ρ	kg m^{-3}	Density
ρ_s	kg m^{-3}	Density of the solid or sediment grain
ρ_f	kg m^{-3}	Density of the fluid
σ_b^2	m^2	Temporal variance of the bottom level
$\sigma_{b,mov}^2$	m^2	Moving bottom variance
$\sigma_{b,int}^2$	m^2	Bottom variance of flow speed interval
$\sigma_{b,norm}^2$	m	Normalized bottom variance, proxy for bed mobility
σ_y^2	m^2 s^{-2}	Spatial variance of cross-stream velocity component
σ_z^2	m^2 s^{-2}	Spatial variance of vertical velocity component
τ	N m^{-2}	Shear stress
τ_0	N m^{-2}	Bed shear-stress
τ_{cr}	N m^{-2}	Critical shear-stress
Φ	°	Pivoting angle
ω	rpm	Rotational speed of the flume lid

Content

1. Outline and objectives

Describing sediment erosion is an important component for the understanding of sediment transport processes in coastal and fluvial environments. If the natural hydrodynamics are interfered or interrupted, the sediment dynamics are affected and unwanted erosion or deposition can be a consequence (Reeve et al., 2004).

Coastal structures, such as ports, jetties, or wave breakers, affect the coastal hydrodynamics (e.g. by blocking off or changing currents, or by reflecting waves) and subsequently the sediment transport. As about one quarter of the world's population lives within 100 horizontal km and 100 vertical metres of the coastline (Small and Nicholls, 2003), radical changes of the environment (e.g. major erosion events) have a significant effect on human lives and infrastructure. Especially in view of sea level rise and increasing occurrence of extreme events, such as storm surges, coastal regions will face severe erosion events and threats to infrastructure in the future. A thorough, broad understanding of coastal sediment dynamics is crucial to improve the sustainable development of coastal areas and to optimize coastal protection.

Similarly, the damming and training of rivers affects the fluvial sediment dynamics. River damming can lead to the deposition and accretion of fluvial sediment upstream of the structure, i.e. in the reservoir (Yang, 2006). In addition, a sediment deficiency will develop downstream of the structure which can then affect the river's flora and fauna, e.g. lead to the loss of spawning grounds for fish (Randle et al., 2006). In these cases, mitigation measures, such as sediment bypass devices, have to be constructed (Yang, 2006). If a natural waterway is modified by human activity, a careful evaluation of the hydrodynamics and the resulting sediment dynamics is necessary to understand, prevent or incorporate possible consequences like unwanted erosion or deposition.

Sediment erosion, i.e. the motion of single sediment grains, is initiated when the hydrodynamic driving force outweighs the grain resistance force (see 2.4). The erosion of unimodal sediment (i.e. sediment of a single grain size) has been described initially by Hjulström (1935) and Shields (1936) and has since been modified and extended by many studies (a summary is given e.g. in Miller et al., 1977). In addition to the flow field and the grain size, other parameters can control the stability, i.e. the resistance to erosion, and the transport behaviour of natural sediment (see 2.5).

Cohesion, i.e. adhesive forces between electrostatically charged clay particles, leads to an increased bed stability (e.g. Teisson et al., 1993; Mehta and Lee, 1994; Panagiotopoulos et al., 1997; Torfs et al., 2001; Le Hir et al., 2008; Jacobs et al., 2011). Biological activity, such as marine micro- and macrofauna living on or in the sediment, can stabilize the bed, e.g. through the secretion of glue-like mucus that binds the particles (e.g. Grant et al., 1986; Paterson et al., 1990; Meadows et al., 1994), or destabilize the bed through bioturbation (e.g. Widdows et al., 1998b; Willows et al., 1998). The grain shape and complexity (e.g. roundness, angularity etc.) affects the frictional strength of the sediment (e.g. Mair et al., 2002; Guo and Morgan, 2004; Kock and Huhn, 2007) and thus the erosion resistance. In addition, in mixed beds comprising a range of grain sizes, the interaction of various grain sizes and grain-size fractions (i.e. the sediment texture) influences the bed stability. These effects can be classified into two cases:

a) Sandy sediment can be *stabilized* through the addition of non-cohesive, finer material (see 2.5.1). Recent studies and conceptual models suggested that the fine particles form networks or so-called caging structures encompassing the coarser grains, block off the water inflow into the bed, and thus stabilize the sediment (e.g. van Ledden et al., 2004; Le Hir et al., 2008; Bartzke et al., 2013). Theoretical models had difficulties to explain this texture-induced stabilization of non-cohesive material (e.g. Mehta and Lee, 1994; Torfs et al., 2001).
b) Coarse sediment (coarse sand, gravel) can be *mobilized* through the addition of non-cohesive, finer material (see 2.5.2). Experimental studies have found that the fines reduce the bed roughness, resulting in an acceleration of the near-bed flow, higher drag forces, and subsequently more particle entrainment of coarse particles that protrude from the bed surface (e.g. Jackson and Beschta, 1984; Iseya and Ikeda, 1987; Wilcock et al., 2001; Venditti et al., 2010a, 2010b; Houssais and Lajeunesse, 2012). Theoretical models attempted to illuminate the texture-induced mobilization of non-cohesive, coarse material (e.g. Komar and Li, 1986; Wiberg and Smith, 1987; Bridge and Bennett, 1992) but could not explain the transition between mobilization and stabilization.

The exact processes that govern the mobility, i.e. the dynamics, of non-cohesive mixed sediment beds are not well understood. Many studies have investigated the stability of mixed beds with different fine-grained fractions, whereas some have suggested that not only the amount of fines, but also the ratio between the sizes of the coarse and the fine grains (hereafter termed the grain-size ratio $RD = D_{50,coarse}/D_{50,fine}$) influences the behaviour of the bed (Le Hir et al., 2008; Venditti et al., 2010a). The research in this dissertation focuses on the mobility of relatively fine-grained, mixed sediment beds (in the sand-silt range) without cohesion, as found in coastal areas or in the downstream reaches of a river. The presented studies investigate the effects of sediment texture on sediment behaviour. In addition, one study will address the effects of particle complexity on sediment behaviour. For simplification, the sediment behaviour is investigated under unidirectional flow, i.e. without the influence of waves or tides, in an annular laboratory flume. A numerical micro-scale model is developed based on these characteristics, representing a “numerical annular flume”.

Based on the observations regarding the influence of texture on sediment stability and the lack of knowledge in this field, this dissertation will address the following research objectives:

Texture-induced bed mobility:

- What are the influences of sediment texture, i.e. the fine-grained fraction and the grain-size ratio $RD = D_{50,coarse}/D_{50,fine}$, on the mobility of a mixed bed and the near-bed flow?

Particle shape:

- What is the influence of the particle complexity (spherical vs. angular) on the mobility of a bed and the near-bed flow?

Two out of the three research papers that contribute to the main part of this dissertation describe laboratory experiments in an annular flume to investigate the mobility of different beds and the

associated near-bed flow (chapters 4 and 6). However, due to the limited resolution of the in-situ instrumentation relative to the grain size, these physical approaches can only give insight into millimetre- to centimetre-scale processes at the sediment bed. As several studies have indicated the importance of grain-scale processes for sediment entrainment, one research paper describes a high resolution numerical model of the bed surface and the upper layers of the bed (chapter 5).
In the following, the chapters of the dissertation and the questions they address are described in more detail.

Chapter 2 introduces the main background knowledge to understand the research presented in this dissertation.

Chapter 3 introduces the methodology that was used to approach the research objectives. The chapter includes a new approach that I developed for the analysis of sediment bed changes and *bed mobility* in laboratory experiments. In addition, the numerical model that I developed to analyse the micro-scale processes at the sediment-fluid interface is introduced.

Chapter 4 describes flume experiments with artificial sediment beds consisting of spherical glass beads with different bimodal grain-size distributions. While modifying both the grain-size ratio *RD* and the fine-grained content, the mobility of the bed was assessed with the method introduced in chapter 3. This study addresses the following questions:

- What are the influences of a) the fine-grained fraction and b) the grain-size ratio $RD = D_{50,coarse}/D_{50,fine}$ on the near-bed flow and the mobility of a mixed bed composed of spherical particles?

The manuscript entitled “The role of the grain-size ratio in the mobility of mixed beds” is in preparation for submission to *Continental Shelf Research*. All experimental work, data processing, and data visualization were conducted by myself. The manuscript was written by myself, whereas the co-authors provided feedback and edits.

Based on the results of chapter 4 and motivated by the limited resolution of laboratory measurements, **chapter 5** describes a numerical micro-scale model of the fluid-sediment interface. A particle model and a flow model were coupled to simulate the fluid flow at the bed surface and in the upper layers of a sediment bed and to investigate micro-scale processes that are controlled by the bed texture. The grain-size ratio in the particle model was varied and the flow through the sediment matrix investigated to answer the following research objective:

- What is the influence of the grain-size ratio *RD* on micro-scale flow processes at the bed surface?

The manuscript entitled “A numerical micro-scale model of the flow inside a sediment matrix” is in review for publication in the *Proceedings of the 7th International Short Course/Conference on Applied Coastal Research* that took place on 28 September – 01 October 2015 in Florence, Italy. The commercial software tools Itasca PFC3D and FLAC3D were used for the development of the numerical model. The particle and the flow model were set up by myself. The coupling between the two model parts is based on a pre-existing code example from Itasca, Inc. that I modified and expanded for my specific application. All numerical work, data processing, and data visualization were conducted by myself. I wrote the manuscript, whereas the co-authors provided feedback and edits.

Based on the outcome of chapter 4 and chapter 5, **chapter 6** transfers the findings to sandy sediment. In a second series of flume experiments with natural, bimodal sediment, the grain-size ratio of the treatments was varied, whereas the same quantity of fine material was used. The results were compared to the outcome of chapter 4 and used to address the following questions:

- What is the influence of the grain-size ratio *RD* on the near-bed flow and the mobility of a mixed bed composed of natural sediment?
- How does the particle shape affect the mobility of a bed and the near-bed flow?

The manuscript entitled “Stabilization and mobilization of a mixed sandy sediment bed through the addition of fines with various grain sizes” is in preparation for submission to *Earth Surface Processes and Landforms*. I conducted all experimental work, data processing, and visualization. The manuscript was written by myself, whereas the co-authors provided feedback and edits. Parts of the preparation for the experiments (sand sampling and sieving) were conducted by a student helper.

Chapter 7 provides a summary of the results and draws overall conclusions based on the previous chapters. The study is set into a global context and an outlook provides suggestions for further works.

Note on INTERCOAST

The research for this thesis was conducted with the support of the International Research Training Group INTERCOAST and was funded by the German Research Foundation (DFG). Within the framework of INTERCOAST’s main theme “Integrated Coastal Zone and Shelf-Sea Research”, PhD students from different scientific backgrounds investigate recent research objectives related to marine geosciences, marine biology, social sciences, geography and law at the University of Bremen, Germany, and the University of Waikato, New Zealand. The laboratory experiments presented in this thesis were conducted during two research stays at the University of Waikato (3.5 months in 2014, 1.5 months in 2015).

2. Background

2.1 Aquatic environments

Inspiration for the research objectives in this dissertation came from both the coastal marine environment (including estuaries) as well as the fluvial environment (i.e. rivers). Studies of the estuarine and marine environment mostly investigate the influence of very fine sediment (cohesive clay particles, but also non-cohesive silt) on the erosion resistance of a sandy sediment bed, whereas many studies dealing with riverbed stability investigate the influence of non-cohesive sand on the erosion resistance of larger grains (gravel, coarse sand). If cohesion between particles is not important, the basic concepts of sediment entrainment are identical in these two environments (see 2.4), although grain characteristics and hydrodynamic forcing might differ. Nonetheless, research of scientific literature from the two fields reveals differences in sediment behaviour (texture-induced stabilization vs. mobilization) that have not been elucidated so far (see 2.5.1 and 2.5.2). For this study, we will take a broader perspective to draw comprehensive conclusions for sediment transport dynamics.

2.1.1 Fluvial environment

River systems are the main providers of sediment to all other sedimentary systems, including the ocean (Leeder, 1999). The morphology of a river depends on the river discharge, the input load and characteristics of the sediment, and the composition of riverbed and banks (Dey, 2014). The sediment, which originates from the river catchments, is flushed into the rivers by precipitation or through bank erosion and transported downstream (*fluvial transport*). During the transport, the grains are further broken down (*abrasion*) and grain diameters decrease with increasing downstream distance (Robert, 2003). The river channel morphology changes with the downstream distance and can be classified by different characteristics and processes (Robert, 2003): In the upstream reaches of a river, large grains like gravel or cobbles (D > 64 mm) that partly protrude the water surface, a high bed gradient, and cascades can be found. This part of the river, the so-called *small* channel, is characterized by a low ratio of flow depth d to grain size D (d/D < 1), with large grain sizes, high energy, and a relatively shallow flow depth. Downstream, in the *intermediate* channel, the bed gradient reduces and grain sizes decrease, yielding a ratio of flow depth to grain size of $1 < d/D < 10$. The river widens and starts meandering. Finer sediment is flushed further downstream and settles out in the flat stretches of the *large* channel, characterized by relatively small grain sizes (d/D > 10), low energy, and a wide, meandering or braiding river with large floodplains.

Although river sediment is sorted along the downstream distance of the river, fine sediment (i.e. sand) is added to the flow frequently, e.g. through surface or bank erosion, and a mixed bed develops as the pulse of fine material travels downstream (Robert, 2003). The addition of fine material is known to lead to a higher erosion rate (e.g. Jackson and Beschta, 1984; Iseya and Ikeda, 1987; Wilcock et al., 2001).

2.1.2 Coastal marine environment

The river ultimately meets the tidally influenced estuary, the transitional zone between the fluvial and the marine environment. Estuaries are complex systems for their part and the estuarine sediment dynamics are influenced by the river inflow, tides, waves, and salinity gradients (Leeder, 1999). Fine, muddy material deposits in the low-energy areas like the intertidal and high-tidal flats or is carried out to sea, whereas coarser sandy material accumulates in the main tidal channel (Wright et al., 1999).

The coast is a highly dynamic environment: Sediment erosion, transport and deposition occur on a variety of spatial scales (µm–km) and time scales (s–a), analogue to the hydrodynamic factors driving and influencing the sediment dynamics, such as currents, tides, and waves (Reeve et al., 2004). Whereas waves influence sediment transport on a micro-scale, the seasons influence the beach evolution over the course of one year, e.g. winter storms cause massive erosion and offshore transport of sediment, followed by a moderate wave regime in summer that transports the material back to the shore (Reeve et al., 2004). Similar to the fluvial environment, grain sizes in the marine environment vary with the energy regime: In the surf zone, where wave energy is high, coarser grain sizes prevail (sand, gravel) because fine grains are washed out. Seaward, the grain sizes decrease, as the finer grains (fine sand, silt) deposit in the less energetic areas (Reeve et al., 2004). The process of land- and seawards movement of sediment is called the *cross-shore* transport (Seymour, 2005). Longshore transport or *littoral drift* describes the sediment transport in parallel to the coast, induced by waves that break at an oblique angle to the shore (Wright et al., 1999).

2.2 Sediment grain sizes, densities, and shapes

A sediment *grain* or *particle* can be characterized by various properties, e.g. size, density, and shape. A common classification for the sediment grain size is the so-called Wentworth scale (Wentworth, 1922) which comprises six major categories: clay (< 4 µm), silt (4–62.5 µm), sand (62.5 µm–2 mm), pebbles or gravel (2–64 mm), cobbles (64–256 mm) and boulders (> 256 mm). Furthermore, subcategories exist to divide the grain sizes into (very) fine, medium and (very) coarse grains. Sediment with grain sizes < 63 µm (i.e. the silt and clay fractions) are commonly referred to as “mud” (Whitehouse et al., 2000) and the mud content – the content of cohesive fine material – has been used as a significant attribute for the stability of a sediment bed (see 2.5). The grain sizes occurring in a sediment sample can be determined using e.g. sieve analysis or laser diffraction analysis (Loveland and Whalley, 2001) and can be summarized in a grain-size or particle-size distribution curve (PSD), as shown in Figure 2.1. The PSD contains information about the various grain sizes occurring in a sediment sample and about the sorting of the sample, i.e. whether a sample contains a wide range of grain sizes (*well-graded*) or a narrow range of grain sizes (*poorly graded*). The PSD, incorporating both qualitative and quantitative information about the grain sizes, represents the *texture* of the sediment (Hillel, 2004). A common description of a sediment sample is the median diameter D_{50}, the diameter for which 50 % of the grains in the sample are smaller

(Soulsby, 1997). Similarly, D_{10}, D_{60}, or D_{90} can be used to characterize a sediment sample (i.e. 10 % of the grains are smaller than D_{10} etc.).

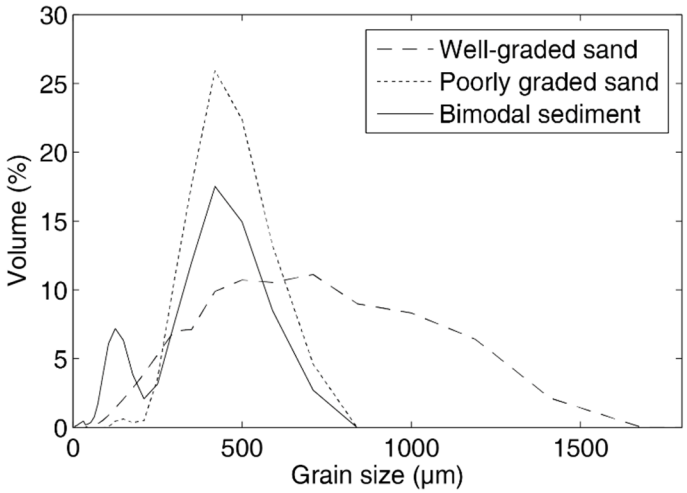

Figure 2.1: Grain-size distribution for a well-graded sand sample (commercial play sand with D_{50} = 481 µm), a poorly graded sand sample (sieved sand from the east coast of New Zealand's North Island with D_{50} = 393 µm), and a bimodal sand mixture used in the laboratory experiments (with D_{50} = 387/111 µm and 40 % (weight) fines, see chapter 6). The grain-size analysis was conducted using a laser diffraction particle size analyser (Mastersizer 2000, Malvern Instruments Ltd., UK).

The studies in this dissertation investigate the behaviour of mixed sediment beds. For the experiments, artificial sediment mixtures and numerical particle assemblages were created using a coarse and a fine fraction. As such a mixture comprises two main modes, the sediment is termed *bimodal* (Figure 2.1). The grain-size ratio $RD = D_{50,coarse}/D_{50,fine}$ is introduced to characterize bimodal sediment in addition to the grain sizes and grain-size fractions. *RD* describes the ratio between the median grain size of the coarse fraction and the median grain size of the fine fraction. A bimodal sediment mixture can for example be found in a river when a sand pulse passes along a coarse gravel bed after an erosion event (Robert, 2003).

The most prevalent mineral in sandy sediments, such as the natural sediment samples used in chapter 6, is quartz with a density of 2650 kg m^{-3} (Soulsby, 1997). Silt has similar mineralogical and physical properties (Hillel, 2004). The properties of the particles in the numerical model (see 3.2 and chapter 5) were chosen accordingly, and the density of the artificial sediment (glass beads, see 3.1.2 and chapter 4) is similar to that of quartz.

Another important attribute of sediment is the shape of the grains. The grain shapes influence several properties of the sediment, e.g. the bulk density, the grain packing, and grain interlocking or frictional strength (Hillel, 2004). The shape can be characterized e.g. by the flatness or elongation of single particles. Although grain shapes within a sediment sample can vary significantly, some general assumptions about the shape of different sediment types are usually made (Hillel, 2004): Cobbles are spherical or ellipsoid particles with a smooth surface. Sand grains are more or less round (i.e. have uniform dimensions), but can still have a very jagged surface (i.e. higher angularity).

Silt particles have a shape that is similar to sand, whereas clay minerals have a plate or rod-like, elongated shape.

In the experimental studies presented in this dissertation, the shape of individual particles was not analysed in detail. However, for the experiments in chapter 4 the particle shape was controlled by using spherical, industrially manufactured glass beads. By conducting flume experiments with two types of particles with extremely different complexity (spherical glass beads vs. angular sand grains), conclusions could be drawn on the effect of the particle shape on bed mobility and near-bed flow (chapter 6). Examples for the different complexity of sand grains and glass beads are shown in Figure 2.2 (Mair et al., 2002).

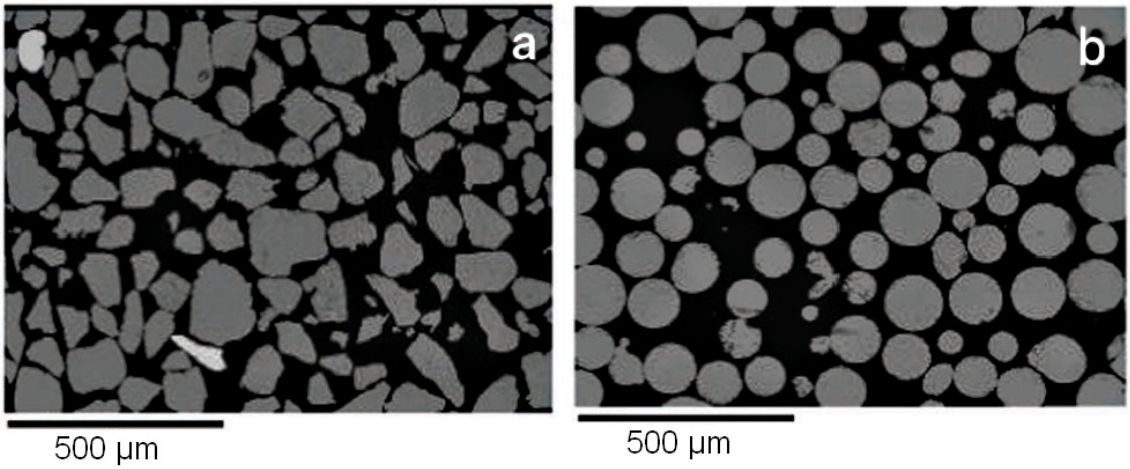

Figure 2.2: Scanning electron microscope (SEM) images of different grain shapes similar to those used in the laboratory experiments: a) Angular sand grains with D_{50} ≈ 110 µm and b) spherical glass beads with D_{50} ≈ 120 µm. From Mair et al. (2002).

2.3 Fluid flow

By definition, a fluid deforms immediately and continuously under the influence of an applied shear force and cannot regain its original form (Leeder, 1999; Dey, 2014). Two important properties for the behaviour of the fluid are the fluid's density and viscosity. The density describes the mass of one unit volume of the fluid:

$$\rho = \frac{m}{V} \qquad [2.1]$$

where ρ (kg m^{-3}) is the density, m (kg) is the mass, and V (m^3) is the volume of the fluid (Dey, 2014). The viscosity indicates the ease to deform or stir the fluid: A fluid with a low viscosity (e.g. water or air) is easier to deform than a fluid with a high viscosity (e.g. honey). If we imagine two "layers" of fluid that are one unit distance apart, the viscosity can be used to relate the applied shear stress to the resulting deformation, i.e. the flow velocity gradient or strain rate (*Newton's law of viscosity*):

$$\tau = \mu \frac{du}{dz} \qquad [2.2]$$

where τ (N m^{-2}) is the shear stress, μ (Pa s) is the (dynamic) viscosity, u (m s^{-1}) is the flow velocity in streamwise direction, and z (m) is the distance between the two layers (Dey, 2014). In other words, the viscosity μ is the shear stress required to move the upper layer of the fluid with one unit velocity past the other layer at one unit distance. The viscosity of a fluid decreases with the fluid's temperature. Water at a temperature of 5 °C has a viscosity of $1.520 \cdot 10^{-3}$ Pa s, whereas water at a temperature of 20 °C has a viscosity of $1.002 \cdot 10^{-3}$ Pa s (Kestin et al., 1978). If the dynamic viscosity is related to the fluid density, we obtain the kinematic viscosity:

$$\nu = \frac{\mu}{\rho} \qquad [2.3]$$

where ν (m^2 s^{-1}) is the kinematic viscosity, μ (Pa s) is the dynamic viscosity, and ρ (kg m^{-3}) is the fluid density (Dey, 2014; Leeder, 1999).

Given the definition of fluid viscosity, we can easily imagine the difference between laminar and turbulent flow. Laminar (or viscous) flow can be visualized as "layers" of fluid moving parallel to each other at relatively low velocity without mass exchange between the layers. The shear stress in laminar flow can be described by equation 2.2. As the flow velocity increases, eddies form and mixing occurs between the fluid layers. As the eddies are highly irregular in space and time, i.e. generate and decay instantaneously, the flow velocities start to fluctuate (Dey, 2014).

To account for the stresses introduced by the turbulences, a coefficient for the turbulent mixing has to be added to the description of the shear stress:

$$\tau = (\mu + \varepsilon)\frac{du}{dz} \qquad [2.4]$$

where τ (N m^{-2}) is the shear stress, μ (Pa s) is the viscosity, ε (Pa s) is the coefficient of eddy viscosity, u (m s^{-1}) is the flow velocity in streamwise direction, and z (m) is the distance between the two fluid layers (Robert, 2003).

The transition between laminar and turbulent flow can be described using the Reynolds number which relates the inertial forces to the viscous forces in a fluid:

$$Re = \frac{uL}{\nu} \qquad [2.5]$$

where Re is the dimensionless Reynolds number, u (m s^{-2}) is the flow velocity or the velocity of an object relative to the fluid, L (m) is the characteristic length, and ν (m^2 s^{-1}) is the kinematic viscosity of the fluid (Leeder, 1999). The Reynolds number allows comparison of the flow behaviour or the nature of flow in different environments. The characteristic length used for the calculation of Re depends on the flow problem. To describe flow in a pipe, the pipe diameter is the characteristic length. For free surface flow, such as in a flume channel or river, the characteristic length is the hydraulic diameter $D_h = 4\,A\,/\,P$ (where A is the cross-sectional area of the flow and P is the wetted perimeter). For the determination of the grain Reynolds number for a particle in a fluid or the flow through a packed bed of particles, the particle diameter is used as the characteristic length (Leeder, 1999; Rhodes, 2008).

The transition between laminar and turbulent flow cannot be narrowed down to a threshold, but occurs in a range of Reynolds number where both laminar and fluid flow patterns exist. In open channels, the transition from laminar to turbulent flow occurs at *Re* = 500–2000, i.e. fully laminar flow occurs at *Re* < 500 and fully turbulent flow occurs when *Re* exceeds 2000 (Leeder, 1999). In pipes, the transition between laminar and turbulent flow is usually assumed to occur at Re ≈ 2300 (Siekmann and Thamsen, 2008). For the flow through a packed bed of spherical particles, the transition occurs at *Re* = 10–2000, with fully laminar flow at *Re* < 10 and fully turbulent flow at *Re* > 2000 (Rhodes, 2008).

For the steady flow of an incompressible fluid through a channel, flume, pipe, or sediment bed, the *continuity equation*, which is based on the law of the conservation of mass, describes the relation between discharge, flow cross-sectional area and flow velocity:

$$Q = A_1 \cdot u_1 = A_2 \cdot u_2 = const. \qquad [2.6]$$

where Q ($m^3\ s^{-1}$) is the discharge, A (m^2) is the cross-sectional area of the flow, and u ($m\ s^{-1}$) is the flow velocity (Dey, 2014). As the fluid is incompressible and mass can neither be created nor destroyed, the mass influx at cross section 1 equals the mass efflux at cross section 2 (Julien, 1998). This indicates that the flow velocity increases if the cross-section of the flow narrows, and vice versa.

2.3.1 The boundary layer

Most fluid flows in the marine or fluvial environment are turbulent (Leeder, 1999; Stanley and Swift, 1976). The current-driven flow along a boundary, e.g. above the seabed or riverbed, is influenced by the frictional effects of the boundary on the flow velocity. The layer of the flow that is affected by these boundary effects is termed the *boundary layer* (Allen, 1985; Leeder, 1999). Above the boundary layer is the outer layer, where the fluid is moving at free stream velocity (Figure 2.3). The flow velocity in the vicinity of the boundary decreases approximately logarithmically and is assumed to be zero right at the boundary (no-slip condition, Leeder, 1999). The velocity profile within the logarithmic boundary layer can be described by the following logarithmic equation:

$$u(z) = \frac{u_*}{\kappa} ln\left(\frac{z}{z_0}\right) \qquad [2.7]$$

where u ($m\ s^{-1}$) is the flow velocity at height z (m) above the bed, u_* ($m\ s^{-1}$) is the friction velocity, κ (-) is von Karman's constant (κ = 0.4), and z_0 (m) is the bed roughness length (Whitehouse et al., 2000). The roughness length is the height above the bed at which the velocity hypothetically reaches zero. It can be related to the roughness of the bed or the grain size of the bed material: A bed of coarse sand has a higher roughness length than a bed of mud (Soulsby, 1997).

In contrast to a unimodal bed, a mixed bed of coarse and fine grains has a relatively low roughness length, as the fine particles fill the surface gaps between the coarser particles (Soulsby, 1983). The reduced *bed roughness* can lead to flow accelerations above mixed beds (e.g. Sambrook Smith

and Nicholas, 2005; Venditti et al., 2010a). This indicates that the logarithmic shape of the velocity profile is an idealized case, as mentioned by Soulsby (1983) and also shown later in this dissertation. In this context, the near-bed flow data in the laboratory experiments (chapters 4 and 6) was used to draw conclusions on the texture-induced differences in bed roughness of the various sediment treatments.

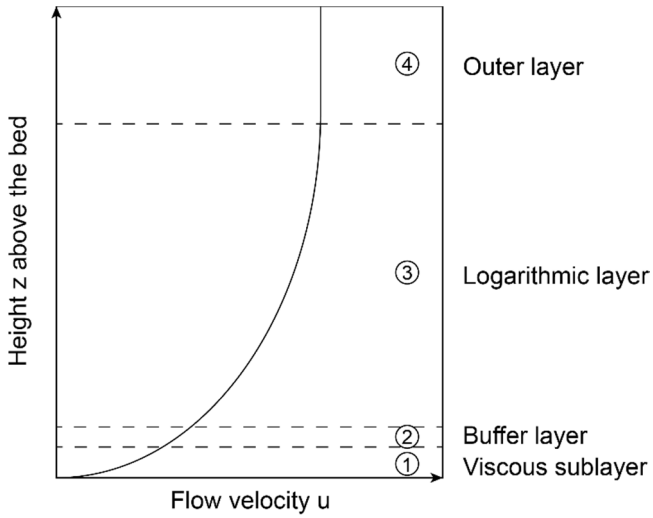

Figure 2.3: Velocity profile in the turbulent boundary layer (after Robert, 2003). Layer thickness not to scale.

The friction velocity or shear velocity u_* in equation 2.7 does not correspond to a measureable flow velocity, but is a different expression of the shear stress exerted on the bed by the fluid flow (Soulsby, 1997; Leeder, 1999; Wright et al., 1999). It describes the ratio between the bed shear-stress and the fluid density:

$$u_* = \sqrt{\frac{\tau_0}{\rho}} \qquad [2.8]$$

where u_* (m s^{-1}) is the shear velocity, τ_0 (N m^{-2}) is the bed shear-stress, i.e. the shear stress exerted on the bed by the fluid flow, and ρ (kg m^{-3}) is the density of the fluid. The use of the shear velocity u_* therefore allows to formulate the bed shear-stress (see also 2.4) in units of velocity.

At the bottom of the otherwise turbulent boundary layer, the so-called viscous sublayer is a thin layer of purely laminar flow, i.e. where viscous shear stresses dominate (Figure 2.3). The layer develops close to a smooth surface when flow velocities are not excessively high and is adjoined by a thin buffer or transitional layer (Wright et al., 1999; Robert, 2003). Above the buffer layer we find the fully turbulent logarithmic layer (Figure 2.3), where Reynolds shear stresses dominate. For the investigation of sediment transport processes, the logarithmic layer is the most interesting zone of the fluid flow: The flow velocities within this layer can be used to estimate the shear velocity and the bed shear-stress, parameters which are crucial for sediment entrainment (see 2.4). Shear velocity and bed shear-stress can be derived from the flow using various approaches. In the idealized logarithmic flow profile, the shear velocity is related to the slope of the velocity increase with log height and can be approximated using the following equation:

$$u_* = \frac{1}{5.75} \cdot \frac{du}{dlogz} \quad [2.9]$$

where u_* (m s^{-1}) is the shear velocity, u (m s^{-1}) is the flow velocity, and z (-) is the height above the bed. In this relation, z is a dimensionless number, thus u_* has the units of velocity (Wright et al., 1999). With knowledge of u_*, the bed shear-stress can be calculated according to equation 2.8.
The bed shear-stress can also be determined from the turbulent fluctuations of the near-bed flow, i.e. the turbulent kinetic energy (*TKE*) in the boundary layer:

$$TKE = \frac{1}{2}\rho \cdot \left(\overline{u_x{}'^2} + \overline{u_y{}'^2} + \overline{u_z{}'^2}\right) \quad [2.10]$$

$$\tau_0 = C_1 \cdot TKE \quad [2.11]$$

where *TKE* (N m^{-2}) is the turbulent kinetic energy, ρ (kg m^{-3}) is water density, u_x', u_y' and u_z' (m s^{-1}) are the flow velocity fluctuations in stream-wise, cross-stream and vertical directions, respectively, and τ_0 (N m^{-2}) is the bed shear-stress (Kim et al., 2000). The bed shear-stress is related to *TKE* through a constant C_1 = 0.19 (Soulsby, 1983). Other methods for the determination of shear velocity and bed shear-stress are the eddy correlation (EC) and the inertial dissipation (ID) method. More information about these methods and their applicability can be found in Inoue et al. (2011).

2.4 Sediment threshold

Sediment entrainment, i.e. the motion of a single sediment grain, is initiated when the hydrodynamic driving force outweighs the resistance force of the grain. The hydrodynamic driver is the drag force exerted on a single grain, or the bed shear-stress exerted on the bed area by the fluid flow, whereas the grain resistance force includes the immersed weight of the grain(s) resting on the bed as well as the intergranular friction.
A single grain on the sediment surface will start moving if the drag and the lift force are high enough to overcome the gravitational and the frictional force (Figure 2.4a). The drag force resulting from the flow of water around the grain is:

$$F_D = \frac{1}{2}\rho_f u^2 C_D A \quad [2.12]$$

where F_D (N) is the drag force, ρ_f (kg m^{-3}) is the density of the fluid, u (m s^{-1}) is the flow velocity, C_D (-) is the drag coefficient, and A (m^2) is the cross-sectional area of the grain (Dey, 2014). F_G (N) is the immersed weight of the grain:

$$F_G = V\left(\rho_s - \rho_f\right)g \quad [2.13]$$

where V (m^3) is the grain's volume, ρ_s (kg m^{-3}) is the density of the grain or solid, ρ_f (kg m^{-3}) is the fluid density, and g is the gravitational constant (9.81 m s^{-2}).
If we take a closer look at Figure 2.4a, we realize that the grain is resting on top of two other grains. To overcome the resistance F_R it has to turn around the pivoting point (Figure 2.4b). In this case, the force required to set the grain in motion depends on the pivoting angle Φ.

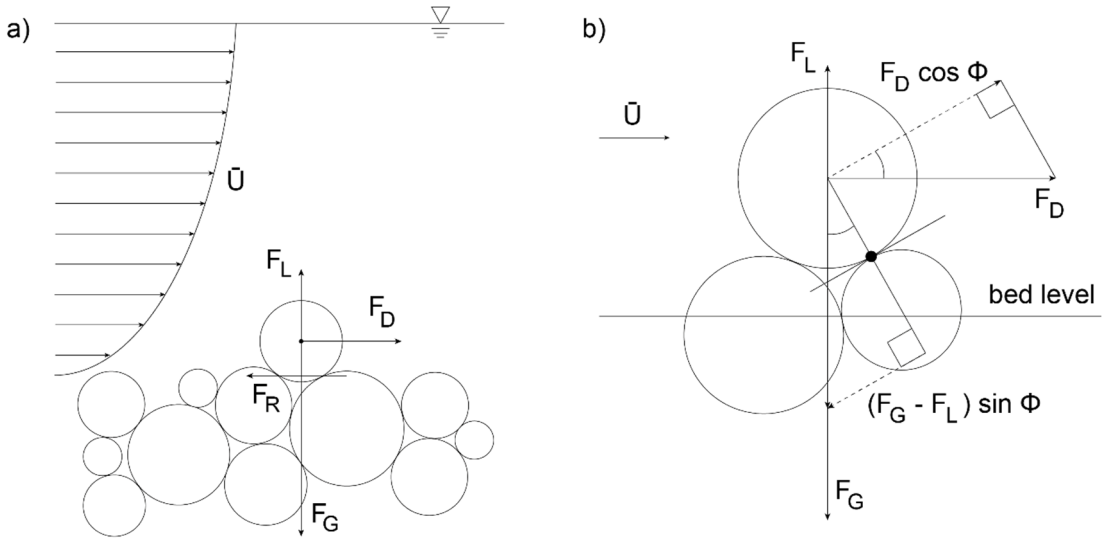

Figure 2.4: a) Balancing of the forces acting on a grain on the sediment bed. Drag F_D and lift force F_L are tending to mobilize the grain, while immersed grain weight F_G and frictional (or resisting) force F_R are resisting the movement. After Dey (2014). b) Detailed balancing of the forces acting on a sediment grain on the bed surface. If drag and lift force are high enough to overcome the resisting forces, the grain will turn around the pivoting point (black dot). In the case pictured here, the mobilizing force (F_D cos Φ) outweighs the resisting force ((F_G – F_L) sin Φ), as indicated by the longer vector (dashed arrow). The particle would subsequently start to move. Modified after Bridge and Bennett (1992).

If the grain is not moving, the forces are in equilibrium:

$$F_D \cos \Phi = (F_G - F_L) \sin \Phi \qquad [2.14]$$

where F_D (N) is the drag, Φ (°) is the pivoting angle, F_G (N) is the immersed grain weight, and F_L (N) is the lift force. If F_D, resulting from the flow velocity, is high enough, the grain will turn around the pivoting point and start moving. For a more detailed description of grain pivoting see Bridge and Bennett (1992).

Thinking of a sediment bed under flow conditions, it is impossible to measure the forces acting on each single grain. It is therefore more convenient to consider the sediment bed as a whole, and to examine the frictional force of the water that acts upon an area of the bed. A mass of grains on the sediment bed will start moving if this frictional force of the fluid, the bed shear-stress τ_0, is high enough to overcome the critical shear-stress τ_{cr} of the bed:

$$\tau_0 > \tau_{cr} \qquad [2.15]$$

The bed shear-stress describes the frictional force per unit area of sediment bed exerted by the fluid flow over it:

$$\tau_0 = \rho_f C_D \overline{U}^2 \qquad [2.16]$$

where τ_0 (N m^{-2}) is the bed shear-stress, ρ_f (kg m^{-3}) is the density of the fluid, C_D (-) is the drag coefficient of the bed, and $\overline{U}$ (m s^{-1}) is the depth-averaged flow velocity (Whitehouse et al., 2000). The drag coefficient of the bed can be related to the roughness length (see 2.3.1, Soulsby, 1997).

However, the critical shear-stress τ_{cr} of a sediment bed is difficult to determine, as many characteristics of the bed and the grains cannot be measured easily. In a semi-empirical model based on a series of flume experiments, Shields (1936) introduced the dimensionless Shields parameter as the ratio between the critical bed shear-stress τ_{cr} required to set the grain in motion and the immersed grain weight:

$$\theta_{cr} = \frac{\tau_{cr}}{g(\rho_s - \rho_f)D} \qquad [2.17]$$

where θ_{cr} (-) is the threshold Shields parameter, τ_{cr} (N m^{-2}) is the critical bed shear-stress, ρ_s and ρ_f (kg m^{-3}) are the densities of the sediment grain and the fluid, respectively, g is the gravitational constant (9.81 m s^{-2}), and D (m) is the grain diameter (Soulsby, 1997). Many studies have since focused on the extension, validation, and modification of Shields' approach (summaries are given by e.g. Miller et al., 1977, or Dey, 2014). Figure 2.5 shows the variation of the threshold Shields parameter over varying dimensionless grain size D_*, based on data collected by Shields and expanded by a correction from Soulsby (1997) for small grain sizes. The dimensionless grain size D_* is given by:

$$D_* = \left[\frac{g(s-1)}{\nu^2}\right]^{1/3} \cdot D \qquad [2.18]$$

where ν (m^2 s^{-1}) is the kinematic viscosity of water, g is the gravitational constant (9.81 m s^{-2}), D (m) is the grain diameter, and $s = \rho_s / \rho$ (Soulsby, 1997). For small grain sizes with D_*< 10, an increase in the threshold Shields parameter is visible, i.e. higher shear stresses and thus flow velocities are required to entrain the finer grain sizes. This increase is attributed to the smooth bed surface which results in the presence of a laminar sublayer that completely covers the fine-grained bed (Shields, 1936).

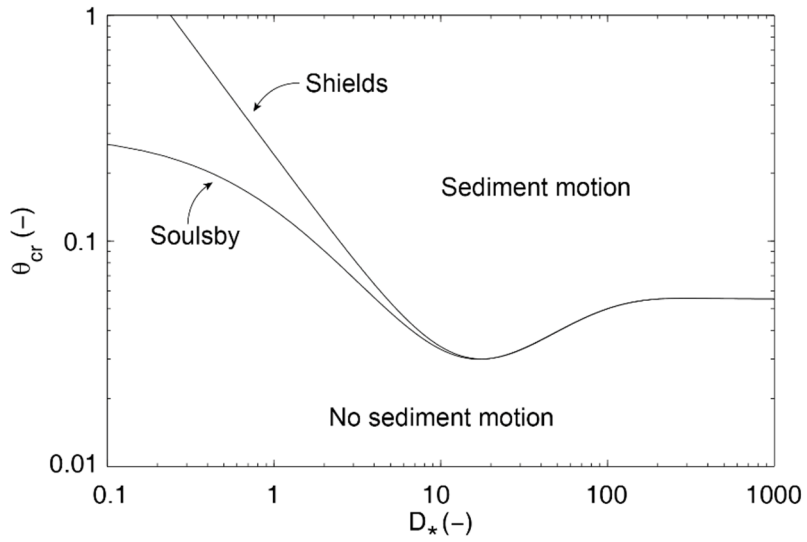

Figure 2.5: Shields diagram showing the critical Shields boundary shear-stress for sediment motion over the dimensionless grain size D_* (modified after Soulsby, 1997).

2.4.1 Modes of transport

If the flow is strong enough to initiate grain entrainment, the grain will start to roll, slide or hop along the bed. The grain is moving along the bed horizontally (with occasional saltation) but vertical turbulent velocities are not high enough to permanently lift it off the bed. This mode of transport, during which contact between the moving grains and the bed persists, is called *bedload*. A sandy bed (D_{50} < 0.8 mm) in a current will tend to form so-called ripples, i.e. small bed features or bed forms (Soulsby, 1997; Leeder, 1999). Ripples have a height and length that is relatively small compared to the water depth. As bedload material is deposited on the downstream side, the bed form slowly moves along the bed. At very high flow speeds, the material forming the bed form is washed out (Soulsby, 1997; Reeve et al., 2004). Bed forms can also develop below the threshold of motion, due to disturbances or irregularities in the bed surface. These irregularities disrupt the flow, leading to turbulence and vortices, and consequently, particle transport is initiated (Leeder, 1999). The measurement of bedload transport is complex and no standard procedure is available (e.g. Julien, 1998; Allen, 2009). To quantify bedload transport, sampling devices, such as sediment traps, bedload samplers (e.g. a Helley-Smith sampler), or a vortex tube can be used (Julien, 1998). These intrusive methods involve the removal of sediment from the system. A non-intrusive method for bedload quantification is the tracer technique, i.e. the visual observation of painted or marked particles (sometimes with the assistance of high-speed cameras). As these methods are not suitable for application in the annular flume, a new approach for the evaluation of bed movement is presented in 3.1.3.

If the flow significantly exceeds the threshold of motion and the vertical turbulent velocity overcomes the grain's settling velocity, the grain moves upwards and is transported in *suspension* (Soulsby, 1997). While coarse, non-cohesive material starts moving as bedload first, finer silt or clay particles usually enter suspension right after the threshold of motion is exceeded (Julien, 1998). Suspended sediment can be measured optically, i.e. using an optical backscatter sensor (OBS) which detects the light attenuation as a proxy for sediment concentration of the water column (Allen, 2009). In addition, suspended material can be detected acoustically, i.e. derived from the acoustic backscatter of the suspended particles measured by an acoustic Doppler velocimeter (ADV) or an acoustic Doppler current profiler (ADCP). The use of acoustic methods to measure sediment transport is still advancing and developing (Thorne and Bell, 2009).

2.5 Factors influencing the bed stability

Although the accuracy of the Shields diagram (Figure 2.5) has improved with the incorporation of additional data from laboratory experiments collected under a variety of flow conditions, the applicability of the concept for natural sediment beds is limited, as natural sediment consists of a range of grain sizes that interact with each other. In addition, the stability of a sediment bed does not only depend on the grain sizes and the flow field, but can be influenced by other parameters controlling the initiation of sediment motion:

- Cohesive forces between clay particles lead to an increased stability of a mixed bed with a threshold clay or mud content. At this threshold, the behaviour of the bed traverses from non-cohesive, sand-dominated to cohesive, mud-dominated behaviour (e.g. Teisson et al., 1993; Mehta and Lee, 1994; Panagiotopoulos et al., 1997; Torfs et al., 2001; Hillel, 2004; Le Hir et al., 2008; Jacobs et al., 2011).
- Biological activity, such as marine micro- and macrofauna living on or in the sediment, can influence the stability of the bed. While some species (e.g. diatoms) secrete glue-like mucus that binds the particles and increases bed stability (e.g. Grant et al., 1986; Paterson et al., 1990; Meadows et al., 1994), bioturbating species create burrows in the sediment, thus increasing the water inflow and subsequently leading to higher erosion (e.g. Widdows et al., 1998a; Willows et al., 1998).
- Sediment texture, i.e. the interaction of grain sizes and grain-size fractions, plays another important role in sediment stability, as it can influence the stability in different ways: Texture-induced stabilization and texture-induced mobilization (see 2.5.1 and 2.5.2).
- Particle complexity (e.g. plate- or rod-like clay particles) can affect the frictional strength of the sediment (e.g. Mair et al., 2002; Guo and Morgan, 2004; Kock and Huhn, 2007) and thus the erosion resistance. Complex grain shapes can lead to the interlocking of grains and an increase of the intergranular friction of a sediment bed (see 2.5.3).

The research in this dissertation focuses on the sediment texture influencing the stability of a mixed bed and provides indications for the role of the particle shape. In the following, each of these factors is described in more detail.

2.5.1 Texture-induced stabilization

In many studies investigating sediment erosion in estuaries or the marine environment, the stabilizing effect of fine particles on a coarse bed has been described. Laboratory experiments with sand-mud mixtures (e.g. Torfs, 1996; Mitchener and Torfs et al., 2001; Le Hir et al., 2008; Jacobs et al., 2011; Bartzke et al., 2013) concluded that the addition of fines leads to an increase of the critical bed shear-stress. This stabilization has been widely accredited to the transition between non-cohesive and cohesive sediment behaviour: As the amount of cohesive fine material exceeds a critical threshold, the bed as a whole starts behaving like a cohesive sediment. Mitchener and Torfs (1996) suggested a threshold mud fraction of 3–15 % (weight), which was later adjusted to 5–10 % clay content by van Ledden et al. (2004). Le Hir et al. (2008) determined a sharp transition between non-cohesive and cohesive behaviour at a threshold mud fraction of 35–40 % (volume). In addition, the authors suggested to investigate a size ratio between sand and mud grains as a measure to characterise the threshold.

Mehta and Lee (1994) have tried to develop a theoretical model to elucidate the transition between the different threshold conditions for the transport of non-cohesive and cohesive sediment grains. They concluded that the behaviour of the silt fraction (≈ 2–63 µm) could neither be explained properly by the model for cohesive transport, nor by the model for non-cohesive transport, although

cohesion does not play a role for grain sizes larger than 20–40 µm. A transition between cohesive and non-cohesive transport behaviour seems to occur in the silt range.

In a conceptual model van Ledden et al. (2004) described the stabilization of a sand-mud mixture through a "network structure" of fines, that acts in addition to the cohesive effects of the mud fraction. A mixed bed with a high amount of coarse material and only little fine grains behaves similar to a unimodal coarse-grained bed. If the fine-grained content exceeds a certain percentage, the fine particles form a network around the coarse grains, interrupting the intergranular contacts, and the erosion behaviour of the bed is dominated by the fine-grained fraction. Even if cohesive forces are not considered at all, the network structure, resulting from the size differences of the coarse and fine grains alone, leads to increased bed stability. Based on these findings, Bartzke et al. (2013) conducted erosion experiments with sand (D_{50} = 300 µm) and silt (D_{50} = 55 µm) with little to no cohesion. The results showed that even small amounts of silt (300 g m^{-3}) can increase the stability of a sand bed and shift the critical bed shear-stress for erosion to higher flows velocities.

In recent years, numerical models have been used to investigate texture-related processes that could contribute to sediment stabilization. Morgan (1999) simulated the intergranular mechanics of (dry) sediment using the discrete element method (DEM) and concluded that the particle-size distribution has a significant influence on particle rolling and rotating, and on strain localizations in particle assemblages. Bartzke and Huhn (2015) coupled a particle and a flow model to simulate the sediment-fluid interaction at the sediment surface. They suggested that the fine particles do not only form stabilizing network structures around the coarser particles, as described by van Ledden et al. (2004), but also block off the water flow into the sediment bed. This blocking of the pore space leads to an additional stabilization of the bed, as particle entrainment is prevented.

2.5.2 Texture-induced mobilization

In contrast to the stabilizing behaviour of the fine fraction described above, for fully non-cohesive, coarser sediment mixtures (e.g. in rivers), it is commonly known that the addition of fine particles can lead to the mobilization of the coarser bed fraction (e.g. Jackson and Beschta, 1984; Iseya and Ikeda, 1987; Wilcock et al., 2001; Venditti et al., 2010a, 2010b; Houssais and Lajeunesse, 2012).

Many theoretical studies have tried to incorporate the grain-size distribution into the erosion equation for mixed, non-cohesive sediment. Einstein (1950) developed a model for bedload transport and introduced a "hiding" factor that affects the calculated bedload of fine material if the fines are small enough to hide behind larger grains or within the laminar sublayer, thus evading entrainment. Wiberg and Smith (1987) described the force balancing on a single particle on a mixed bed in relation to the ratio between grain diameter and roughness length, accounting for the reduced erosion of very fine material and increased erosion of coarse material from a mixed bed. Similarly, Bridge and Bennett (1992) described particle entrainment on a small scale, introducing both a relation between particle sizes and bed roughness, and a particle shape factor. Wilcock and Kenworthy (2002) developed a two-fraction approach to describe the erosion of a bimodal gravel-sand bed, based on experimental data (Wilcock et al., 2001).

In laboratory experiments Jackson and Beschta (1984) observed that the addition of sand pulses to a gravel-sand bed leads to an increase in bedload transport of gravel and sand, and to the scour of bed features. The authors hypothesized that the sand grains in the near-bed flow facilitate further sediment entrainment (due to increased fluid density and fluid viscosity through the addition of sand to the flow). In addition, the bed surface roughness decreases due to the sand filling "pools" between the gravel and due to the scouring of the bed features. While many other studies have investigated the mobilization of coarser particles on a mixed bed (e.g. Iseya and Ikeda, 1987; Wallbridge et al., 1999; Houssais and Lajeunesse, 2012), only the recent development of flow measurement techniques (such as acoustic Doppler velocimetry or particle image velocimetry, PIV) could provide the near-bed hydrodynamics that are associated with these processes. Using near-bed flow measurements in a flume experiment, Sambrook Smith and Nicholas (2005) found that with the addition of fine sand to a gravel bed and the subsequent reduction of the surface roughness, turbulences above the bed decrease and the flow velocities increase. Venditti et al. (2010a) made similar observations using a pulse of fines on a gravel bed. They hypothesized that the higher near-bed flow velocities result in a higher drag that is exerted on the coarse particles on the bed surface, which then leads to increased erosion of coarse bed material. Venditti et al. (2010a) also suggested to investigate the effect of the fine grain size relative to the coarser bed material.

2.5.3 The effect of particle shape

In most laboratory studies investigating the stability of a sediment bed under flow conditions, the bed is only described using grain sizes (D_{50}) or the grain-size distribution. Laboratory shear tests (e.g. Mair et al., 2002) and numerical models (e.g Guo and Morgan, 2004; Kock and Huhn, 2007) have shown that the angularity of complex grains leads to an increase in intergranular friction, and to a higher bed stability. Based on these results it becomes clear that the characterization of a sediment bed by the grain diameter only is a strong simplification. One approach to incorporate the particle complexity is the incorporation of the fine content (i.e. the amount of mud with $D_{50} < 63$ µm, see 2.2). The fine content can be used as a measure for the amount of very complex clay particles, i.e. particles that increase the critical shear stress of a sediment bed.

Some theoretical studies (e.g. Komar and Li, 1986; Bridge and Bennett, 1992) incorporated the particle shape into a model describing pivoting and sediment entrainment. For more complex (i.e. less "rollable") grains, a higher flow velocity is required for grain entrainment (see 2.4). The effects of different particle shapes on the near-bed flow field, however, are mostly unknown. Latest development of in-situ instrumentation, such as profiling acoustic Doppler velocimetry, has allowed to measure flow profiles at high resolutions (mm scale). This enables us to investigate the flow velocities above different sediment beds, and to draw conclusions about possible relations between the particle shapes and the near-bed flow (chapter 6).

2.6 Scope of the study

The literature research on varying sediment mobility in coastal as well as fluvial environments inspired the focus on the relative particle size of the fine and coarse particles, i.e. the grain-size ratio $RD = D_{50,coarse}/D_{50,fine}$, as a factor controlling sediment mobility in addition to the amount of fines. As described in the theoretical models for non-cohesive, coarse sediment (Komar and Li, 1986; Wiberg and Smith, 1987; Bridge and Bennett, 1992), the size of a grain on the bed surface relative to its neighbouring grains can control the particle stability. Likewise, the surface roughness of a bed is only reduced by the addition of fines (as described by e.g. Jackson and Beschta, 1984; Venditti et al., 2010a), if the fine particles are small enough to hide in the surface gaps between the coarse particles. It is hypothesized that in a similar fashion, the formation of stabilizing network structures depends on the grain-size ratio: The ability of fines to form stabilizing networks and to break up the inter-particle contacts of the coarser grains (van Ledden et al., 2004) depends on the relative sizes of the coarse and fine particles. The blocking of pore space by fine particles (as described by e.g. Bartzke and Huhn, 2015) can only inhibit bed inflow if the fines are small enough to completely fill the pore space between the coarser particles. I hypothesize that in all these scenarios not only a critical amount of fines but also a certain grain-size ratio is required.

The major part of this dissertation investigates the influence of the grain-size ratio *RD* on the near-bed flow processes and on the bed mobility. One research paper addresses both the grain-size ratio and the amount of fines. Furthermore – based on the different sediment behaviour with the addition of fines – the studies aim to elucidate the transition between stabilization and mobilization of a mixed bed through the addition of fines. As grain shapes vary significantly within one size class, the median grain diameter is only a rough approximation to describe the grain. Therefore, an additional aim of the dissertation is to validate the findings for naturally occurring, more complex grain shapes, and to test the influence of the shape on the bed mobility and the near-bed flow. To achieve this goal, a controlled environment with unidirectional flow (laboratory flume, numerical model) was set up to investigate the behaviour of mixed beds with known parameters (grain sizes, grain-size fractions, *RD*).

3. Methodology

3.1 Laboratory experiments

Erosion experiments in an annular flume were conducted to investigate the effects of the grain-size ratio *RD*, the effect of the amount of fine material (i.e. the fine fraction), and the effect of the particle shape on the near-bed flow field and the mobility of mixed beds.

3.1.1 Annular flume

The flume that was used in the laboratory experiments is a replica of an annular flume developed by Widdows et al. (1998b). Two concentric cylinders of 63 and 43 cm diameter form a circular flow channel of 10 cm width (Figure 3.1a). A motor driven lid is placed on top of the flume. The flume is filled with bed material to a height of 5 cm and water is added to a height of 25 cm. The flume lid is submerged in water to a depth of 3 cm. When the lid starts rotating, a current is induced through the friction between the lid and the fluid. For the flume experiments described in this thesis, the current velocity was increased in 12 intervals and each interval was run for 15 min to receive an equilibrium between the flow field and the particle transport, yielding a total duration of 180 min for one experimental run. The maximum free flow velocity in the flume was U = 18.5–23.0 cm s^{-1}. Detailed descriptions of the hydrodynamics of the two experimental series can be found in the corresponding chapters 4 and 6.

A major advantage of annular flumes compared to other flume shapes is the full development of a boundary layer, due to quasi infinite flow length (Amos et al., 1992). This makes the hydrodynamics in the flume comparable to flow in the field. Furthermore, the absence of a pump (typically used in recirculating flow tanks) results in uninterrupted sediment transport. The circular shape of the flume may lead to the development of a secondary flow (Spork, 1997), however, in a channel of 10 cm width this is minimal compared to in wider annular flumes (Widdows et al., 1998b).

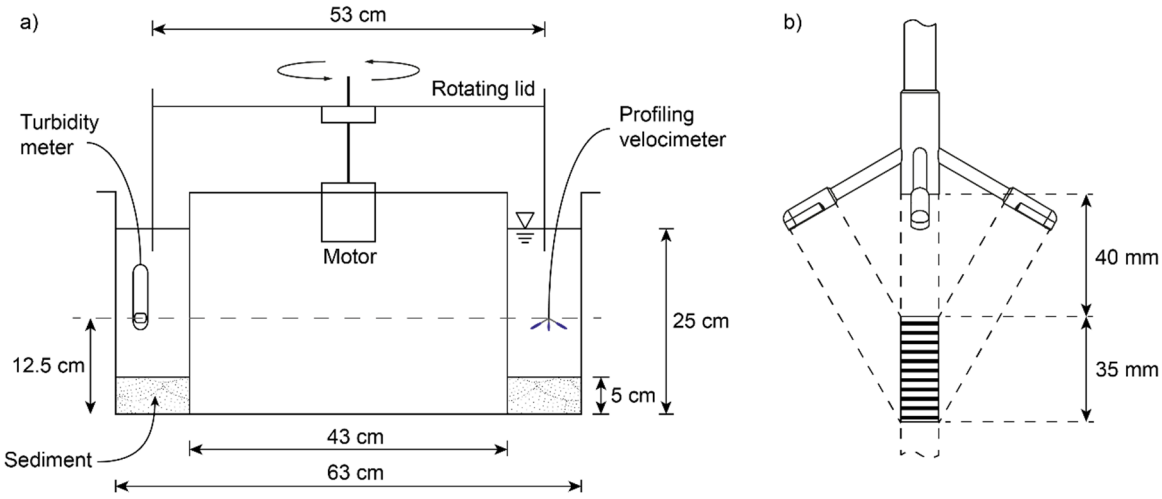

Figure 3.1a) Sketch of the annular flume used in the laboratory experiments. b) Probe of the profiling ADV (modified after Nortek Inc., 2012). The shaded area indicates the velocity sampling volume.

The near-bed flow profiles over a vertical extent of 35 mm were recorded with a profiling ADV (10 MHz Vectrino Profiler, Nortek AS, Norway, Figure 3.1b). As the grain sizes ranged from silt- to sand-sized (≈ 40–400 µm), the eroded material moved partly as bedload and partly in suspension (2.4.1). Therefore, bed erosion and mobility in the laboratory experiments were analysed in a twofold way:

- Changes of the bed level as indicators for bed mobility were derived from the distance between the ADV and the bed (i.e. the so-called bottom distance). The temporal variance of the bottom distance served as a proxy for bed movement underneath the instrument (see 3.1.3).
- To detect suspended sediment transport, i.e. changes of the suspended sediment concentration (*SSC*) or suspended particulate matter concentration (*SPM*) in the water column, an optical backscatter sensor (Seapoint Turbidity Meter, Seapoint Sensors, Inc., USA) and the acoustic backscatter signal from the ADV were used. The *SPM* measurements were calibrated with water samples that were taken in regular intervals during each experimental run.

3.1.2 Material

To separate the effect of the grain-size ratio on bed mobility from other factors influencing erosion (e.g. particle complexity, cohesion, bioactivity), spherical glass beads (Sigmund Lindner GmbH, Germany, Figure 3.2) were used for the first experimental series (chapter 4). These industrial glass beads are made of soda-lime glass with a density (ρ = 2500 kg m^{-3}) that is similar to quartz. With a very smooth surface and high sphericity (≥ 0.89), the contact area between the particles is minimized resulting in very low intergranular friction. In addition, the use of well-sorted, spherical particles allows the accurate determination of the grain-size ratio, which improves the reproducibility of the experiments. In the flume experiments, particle sizes ranged from 39 µm to 367 µm, comparable to the grain sizes of coarse silt to medium sand. As described in 2.2, the bimodal mixtures were characterized by the grain-size ratio *RD* and the amount of fine material. One unimodal bed and three mixed beds with various *RD* (3.9; 5.8; 9.4) were created. In addition, the amount of fines in the mixed beds was varied (10; 20; 40 % dry weight) to obtain ten different glass-bead mixtures in total (Table 3.1a). The coarse 367 µm-material was dyed red to allow visual differentiation of the grain-size fractions (Figure 3.2).

Figure 3.2: Dyed, saturated glass beads of the coarse fraction with D_{50} = 367 µm.

To investigate the effect of particle complexity and bed roughness on the bed mobility and the near-bed hydrodynamics, and to transfer the findings from artificial bed material to nature, bimodal sediment mixtures consisting of sand and silt were used for the second experimental series (chapter 6). The grain sizes ranged from 53 µm to 410 µm. Sediment of these grain sizes is assumed to be

non-cohesive (e.g. Mehta and Lee, 1994; Whitehouse et al., 2000) and can be found e.g. in high-energy near-shore or beach environments (Reeve et al., 2004). One unimodal bed and three mixed beds with various *RD* (2; 3.5; 7.7) and 40 % fines (dry weight) were created (Table 3.1b). The results of the natural experimental series were compared with the results from the glass-bead experiments with 40 % fine content.

Table 3.1: Outline for laboratory experiments.

a) Glass beads

RD	D_{50} (µm)	Fine content (% dry weight)		
unimodal	367		0	
9.4	367/39	10	20	40
5.8	367/63	10	20	40
3.9	367/93	10	20	40

b) Sand/silt

RD	D_{50} (µm)	Fine content (% dry weight)
unimodal	389	0
7.7	410/53	40
3.5	387/111	40
2	393/193	40

3.1.3 Development of a new approach for the evaluation of bed mobility

Studies analysing erosion and stability of fine-grained sediment commonly use the erosion rate *E*, derived from changes in the *SPM* concentration in the water column, as a proxy for particle entrainment (e.g. Amos et al., 1992; Widdows et al., 1998; Andersen, 2001; Andersen et al., 2005). Although this is a reliable method to determine particle entrainment and transport in suspension, erosion of coarser material can occur without it being detectable in the *SPM* data, e.g. particles are entrained and start moving as bedload. Only at very high flow speeds the material is suspended. While bedload transport can lead to a significant change of the bed morphology (e.g. through the development of bed forms, see 2.4.1), the turbidity of the water column does not necessarily increase, thus these changes take place unnoticed. Vice versa, the entrainment of a large amount of very fine particles leads to an increase in turbidity and *SPM*, but is not necessarily connected to major changes of the bed level. The combined measurement of both *SPM* and changes of the bed level can resolve this difficulty.

As mentioned in 2.4.1, no standard technique exists for the measurement of bedload transport, (Julien, 1998; Allen, 2009). Common intrusive methods like sediment samplers remove material from the system and are difficult to apply in a confined laboratory environment. In a recirculating laboratory environment like the annular flume used in the studies presented here, the in-situ assessment of the particle transport is preferable. However, the visual tracking of individual painted or marked particles is only practicable for coarser grains. In addition, there are methods that derive the bedload transport from the shape and movement of bed features (e.g. Simons et al., 1965; Engel and Lau, 1980). For these methods however, undisturbed bed-form development and bed-form migration are required.

Modern acoustic measurement techniques allow the precise determination of the bed level over time. In this dissertation, an approach is made to use these high-resolution (in both time and space) acoustic data to evaluate bed level changes as an indicator for the “bed mobility”. It has to be noted

that the measurements do not represent the bedload transport (in terms of a volumetric transport rate), as no calibration was conducted.

The profiling ADV records the distance between the instrument's central transducer and the bed, i.e. the "bottom distance" d_b, at a sampling rate of 10 Hz. The "bottom", as detected by the ADV, is located at the depth with the strongest acoustic backscatter (*BS* = max), coinciding with the maximum particle concentration within the measurement range of the ADV. To quantify the changes of the bed level over time, the temporal variance of the bottom distance is calculated:

$$\sigma_b^2 = \frac{1}{N-1}\sum_{i=1}^{N}(d_{bi} - \overline{d_b})^2 \qquad [3.1]$$

where σ_b^2 (m²) is the bottom variance, N (-) is the number of measurements, d_{bi} (m) is the bottom distance and $\overline{d_b}$ (m) is the mean bottom distance averaged over N measurements. The bottom variance is an indicator for the mobility of the bed, i.e. a proxy for the bed movement underneath the ADV.

To evaluate the *onset* of sediment motion and major events of particle movement in relation to the flow velocity, the moving bottom variance $\sigma_{b,mov}^2$ was calculated with N = 20, i.e. over a time span of 2 s. Peaks in the moving bottom variance are indicators for major changes of the bottom level over a time span of 2 s (i.e. a rise or fall of the bottom level). At increasing flow velocities, the first peak in the moving bottom variance, i.e. the first major change of the bottom level, can be used to determine a critical flow velocity for the sediment entrainment. In chapter 6, a threshold moving variance of $\sigma_{b,mov}^2$ = 0.025 mm² is used to determine the critical flow velocity U_{cr}.

In addition to the moving bottom variance, a method was developed to quantify the bed mobility for the complete experimental run. For each interval with constant flow speed, equation 3.1 was used to calculate the bottom variance $\sigma_{b,int}^2$ over the time span of Δt = 15 min (i.e. N = 9000), i.e. the variance of the bottom level from the mean bottom distance during the interval. The bottom variance in each flow speed interval was then normalized, dividing it by the average flow speed U of the respective interval and the duration of the interval (Δt). Finally, the normalized mobility was averaged over all flow speed intervals:

$$\sigma_{b,norm}^2 = \frac{1}{n_{Int}}\sum\frac{\sigma_{b,int}^2}{U \cdot \Delta t} \qquad [3.2]$$

where $\sigma_{b,norm}^2$ (m) is the normalized bottom variance as an indicator for the bed mobility, n_{Int} (-) is the number of intervals with constant flow velocity, $\sigma_{b,int}^2$ (m²) is the bottom variance calculated over one flow speed interval, U (m s^{-1}) is the flow velocity in the respective interval, and Δt (s) is the duration of the interval. The obtained value $\sigma_{b,norm}^2$ is independent of the prevailing flow velocity and the duration of the measurement, thus allowing comparison with experiments that follow a different experimental procedure.

In addition to the *SPM* measurement, this method using the temporal variance of the bottom level provides a proxy for changes of the bed morphology in the laboratory experiments (chapters 4 and 6). The experimental data of the experiments was processed and analysed using MATLAB R2013b (MathWorks, Inc., USA, 1984–2013).

3.2 Numerical model

In analogue experiments and field measurements, the in-situ quantification of the controlling parameters (such as flow speed, porosity, sediment properties etc.) proves to be difficult, thus numerical models have gained importance in the simulation and analysis of sediment erosion. These models are used to simulate the water flow above and the inflow into the sediment bed; thereby processes inside the sediment matrix (i.e. flow around individual grains, porosity changes etc.) can be investigated on a grain scale (e.g. Drake and Calantoni, 2001; Schmeeckle and Nelson, 2003; Bartzke and Huhn, 2015). In contrast to physical models, numerical models provide detailed, continuous data collection of the critical parameters. These results form the basis for larger scale sediment movement and erosion models.

A high-resolution numerical model was developed to investigate the effects of the grain-size ratio *RD* on the micro-scale flow processes at the bed surface and in the upper millimetres of the bed, and subsequently on particle entrainment (chapter 5). The coupled, three-dimensional model (Figure 3.3) comprised a particle simulation and a flow simulation. The commercial software Itasca PFC3D 3.10 (Particle Flow Code in Three Dimensions, Itasca Consulting Group, Inc., USA, 1993–2005) was used to simulate the particle movements and interactions. PFC3D uses the discrete element method (DEM) that describes the interaction (i.e. contacts and motions) of a large number of particles (Cundall and Strack, 1979). In the calculation cycle of PFC3D, the particle and wall positions are used to determine a set of contacts in the modelling domain. The force-displacement law is applied to every contact and the law of motion is applied to each particle, resulting in particle motion. Subsequently, the particle and wall positions are updated and the calculation cycle is repeated (Itasca Consulting Group, 2006a). The model parameters of the particle model, such as particle stiffness and density, are summarized in Table 3.2a.

The flow simulation was conducted with Itasca FLAC3D 3.10 (Fast Lagrangian Analysis of Continua in Three Dimensions, Itasca Consulting Group, Inc., USA, 1993–2006). FLAC3D uses the finite difference method (FDM) to simulate laminar flow according to designated boundary conditions, e.g. specific discharge, pore pressure and fluid density (Itasca Consulting Group, 2006b). The modelling domain is discretized into cubic grid cells and Darcy's law for fluid transport is applied to calculate the flow velocities in each cell (Itasca Consulting Group, 2006b). Benchmark tests were conducted to find suitable parameters for porosity and permeability of the cells to mimic "free flow" (Table 3.2b). The dimensions of the modelling domain, the particle sizes in the DEM model and the grid sizing in the FDM model were chosen to obtain a reasonable compromise between model resolution and computational effort.

Table 3.2: Model parameters of the coupled particle-flow model.

a) Particle model	
Particle density ρ_s	2650 kg m^{-3}
Normal stiffness k_n	10^8 N m^{-1}
Shear stiffness k_s	10^8 N m^{-1}
Friction coefficient μ	0.5
Gravitational acceleration g	9.81 m s^{-2}
Particle diameter D	100; 125; 150; 600 µm
Box length; height; width	2.4; 1.8; 1.8 mm

b) Flow model	
Fluid density ρ_f	1000 kg m^{-3}
Pore pressure p	2500 Pa
Porosity n	1.0
Mobility coefficient k	100 m^2 Pa^{-1} s^{-1}
Fluid bulk modulus k_f	$2.2 \cdot 10^{-9}$ Pa
Saturation	1.0
Specific discharge q_s	0.1; 0.2; 0.3; 0.4 m s^{-1}
Model length; height; width	4.0; 3.6; 1.8 mm
Number of cells	405,000

3.2.1 Model coupling

In the particle model (Figure 3.3a), spherical particles were generated and settled under gravity into a numerical box with a size of 2.4 mm x 1.8 mm x 1.8 mm (length x height x width). The particles had properties that are similar to the glass beads and quartz grains used in the laboratory experiments (Table 3.2a). The up- and downstream boundaries of the particle model (corresponding to the in- and outflow boundaries in the flow model) were periodic, i.e. particles exiting the model on the downstream side re-entered the model on the upstream side, mimicking a recirculation flume similar to the annular flume described in 3.1. For better comparability of the data at specific sampling locations, a cubic assemblage of 4 x 3 x 3 = 36 coarse particles (D_{coarse} = 600 µm) was used in each simulation. One unimodal reference bed was created with coarse particles only. The pore space of the coarse particles was filled with fine particles of different diameters (D_{fine} = 100; 125; 150 µm) to obtain three mixed beds with a similar fine fraction and various *RD* (Figure 3.4, Table 3.3).

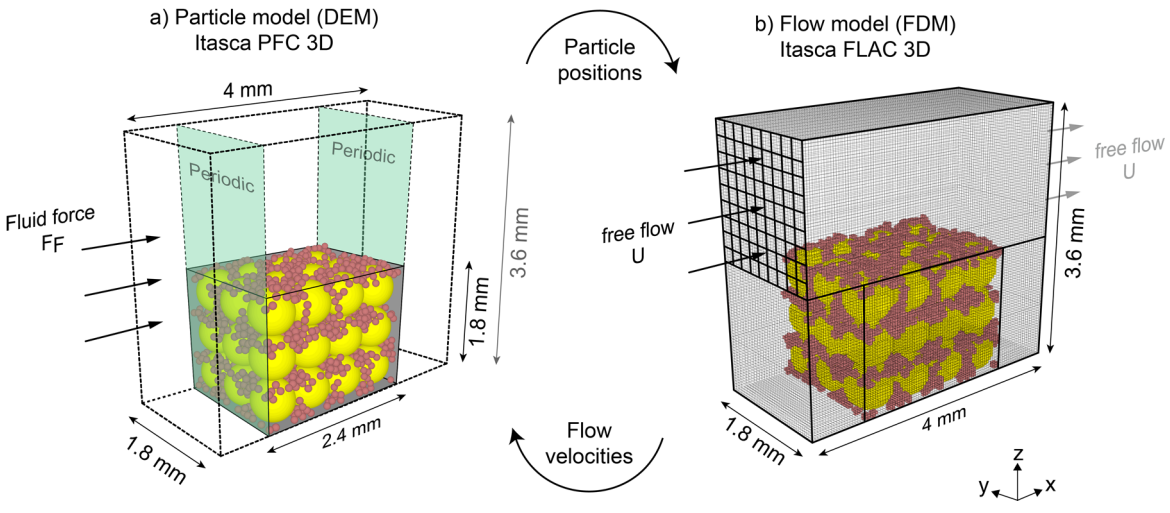

Figure 3.3: Coupled particle-flow model using the discrete element method and the finite difference method.

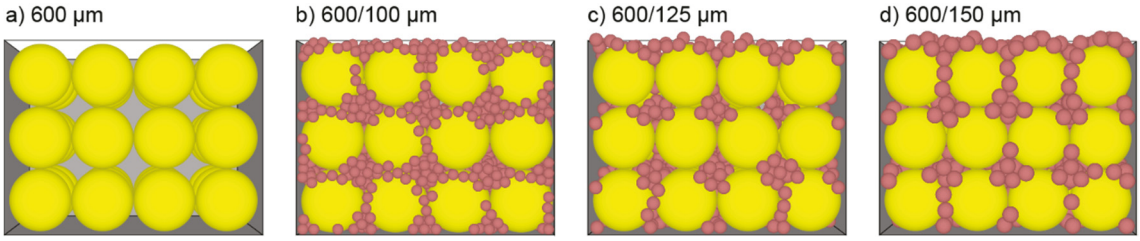

Figure 3.4: Grain-size combinations for the numerical simulations. a) Unimodal reference experiment, b) mixed bed with RD = 6, c) mixed bed with RD = 4.8, and d) mixed bed with RD = 4 (see also Table 3.3).

The coupling process was started by transferring the particle sizes and positions from the particle model to the flow model where each particle was discretized in the 3D grid. The flow model (Figure 3.3b) had a size of 4.0 x 3.6 x 1.8 mm (length x height x width) and comprised 100 x 90 x 45 = 405,000 cubic cells with an edge length of 0.04 mm each. The grid size was chosen according to the smallest particle size to ensure that every particle was represented by at least 2 x 2 x 2 cells in the flow model. Boundary effects, such as cells with irregular flow velocities (exceeding the boundary inflow velocity), can occur in the vicinity of the in- and outflow boundaries of the flow model. To minimize the influence of these boundary effects on the particle movement, and to obtain a smooth flow field above the bed, the flow model exceeded the discretized particle matrix by 0.8 mm on either side in flow direction. Using a pore pressure of 2500 N m^{-2}, a water depth of 0.25 m (i.e. similar to the laboratory flume) was simulated. A constant specific discharge (q_s = 0.10; 0.20; 0.30; 0.40 m s^{-1}) at the in- and outflow boundaries of the model was simulated, which induced a laminar flow in positive x-direction (U = 0.08; 0.15; 0.23; 0.31 m s^{-1}) above the particle matrix. The simulations were repeated with various flow velocities for every particle-size combination. One coupling circle was completed by transferring the flow velocities from each cell back to the particle model. The velocities of all the cells within a distance of 1.5 * r from the centre of each particle were averaged. To obtain the particle movement in horizontal (x- or y-) direction, the drag force resulting from the averaged horizontal flow component was applied on the according particle (see equation 2.12). The particle movement in vertical (z-) direction was calculated using Stokes' law for the movement and settling of small spheres under low Reynold's numbers:

$$F = 6\pi \cdot \mu \cdot u \cdot r \qquad [3.3]$$

where F (N) is the Stokes' drag, μ is the dynamic viscosity of the fluid (μ = 1.002 · 10^{-3} Pa s), u (m s^{-1}) is the particle's relative velocity and r (m) is the particle radius (Dey, 2014).
When a steady state in the particle model was reached, the updated particle positions were transferred to the flow model again, restarting the coupling process.

The coupling between particle and flow model was repeated for 100 cycles. While the flow model used a predefined timestep, the particle model calculated the timestep depending on the number of contacts in the model. Subsequently, the different models with various amounts of particles reached a different simulated time t at the end of the 100 steps. The data from the different models were analysed at the common simulated time of 6 ms.

The used fluid model describes a laminar flow both above and inside the discretized particle matrix (Itasca Consulting Group, 2006b), i.e. the surface of the numerical bed is assumed to be located within the laminar sublayer (Dey, 2014). The laminar flow through the particle matrix is an accurate representation of the Darcy flow inside a sediment bed. Turbulences are absent, i.e. for flow processes outside of the laminar sublayer the applied fluid model would depict a significant simplification compared to nature.

Table 3.3: Outline for numerical experiments.

Numerical particle matrix		
RD	D_{50} (µm)	% fines
unimodal	600	0
6	600/100	17.4
4.8	600/125	13.8
4	600/150	17.6

3.2.2 Data analysis

For the analysis of the micro-scale flow processes at the bed surface, the flow velocity data from every cell of the flow model was evaluated at t = 6 ms. At two sampling points located in the pore space of the coarse particle matrix, halfway through the flow model in x-direction (Figure 3.5a), two flow profiles were extracted. Each sampling volume covered 12 cells horizontally and had a vertical extent of 85 cells. The flow velocities were averaged over the two locations, yielding one flow profile for each model at each flow velocity *U* (Figure 3.5b). Due to voidage or porosity variation in the vicinity of the wall in the mixed beds (so-called wall effects which lead to the overestimation of flow velocities, e.g. Cohen, 1981), the lower five cells were excluded from the analysis.

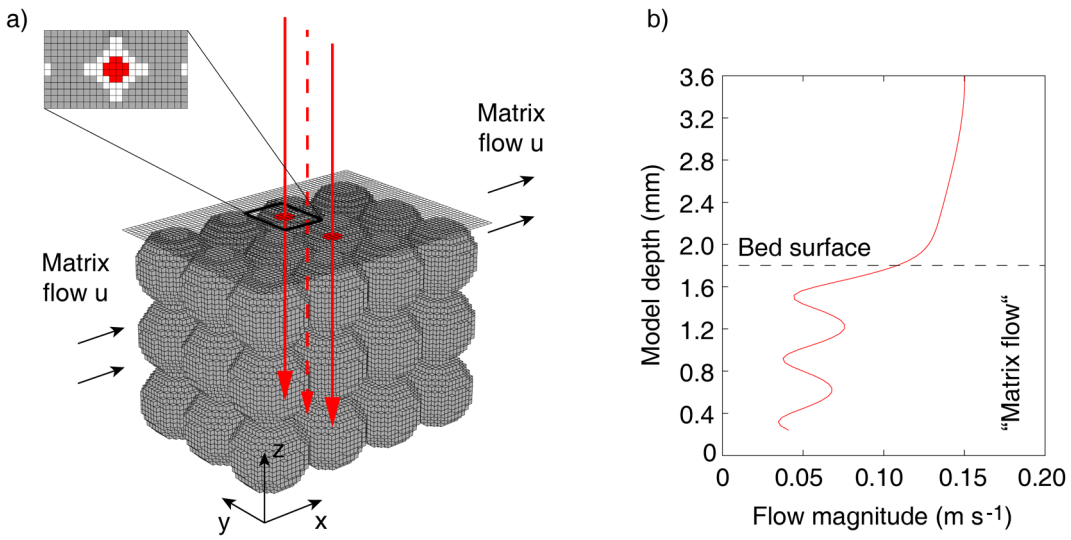

Figure 3.5: a) Sampling locations for the extraction of flow profiles, shown for the example of the unimodal model setup. Each sampling volume covers an area of 2 + 4 + 4 + 2 = 12 cells horizontally and has a vertical extent of 85 cells. The dashed arrow indicates the averaging of the two profiles. b) Flow velocity magnitude averaged over the two extracted profiles.

The streamwise flow is channelled through the pore space between the numerical particles and deflected in cross-stream and vertical direction, depending on the various grain-size distributions. To evaluate differences between the series, the flow magnitude as well as the cross-stream and vertical flow components from every simulation were investigated separately. The cross-stream and vertical flow velocities are indicators for flow deflections that occur inside the particle matrix. Figure 3.6 shows an example of the cross-stream flow component in one of the models.

To quantify and compare the *degree* of flow deflections, the spatial variance of the according cross-stream and vertical flow components over model depth z (i.e. over a vertical extent of N = 85 cells) was calculated:

$$\sigma_y^2 = \frac{1}{N-1}\sum_{i=1}^{N}\left(u_{yi} - \overline{u_y}\right)^2 \quad \text{and} \quad \sigma_z^2 = \frac{1}{N-1}\sum_{i=1}^{N}(u_{zi} - \overline{u_z})^2 \qquad [3.4]$$

where σ_y^2 and σ_z^2 (m^2 s^{-2}) are the variances of the respective y- and z-velocity components, *N* is the number of velocity measurement (*N* = 85), u_{yi} and u_{zi} (m s^{-1}) are the respective velocity components, and $\overline{u_y}$ and $\overline{u_z}$ (m s^{-1}) are the respective depth-averaged velocities.

The data of the numerical model was analysed and visualized in Itasca PFC3D 3.10, Itasca FLAC3D 3.10, and MATLAB R2013b (MathWorks, Inc., USA, 2013), and is presented in chapter 5.

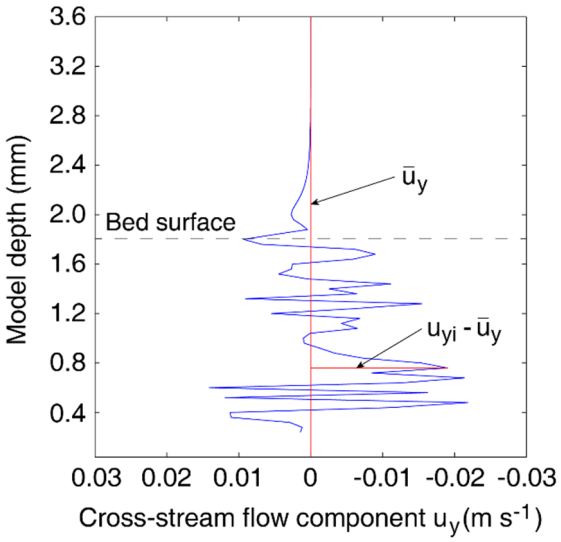

Figure 3.6: Example of the cross-stream flow component (u_y) over model depth z, and demonstration of how to determine the variance σ_y^2 (in this case) to quantify the cross-stream flow deflections inside the particle matrix. σ_y^2 is calculated using equation 3.4.

4. The role of the grain-size ratio in the mobility of mixed beds

Franziska Staudt [a], Julia C. Mullarney [b], Conrad A. Pilditch [b], Katrin Huhn [a]

[a] MARUM – Center for Marine Environmental Sciences, University of Bremen, Leobener Str., 28359 Bremen, Germany
[b] School of Science, Faculty of Science and Engineering, University of Waikato, Private Bag 3105, Hamilton 3240, New Zealand

Erosion experiments in an annular flume were conducted using different size compositions of spherical glass beads. The main goal of the study was to gain a deeper insight into texture-induced effects on sediment stability, which is a critical subject in coastal engineering. The stabilizing effect of the fine fraction in cohesive sand-mud but also in non-cohesive sand-silt mixture has been reported in many marine studies. In contrast, studies investigating river sediments and hydraulics have found a mobilizing effect of the fine fraction on a bed of a gravel-sand mixture. Theoretical models have been used to explain the mobilization of a mixed bed, but could not fully explain the stabilizing effect of non-cohesive fine material. To connect these existing findings, in a laboratory experiment we analysed the bed stability in relation to the bed texture, i.e. a) the grain-size ratio $RD = D_{50,coarse}/D_{50,fine}$ (the relative size of coarse and fine grains) and b) the fraction of fines. Several glass-bead combinations with unimodal and bimodal grain-size distributions (D_{50} = 39–367 µm) and varying fine fractions (10–40 % dry weight) were subjected to increasing flow speeds (0.01-0.19 m s^{-1}). Using acoustic Doppler velocimetry (ADV) and optical backscatter, the flow profile in the vicinity of the bed surface, the changes in bed morphology, and the suspended particulate matter concentration (*SPM*) were measured. A new method was developed to evaluate the bed-level changes detected by the ADV as a proxy for the bed mobility. We found different modes of bed mobility depending on the grain-size ratio with a transition at $RD_{cr} \approx 5$. For a grain-size ratio of $RD = 3.9$ (below the critical *RD*), an increase in the fine fraction (to 40 %) led to increased bed-level changes during the experiment and the mobilization of the mixed bed at the highest flow speed. For ratios of $RD = 5.8$ and 9.4 (above the critical *RD*), an increase in fine fraction (to 40 %) led to a decrease of bed-level changes and the beds remained stable, i.e. no bed forms developed even at the highest flow speed. Therefore, increasing the amount of fine particles can lead to contradicting behaviour depending on the grain-size ratio. For a bimodal sediment bed with spherical grains under unidirectional flow conditions, the grain-size ratio can be used to estimate the bed mobility, i.e. to evaluate if a bed is likely to mobilize at a flow speed of up to 0.19 m s^{-1}. Hence, for the stability of a non-cohesive, mixed bed in the sand-silt range, the grain-size ratio plays a fundamental role, while the amount of fine grains is a secondary factor.

Keywords: sediment erosion, texture, laboratory experiment, stability, mobility, bed morphology

4.1 Introduction

Coastal development and offshore structures have a direct impact on local sediment dynamics. In order to determine the stability of a structure in the marine environment and to minimize environmental effects, knowledge of the sediment transport processes in the surrounding area is essential. The behaviour of a single particle in a flow can easily be determined by the flow velocity, the particle size, its density, and its pivoting angle on the sediment bed (e.g. Allen, 1985; Leeder, 1982). The erosion behaviour of a unimodal sediment bed (i.e. consisting of one particle size) has been described by Shields (1936), Miller et al. (1977), McCave (1984), and many others. Numerous studies have since extended this previous work to investigate the behaviour of mixed sediment beds (i.e. comprised of different grain sizes) with the aim of evaluating the complex factors that influence the sediment stability. These are:

1) cohesion, which binds fine clay particles through electrostatic forces (e.g. Teisson et al., 1993; Mehta and Lee, 1994; Panagiotopoulos et al., 1997; Torfs et al., 2001; Le Hir et al., 2008; Jacobs et al., 2011);

2) benthic microorganisms that can secrete mucus films (EPS or extracellular polymeric substances) that act like glue binding sediment particles (e.g. Grant et al., 1986; Paterson et al., 1990; Meadows et al., 1994), and macrofauna that can disrupt the sediment matrix through bioturbation (e.g. Widdows et al., 1998b; Willows et al., 1998);

3) the complexity of grain shapes (e.g. plate- or rod-like clay particles) which affects the frictional strength of the sediment (e.g. Mair et al., 2002; Guo and Morgan, 2004; Kock and Huhn, 2007) and thus the erosion resistance; and

4) sediment texture, i.e. the interaction of different grain sizes and grain-size fractions (e.g. van Ledden et al., 2004; Le Hir et al., 2008; Bartzke et al., 2013).

Here, we focus on how the texture of mixed sediment alters the erosion behaviour. Many marine studies have described the texture-induced stabilization of a mixed sediment bed by a fine-grained fraction; a sand-mud mixture containing a certain threshold fine fraction is more stable against erosion than a sediment bed consisting of e.g. pure sand or pure mud (e.g. Mitchener & Torfs 1996; Torfs et al. 2001; Le Hir et al. 2008; Jacobs et al. 2011). Depending on the relative amounts of sand, silt or clay, the sediment network is dominated by either coarse (sand) or fine (mud with $D_{50} < 63$ µm, i.e. silt and clay) grains and the sediment behaviour changes accordingly (e.g. Mitchener and Torfs, 1996; van Ledden et al., 2004). It is understood that fine particles – even if cohesion is not important – follow a different erosion behaviour than coarser particles (e.g. Mehta and Lee, 1994; Torfs et al., 2001). Van Ledden et al. (2004) described the stabilization of a sand-mud mixture as a “network structure” of fines that acts in addition to the cohesive effects of the mud fraction. A mixed bed with a high amount of coarse material and only little fine grains behaves similar to a unimodal coarse-grained bed. If the fine-grained content exceeds a certain percentage, the fine particles form a network around the coarse grains, interrupting the intergranular contacts, and the erosion behaviour of the bed is dominated by the fine-grained fraction. Even without cohesive forces, the network structure, resulting from the size differences of the coarse and fine

grains alone, leads to increased bed stability. Also Le Hir et al. (2008) suggested that the relative size of the coarse and fine particles in a mixture could contribute to the stabilizing effect of the fine fraction. Based on these findings, Bartzke et al. (2013) conducted erosion experiments with sand (D_{50} = 300 µm) and silt (D_{50} = 55 µm) with little to no cohesion and demonstrated that with the addition of silt to sand, the hydraulic conductivity of the sediment drops, as less water can percolate through the sediment matrix. The results showed that even small amounts of silt (300 g m^{-3}) can increase the stability of a sand bed and shift the critical bed shear-stress for erosion to higher flows velocities. The authors suggested that in addition to the formation of network structures, a blocking of the water inflow into the bed contributes to the stabilization of the sediment. Besides empirical studies, several theoretical models (e.g. Mehta and Lee, 1994; Torfs et al., 2001; Mehta and Letter, 2013) have been developed to account for the increased critical shear stress required to entrain finer particles and mixtures of coarse and fine grains. Mehta and Lee (1994) concluded that in the silt range (2–63 µm) a transition from cohesive to non-cohesive behaviour occurs that could neither be fully described by cohesive nor by non-cohesive erosion models.

Studies investigating coarser, non-cohesive material (like sand and gravel) have observed the mobilization of mixed sediments induced by a fine-grained fraction. Experiments have shown that the addition of sand or fine gravel to a coarse gravel bed increases the gravel transport rate above the bed, i.e. the fine fraction facilitates erosion of the coarser sediment (e.g. Jackson and Beschta, 1984; Iseya and Ikeda, 1987; Wilcock et al., 2001; Venditti et al., 2010a, 2010b; Houssais and Lajeunesse, 2012). Jackson and Beschta (1984) observed in laboratory experiments that the addition of sand pulses to a gravel-sand bed leads to an increase in bedload transport of gravel and sand. The authors hypothesized that the sand grains in the near-bed flow facilitate further sediment entrainment (due to increased fluid density and fluid viscosity through the addition of sand to the flow). In addition, channel flow roughness decreases due to the sand filling “pools” between the gravel and due to the scouring of bed forms. Several theoretical studies have tried to incorporate different grain sizes into the erosion equation and to explain this mobilization of mixed beds. Einstein (1950) developed a model for bedload transport and introduced a “hiding” factor that affects the calculated bedload of fine material if the fines are small enough to hide behind larger grains, thus evading entrainment. Particles that are larger than the roughness length of the bed protrude into the flow and are entrained earlier than the surrounding finer material. Komar and Li (1986) described particle entrainment on a small scale, introducing both a relation between mixed particle sizes and pivoting angle, and a particle shape factor. Also Wiberg and Smith (1987) described the force balancing on a single particle on a mixed bed in relation to the ratio between grain diameter and roughness length, accounting for the reduced erosion of very fine material from a coarser bed and increased erosion of coarse material from a finer bed. Based on the model by Wiberg and Smith (1987), Wallbridge et al. (1999) conducted laboratory experiments with mixed sand beds, investigating initial grain pivoting and selective entrainment of several grain-size fractions over a duration of 5 x 1 s. The authors could confirm the model findings (Wiberg and Smith, 1987) that coarse grains protruding from the bed surface due to their size are entrained at lower flow speeds

than the surrounding finer bed material. In contrast, fine grains on a coarser bed are entrained at higher flow speeds than theoretically needed for these grain sizes because the fines hide between the coarser grains. However, these models indicate that coarse particles on a mixed bed are always entrained at flow speeds below their critical threshold and cannot be stabilized by the surrounding fine material.

In the recent decade, the advance of new measurement techniques, such as acoustic Doppler velocimetry (ADV) and particle image velocimetry (PIV), has allowed the investigation of the near-bed hydrodynamics related to sediment transport. Using these techniques it was possible to observe that the filling of pools and surface gaps on a gravel bed by fine material is accompanied by a reduction in turbulence and an acceleration in near-bed flow (e.g. Sambrook Smith and Nicholas, 2005; Venditti et al., 2010a). Venditti et al. (2010a) suggested that the accelerated near-bed flow subsequently exerts a higher drag force on the larger gravel particles that are exposed to the flow on the sediment surface, which leads to increased erosion of coarse material.

The literature has shown that the addition of a finer fraction to a unimodal bed can lead to a shift of the initiation of motion to an either higher or lower flow regime. It has been suggested that not only the size and percentage of the fine particles but the ratio between coarse and fine particle size influences the stability or mobility of the sediment bed (Le Hir et al., 2008; Venditti et al., 2010a). Some theoretical models for non-cohesive sediment transport (e.g. Einstein, 1950; Komar and Li, 1986; Wiberg and Smith, 1987) include the size relation between a grain on a mixed bed and the roughness length to account for the mobilization of the grain. For the stabilizing effects in non-cohesive beds, i.e. the formation of network structures, the relative size of the fines has not been investigated so far, and theoretical models could not fully explain the transition between the stabilizing and mobilizing behaviour of mixed beds (Mehta and Lee, 1994; Torfs et al., 2001).

Our study investigates the effects of texture on the erosion behaviour of mixed beds and the near-bed hydrodynamics that are associated with it. As experimental studies have investigated either the mobilizing or the stabilizing effect of the fine fraction, we try to find a transition between the different modes of behaviour. The mobility of artificial, non-cohesive sediments was studied using an annular flume. To exclude cohesive forces, bioactivity and grain complexity as possible stabilizing factors and to focus on the effects of grain-size interactions on the bed mobility, we used spherical glass beads instead of natural sediment. One bed with a unimodal grain-size distribution and three mixed beds with bimodal grain-size distributions were used. In the mixed experiments we varied the grain size of the fines as well as the amount of fines. We could thereby investigate the influence of a) the "grain-size ratio" $RD = D_{50\ coarse}/D_{50\ fine}$ and b) the abundance of fine particles on the bed mobility. The erosion behaviour and the near-bed flow field were analysed with respect to the different glass-bead combinations at increasing flow velocities in the flume. We assessed the flow velocities above and at the bed surface as well as changes in water column turbidity and bed topography. In addition, the hydraulic conductivity of all treatments was determined to evaluate the potential for water inflow. The paper presents the next step towards a comprehensive perspective on the textural factors influencing sediment mobility.

4.2 Material and methods

Glass beads (Sigmund Lindner GmbH, Germany) made of soda-lime glass (ρ = 2500 kg m^{-3}) were used for the erosion experiments. Industrial glass beads are very well sorted, with known grain sizes and a high sphericity (≥ 0.89). The particle surface is very smooth and owing to the high sphericity, the contact area between the particles is minimized, resulting in a low intergranular friction. In contrast to natural sediment which contains irregular, complex grain shapes and sizes, the usage of well sorted, spherical glass beads allows the accurate determination of the grain-size ratio, improving the reproducibility of the experiments and providing control not achievable with natural material. The coarse fraction used in the experiments had a median grain size D_{50} = 367 µm (comparable to medium sand). The D_{50} for the three fine fractions were 39, 63 and 93 µm (comparable to coarse silt to very fine sand) which were mixed with the coarse fraction to produce bimodal grain-size distributions. Natural sediment of similar grain sizes has little to no cohesion (e.g. Mehta and Lee, 1994; Whitehouse et al., 2000) and can be found in high-energy near-shore, beach or river environments. Erosion experiments were conducted with just a unimodal grain-size distribution of the coarse fraction (RD_0) and three different glass-bead combinations with a bimodal grain-size distribution ($RD_{9.4}$, $RD_{5.8}$, $RD_{3.9}$, see Table 4.1). The bimodal setups were tested with small (S, approx. 10 % dry weight), medium (M, approx. 20 %), and large (L, approx. 40 %) fine fractions. *RD* for the mixed experiments varies according to the different grain sizes of the fine fractions (Table 4.1). To evaluate the passage of water through our glass-bead mixtures, the hydraulic conductivity *k* of all combinations was determined using a constant-head permeameter (Kresic, 2006). A saturated sample (*L* = 10 cm, *D* = 5.5 cm) of each treatment was filled into a plexiglas pipe and allowed to settle for 15 h. The lower opening of the pipe was closed with a textile mesh to keep the sediment in place but allow water percolation. To measure *k*, the height of the water level above the sample was kept constant (using a pump) while the water percolating through the sample was collected in a container underneath. The hydraulic conductivity was estimated by $k = (V \cdot L)/(A \cdot h \cdot t)$, where *V* is the volume of the percolated water in the time *t*, *L* is the height of the sample, *A* is the cross-sectional area of the pipe and *h* is the height of the water level above the sample.

An annular flume similar to the one developed by Widdows et al. (1998b) was used for the erosion experiments. The annular flume consisted of an outer cylinder with a width of 63 cm and an inner cylinder with a width of 43 cm on a base plate, forming a circular flow channel of 10 cm width. A motor-driven rotating lid with a diameter of 53 cm was placed on top of the flume. Using a water level of 25 cm, the flume lid was submerged in the water at a depth of 3 cm. As the lid started rotating, the friction between lid and water induced a current in the flume. The relation between the lid rotational speed and flow velocity can be described by $U \mathrel{\widehat{=}} \omega \cdot 0.0032 - 0.0066$ where *U* (m s^{-1}) is the flow velocity 3 cm above the bed and ω (rpm) is the rotational speed of the lid. For the erosion experiments, the rotating lid was accelerated from 5 rpm ($\mathrel{\widehat{=}}$ *U* = 0.0094 m s^{-1}) to 60 rpm ($\mathrel{\widehat{=}}$ 0.1854 m s^{-1}) in 5 rpm increments every 15 min. Each velocity increment was left to run for 15 min to ensure the development of an equilibrium between flow and particle transport. The circular

shape of the flume may lead to the development of a (minor) secondary flow, however, in a channel of 10 cm width this is minimal compared to in wider annular flumes (Widdows et al., 1998b). Flow profiles over a vertical extent of 35 mm were recorded at a sampling rate of 50 Hz using a profiling ADV (10 MHz Vectrino Profiler, Nortek AS, Norway) which was positioned at a height of approximately 70 mm above the bed. The distance between the ADV and the bed, the so-called bottom distance, was sampled at a rate of 10 Hz. The latter was used to derive changes of the bottom level as an indicator for bed mobility (see 4.2.1 below). Suspended sediment concentrations were measured using an optical backscatter sensor (Seapoint Turbidity Meter, Seapoint Sensors, Inc., USA) with a sampling rate of 1 Hz at a height of 75 mm above the bed.

The saturated glass-bead mixture filled the flume to a height of 5 cm above the base and was flattened with a spatula. In order to prevent disturbance during filling, the bed was covered with bubble wrap before fresh water was added to a height of 25 cm above the base. To reduce irregularities between experiments, the bed was prepared by the same person for all experimental runs. The material in the flume was left to settle under no-flow conditions for 15 h. The water temperature during the experiments ranged between 16 °C and 21 °C. Water samples were taken in 30 min intervals during each experiment for the calibration of the turbidity meter: The samples were taken with a syringe at a height of 75 mm above the bed surface in the centre of the flow channel and filtered through pre-weighed glass microfiber filters (Whatman GF/C 47 mm, GE Healthcare, UK) using a vacuum pump. The filters were oven-dried at 105 °C for 15 h and weighed. The suspended particulate matter (*SPM*) concentration was determined from the mass of particles trapped on the filter. For each experiment, a linear fit (average R^2 = 0.78, with values ranging from 0.63 to 0.98 between runs) was used to obtain the relationship between turbidity and *SPM*. At the completion of each experiment, a grab sample of the bed was taken to determine the exact fine-grained content using sieve analysis. Major changes in the bed morphology were assessed visually, i.e. the presence or absence of bed forms. The reference experiment (RD_0) was replicated three times. For the mixed series $RD_{9.4}$ one out of three experiments was replicated, while for $RD_{3.9}$ two out of three experiments were replicated. In this study we present one data set from each of the experiments because there were no substantial differences between replicated runs (Table 4.1).

4.2.1 Data analysis

We combined *SPM* variations, changes in bottom level, and observations of bed morphology as criteria for the investigation of the bed mobility. The glass beads used in this experiment were transported as bedload as well as in suspension. The suspended material was measured using optical backscatter. However, given the confined flume dimensions, no sediment samplers or traps could be applied to measure the bedload transport. In addition, removing sediment would change the flume environment and diminish the advantage of the annular flume (uninterrupted sediment transport). Therefore, a non-intrusive approach using the ADV was chosen to evaluate changes of the bed level as a proxy for the “mobility” of the bed.

We identified two boundaries at the bed distinguished acoustically by the profiling ADV: 1. the upper boundary which is the location of the bed surface or bed-fluid interface and 2. the lower boundary which represents the “bottom”, as detected by the ADV:

1. The bed-fluid interface is located at the depth with the maximum change in acoustic backscatter ($\partial BS/\partial z$ = max), i.e. where a distinct boundary between the water column (low backscatter) and the bed (high backscatter) is visible. It represents the boundary between glass beads and water column, i.e. the level where flow from the water column enters the matrix of glass beads. As this boundary is derived from the flow velocity data, it is similarly sampled at 50 Hz. For each velocity interval in our experiment, the bed surface level was averaged over the last 10 min. In the results and figures, z = 0 indicates the location of this bed surface.

2. The lower boundary represents the “bottom”, as sampled by the ADV (at 10 Hz), which is located at the depth with the strongest acoustic backscatter (BS = max). The location of the strongest acoustic signal coincides with the maximum particle concentration (which is directly related to the bulk density) within the bottom-measurement range of the ADV. In our experiment, this layer lies 2–3 mm below the bed surface (i.e. at z = -2 to -3). From the bottom distance between the instrument’s central transducer and the bottom, we calculated the variance σ_b^2 according to the following procedure to provide a quantitative measure for the changes of the bottom level.
For each interval with constant flow speed, equation 4.1 was used to calculate the bottom variance over the time span of Δt = 900 s (i.e. N = 9000), i.e. the variance of the bottom level from the mean bottom distance during the interval:

$$\sigma_{b,int}^2 = \frac{1}{N-1}\sum_{i=1}^{N}(d_{bi} - \overline{d_b})^2 \qquad [4.1]$$

where $\sigma_{b,int}^2$ (m^2) is the bottom variance of the flow speed interval, N (-) is the number of measurements, d_{bi} (m) is the bottom distance and $\overline{d_b}$ (m) is the mean bottom distance averaged over the duration of the interval. The variance of each flow speed interval was then normalized, dividing it by the average flow speed U of the respective interval and the duration of the interval (Δt). Finally, the normalized mobility was averaged over all flow speed intervals:

$$\sigma_{b,norm}^2 = \frac{1}{n_{Int}}\sum\frac{\sigma_{b,int}^2}{U \cdot \Delta t} \qquad [4.2]$$

where $\sigma_{b,norm}^2$ (m) is the normalized bottom variance, n_{Int} (-) is the number of intervals with constant flow velocity, $\sigma_{b,int}^2$ (m^2) is the bottom variance calculated over one flow speed interval, U (m s^{-1}) is the flow velocity in the respective interval, and Δt (s) is the duration of the interval. The obtained value $\sigma_{b,norm}^2$ is independent of the prevailing flow velocity and the duration of the measurement, thus allowing comparison with experiments that follow a different experimental procedure.
The bottom variance is an indicator for the mobility of the bed, i.e. a proxy for the bed movement underneath the ADV. It has to be noted that the “mobility” as determined using this method does

not correspond to the bedload in terms of a quantitative transport rate and that no calibration was conducted.

The turbidity data was used to derive a time series of *SPM* concentration. The data was filtered using a running median and averaged over the last 10 min of each velocity interval. In the reference experiment, the initial increase in *SPM* depicts the onset of entrainment of the coarse particles. The flow velocity at this time of *SPM* increase is the critical flow velocity $U_{cr,failure}$ for the erosion of coarse particles. In the mixed experiments, a slow rise in *SPM* depicts particle entrainment and subsequent transport in suspension of mostly fine particles. For these experiments, the flow velocity at the time of the initial increase in *SPM* is defined as the critical flow velocity $U_{cr,fine}$ for the entrainment of fine particles. An abrupt increase in *SPM* depicts the sudden entrainment of a large amount of particles (coarse and fine) into the flow. In our experiments, this rise in *SPM* coincided with the development of bed forms, i.e. the failure of the bed. After the examination of *SPM* along with particle movement and changes in bed morphology, a critical concentration of SPM_{cr} = 8 mg l^{-1} was found to be a suitable indicator of bed failure in the mixed experiments. The flow velocity at the time of bed-form development and the increase in *SPM* > 8 mg l^{-1} is therefore defined as the critical flow velocity $U_{cr,failure}$ for bed failure.

4.2.1.1 Hydrodynamics

To be able to determine turbulence from the 3D velocity data of an ADV, noise has to be eliminated (Chanson et al., 2008). ADV data was despiked using the phase-space thresholding method (Goring and Nikora, 2002) and poor quality data (beam correlations < 60 % and signal-to-noise ratios < 12) was discarded. In addition, so-called weak spots of very low flow velocities resulting from the acoustic signal echoing off the narrow flume boundaries were identified and removed before the data analyses (Chanson et al., 2008). The velocity data from the last 10 min of each 15 min interval was time-averaged to give a single profile for each flow increment. We used z = 5 mm as a reference height for comparison of the horizontal velocity u_{xy5} at a flow speed of U = 0.17 m s^{-1}, i.e. shortly before failure of (most) unstable beds. The bed shear-stress was calculated from the averaged velocity data from the boundary layer using the turbulent kinetic energy (*TKE*) approach (Kim et al., 2000):

$$TKE = \frac{1}{2}\rho \cdot \left(\overline{u_x{}'^2} + \overline{u_y{}'^2} + \overline{u_z{}'^2}\right) \quad [4.3]$$

$$\tau_0 = C_1 \cdot TKE \quad [4.4]$$

where *TKE* (N m^{-2}) is the turbulent kinetic energy, ρ (kg m^{-3}) is the water density, u_x', u_y' and u_z' (m s^{-1}) are the flow velocity fluctuations in stream-wise, cross-stream and vertical directions, respectively, and τ_0 (N m^{-2}) is the bed shear-stress. The bed shear-stress is related to *TKE* through a constant C_1 = 0.19 (Soulsby, 1983).

4.3 Results

4.3.1 Hydraulic conductivity and bed shear-stress

For the mixed experiments $RD_{9.4}$ (367/39 µm), $RD_{5.8}$ (367/63 µm) and $RD_{3.9}$ (367/93 µm), the hydraulic conductivity *k* was generally lower than in the reference experiment RD_0 (367 µm) and decreased exponentially with increasing fine-grained content (Figure 4.1, Table 4.1). Under a quadrupling of the fine fraction (≈ 10 to 40 %), the strongest decline in hydraulic conductivity occurred with the largest grain-size ratio ($RD_{9.4}$), while the weakest decline was observed with the smallest grain-size ratio ($RD_{3.9}$). At a low fine content (≈ 10 %), *k* varied from $k = 0.063$ cm s^{-1} at the large *RD* to $k = 0.045$ cm s^{-1} at the smallest *RD*. With increasing fine content, the values for *k* of the different glass-bead combinations converged.

The bed shear-stress τ_0 in all treatments was similar at low flow velocities and increased exponentially with rising flow velocity (Figure 4.2). Starting at $U = 0.09$ m s^{-1}, τ_0 in the experiment with a high *RD* and a medium fine content ($RD_{9.4,M}$), exceeded the average shear stress by up to 65 % (at $U \approx 0.14$–0.15 m s^{-1}). In the three experiments with low *RD* ($RD_{3.9,S\text{-}L,}$), τ_0 began to deviate from the exponential curve at a flow velocity of $U \approx 0.05$ m s^{-1}, exceeding the average shear stress by up to 100 % (e.g. $RD_{3.9,M}$ at $U \approx 0.07$ m s^{-1}). With increasing flow velocity, the variance in τ_0 between experiments increased, reaching a maximum at the highest flow speed ($U = 0.19$ m s^{-1}). In runs $RD_{9.4,M}$, $RD_{9.4,L}$, $RD_{5.8,M}$, and $RD_{3.9,L}$, the bed shear-stress decreased in the last flow speed interval.

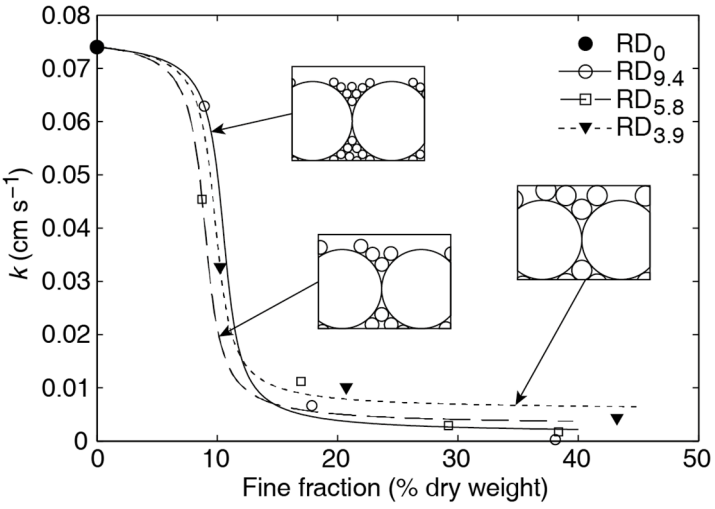

Figure 4.1: Hydraulic conductivity (k) as a function of increasing fine fraction in the different glass-bead combinations (fitted with an arctangent fit): Reference bed RD_0 with coarse particles only (D_{50} = 367 µm), mixed bed $RD_{9.4}$ with large grain-size ratio RD = 9.4 (D_{50} = 367/39 µm), mixed bed $RD_{5.8}$ with medium grain-size ratio RD = 5.8 (D_{50} = 367/63 µm) and mixed bed $RD_{3.9}$ with low grain-size ratio RD = 3.9 (D_{50} = 367/93 µm). Insets show the relative coarse and fine grain sizes (RD to scale).

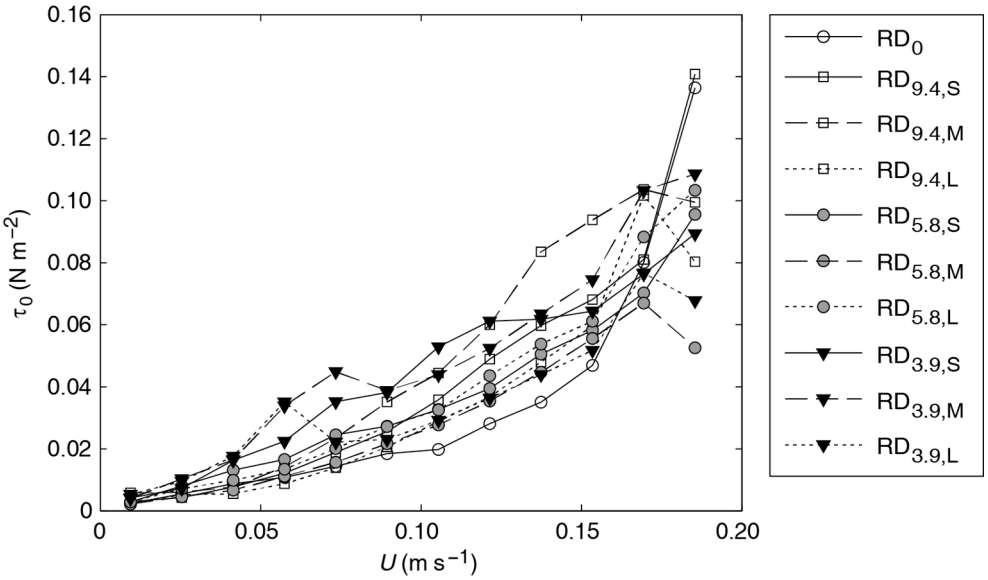

Figure 4.2: Development of bed shear-stresses (τ_0) with increasing flow velocity U for the different glass-bead treatments. The indices S, M and L refer to the different treatments with small (≈ 10 % dry weight), medium (≈ 20 %), and large (≈ 40 %) fine-grained fraction. See Table 4.1 for further information on the different treatments.

4.3.2 Bed mobility

In the unimodal reference experiment RD_0, *SPM* increased slightly starting at $U_{cr,failure}$ = 0.06 m s^{-1} (Figure 4.3a) and bed forms started developing throughout the flume. The normalized bottom variance of RD_0 serves as the reference for the mobility of the mixed beds (solid horizontal line in Figure 4.4). The beds with the largest grain-size ratio ($RD_{9.4}$) were less mobile than RD_0 and mobility decreased with an increase of the fine content from 10 to 20 %. Although the mobility slightly grew with an increase in fine content to 40 %, $U_{cr,failure}$ further increased (Figure 4.4, Table 4.1). In the experiments with small and medium fine content ($RD_{9.4,S}$ and $RD_{9.4,M}$), fine material was entrained and kept in suspension at low flow velocities (Figure 4.3b). Large amounts of bed material eroded during the last two flow speed intervals (U = 0.17–0.19 m s^{-1}), indicated by a high *SPM* (Figure 4.3b), and the bed failed, indicated by the development of bed forms. The bed mobility in $RD_{9.4,S}$ was about 1/3 of the bed mobility observed in RD_0, indicating less changes of the bed level (Figure 4.4, Table 4.1). With a medium fine content ($RD_{9.4,M}$), the bed mobility was reduced to a minimum, but the development of bed forms could still be observed. In the treatment with a high fine content ($RD_{9.4,L}$), fine material was entrained at a slightly higher erosion threshold (+ 0.04 m s^{-1}) for fine grains than for the lower fine fractions ($RD_{9.4,S}$ and $RD_{9.4,M}$). The increase in *SPM* is very low and only slightly visible in Figure 4.3b. The normalized bottom variance is marginally higher than in $RD_{9.4,M}$ (Figure 4.4, Table 4.1); however, no considerable change in bottom morphology and no bed-form development occurred. In summary, the beds with a high *RD* but a low fine content (< 40 %) developed bed forms at high flow speeds, while the bed with a high *RD* and a high fine content (~ 40 %) maintained a smooth surface even at the highest flow speed of U = 0.19 m s^{-1}. In comparison to the uniform reference bed, the mobility of all $RD_{9.4}$ beds was lower and entrainment of coarse material and the subsequent bed failure in $RD_{9.4}$ occurred at higher flow speeds.

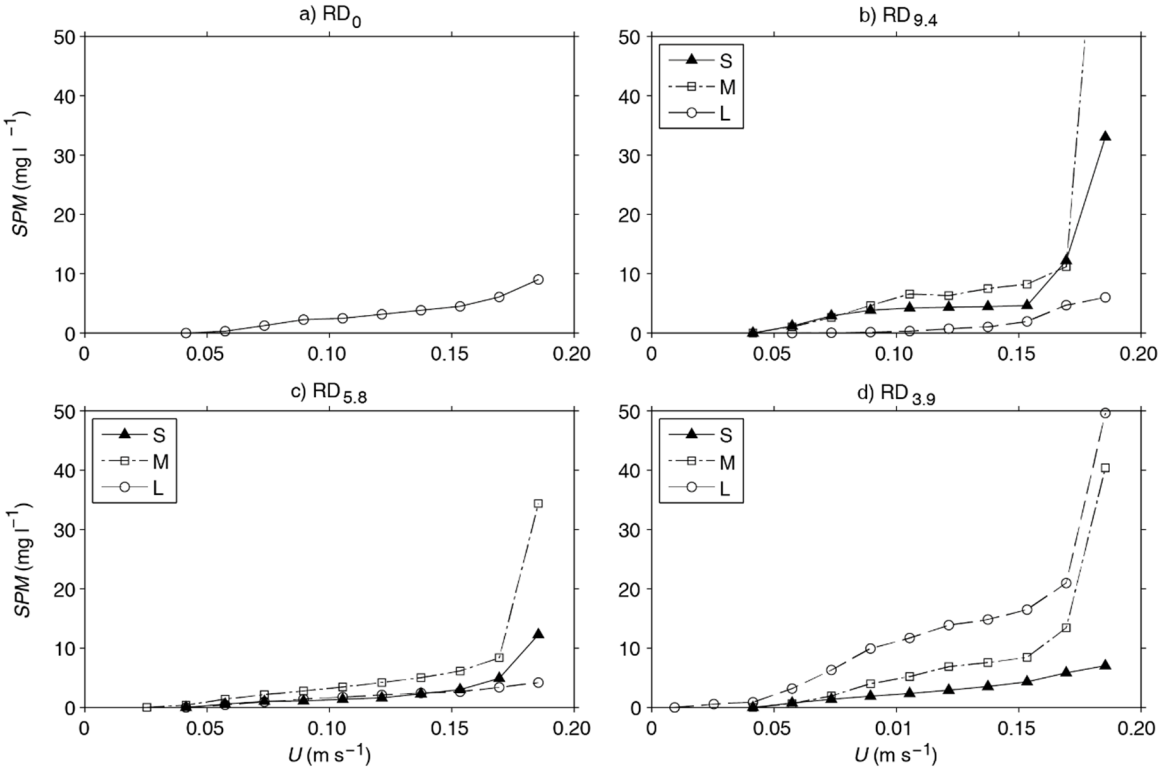

Figure 4.3: Changes in suspended particulate matter (SPM) concentration with increasing flow velocity U: a) Unimodal reference bed RD_0, b) mixed bed $RD_{9.4}$, c) mixed bed $RD_{5.8}$, d) mixed bed $RD_{3.9}$. S, M and L in the panels of the mixed experiment (b, c, d) refer to the different treatments with small (≈ 10 %), medium (≈ 20 %) and large (≈ 40 %) fine-grained fraction. See Table 4.1 for the different grain sizes.

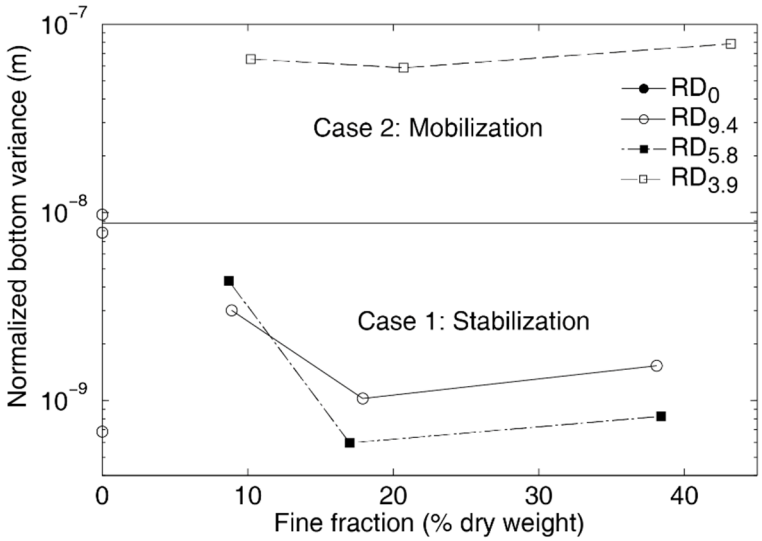

Figure 4.4: Normalized bottom variance (logarithmic scale), as a proxy for bed mobility, with varying grain-size ratio RD and fine fraction. The mobility of the unimodal treatment RD_0 (solid horizontal line) serves as the reference for the mobility of the mixed beds $RD_{9.4}$, $RD_{5.8}$ and $RD_{3.9}$.

As in $RD_{9.4}$, the bed with a medium *RD* = 5.8 generally had a lower mobility than the unimodal bed and became more stable with an increase in fine content from 10 to 20 % (Figure 4.4, Table 4.1), indicated also by an increase in $U_{cr,failure}$ (Figure 4.3c, Table 4.1). Beds $RD_{5.8,S}$ and $RD_{5.8,M}$ with a small and medium fine fraction developed bed forms and experienced a rise in *SPM* at the end of

the experiment (Figure 4.3c). Although $RD_{5.8,S}$ had a lower hydraulic conductivity than the comparable $RD_{9.4,S}$ (Figure 4.1), the bed in this experiment was slightly more mobile (Figure 4.4, Table 4.1). The bed with a large fine fraction ($RD_{5.8,L}$) remained comparably stable during the experiment, no bed forms developed at high flow velocities, although the mobility increased marginally compared to $RD_{5.8,M}$. During the first half of the experiment, the *SPM* concentration was similar to $RD_{5.8,S,}$ but unlike in the scenario with smaller fine fraction, *SPM* did not rise above the critical value at the end of the experiment (Figure 4.3c). As in the runs with large grain-size ratio ($RD_{9.4}$), the beds with a medium grain-size ratio and a low to medium fine content (< 40 %) developed bed forms with increasing flow speed whereas the bed with a large fine fraction (~ 40 %) maintained a smooth surface.

In contrast to $RD_{9.4}$ and $RD_{5.8}$, the beds with a low *RD* (3.9) became more mobile with an increasing fine content. The mobility of the beds is about one magnitude higher than the mobility of the unimodal reference bed. Fine material was entrained at lower flow velocities than in the previous experiments. However, as in the other mixed grain experiments, bed failure and bed-form development occurred at higher flow speeds than in the reference case RD_0 (Figure 4.3d). In the experiment with a small fine fraction ($RD_{3.9,S}$), *SPM* did not exceed the critical value of 8 mg l^{-1} at high flow velocities (Figure 4.3d), still the mobility was more than seven times higher than in the reference experiment RD_0 and about one magnitude higher than in $RD_{9.4}$ and $RD_{5.8}$ (Figure 4.4, Table 4.1). This result indicates the high mobility of $RD_{3.9,S}$ compared to the previous experiments, which is underlined by bed-form development. In the experiments with medium and high fine content ($RD_{3.9,M}$, $RD_{3.9,L}$), *SPM* increased at U = 0.06 m s^{-1} and 0.03 m s^{-1}, respectively, and levelled out until at high flow velocities a clear increase in *SPM* is visible (Figure 4.3d), indicating transport in suspension. The mobility decreased slightly with a rise in fine content to 20 %, then increased further (Figure 4.4, Table 4.1). In $RD_{3.9,L}$ the mobility depicted changes in bottom level about one magnitude higher than in the uniform sediment case RD_0.

4.3.3 Flow behaviour

The flow profile recorded above the reference bed (RD_0) was approximately logarithmic with a boundary layer of ≈ 30 mm height (Figure 4.5). In contrast to the reference experiment RD_0, the flow profiles above the mixed beds with low fine content ($RD_{9.4,S}$, $RD_{5.8,S}$ and $RD_{3.9,S}$) do not show a logarithmic shape (Figure 4.5a). In $RD_{9.4,S}$ and $RD_{3.9,S}$ the horizontal flow velocity is nearly uniform above z = 3 mm and decreases sharply closer to the bed surface. In these experiments, the flow velocities at the reference height (z = 5 mm) were faster than in RD_0 (Figure 4.5, Table 4.1), demonstrating that the near-bed flow was accelerated, and the boundary layer was confined to ≈ 3 mm. The flow profile of $RD_{5.8,S}$ shows faster near-bed flow velocities than the reference experiment, however the velocities are slightly lower than in the other mixed experiments $RD_{9.4,S}$ and $RD_{3.9,S}$ (Figure 4.5a, Table 4.1). In the experiments $RD_{9.4,M}$ and $RD_{3.9,M}$ with medium fine content, a similar near-bed flow acceleration could be observed (Figure 4.5b, Table 4.1). The profile of $RD_{5.8,M}$ is incomplete due to poor data quality above the bed (z = 2–14 mm), however, it is still

apparent that the flow at the bed surface was still slightly higher than the flow in the reference experiment RD_0. In the experiments $RD_{3.9,L}$ and $RD_{9.4,L}$ with high fine content, the near-bed flow velocities were highest (Figure 4.5c, Table 4.1). Both profiles show a confined boundary layer and a near-bed flow that was significantly accelerated in comparison to RD_0. The flow profile of $RD_{5.8,L}$ shows higher near-bed velocities than in RD_0, however lower than in the other mixed experiments with high fine content. It has to be noted that, similar to $RD_{5.8,M}$, a weak layer affects the near-bed flow measurements in $RD_{5.9,L}$ (Figure 4.5b and c).

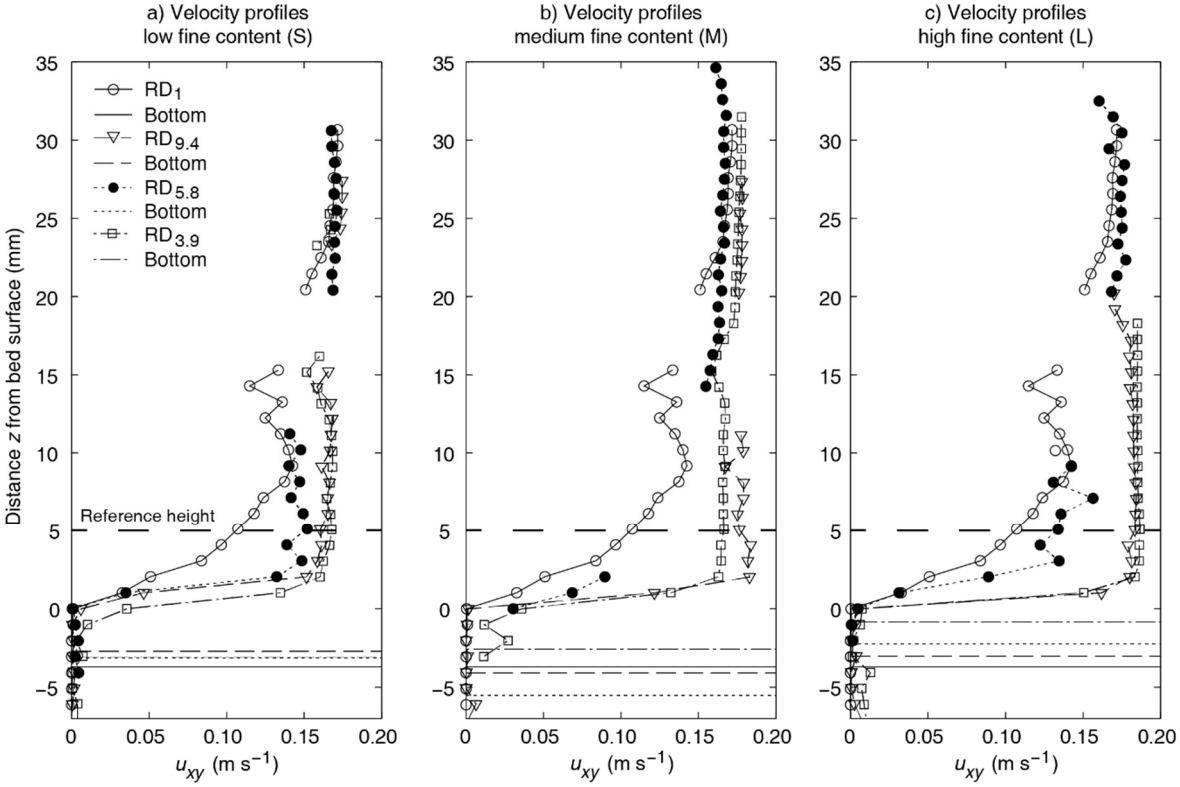

Figure 4.5: Flow profiles from all experiments at flow velocity U = 0.17 m s^{-1}. z = 0 indicates the bed surface or bed-water interface. The horizontal lines at z < 0 indicate the "bottom" detected by the profiling ADV in each experiment (see 4.2.1 for details). At the reference height z = 5 mm the velocity u_{xy5} is measured. Note the gaps in the profiles where data was excluded due to poor quality.

To reveal major differences between the hydrodynamics of the stable and unstable (under the applied flow conditions) combinations, we investigated the changes in near-bed flow profiles of the two end members, $RD_{9.4,L}$ and $RD_{3.9,L}$, in more detail (Figure 4.6). In $RD_{9.4,L}$ (Figure 4.6a) the highest occurring horizontal flow velocity at the bed surface did not exceed $u_{xy(z=0)}$ = 0.006 m s^{-1}. The velocity decreased abruptly at the bed surface and remained below 0.005 m s^{-1} in the upper few mm of the bed, indicating that the bed surface, consisting of coarse and very fine glass beads, is densely packed and the flow cannot enter the bed. In $RD_{3.9,L}$ (Figure 4.6b) the maximum horizontal flow velocity at the bed surface was $u_{xy(z=0)}$ = 0.03 m s^{-1}, i.e. five times higher than in $RD_{9.4,L}$. The flow velocity at the bed surface decreased gradually, i.e. less abruptly than in $RD_{9.4,L}$. This profile indicates that the flow is able to enter the upper layers of the bed, i.e. the surface pockets in between the glass beads.

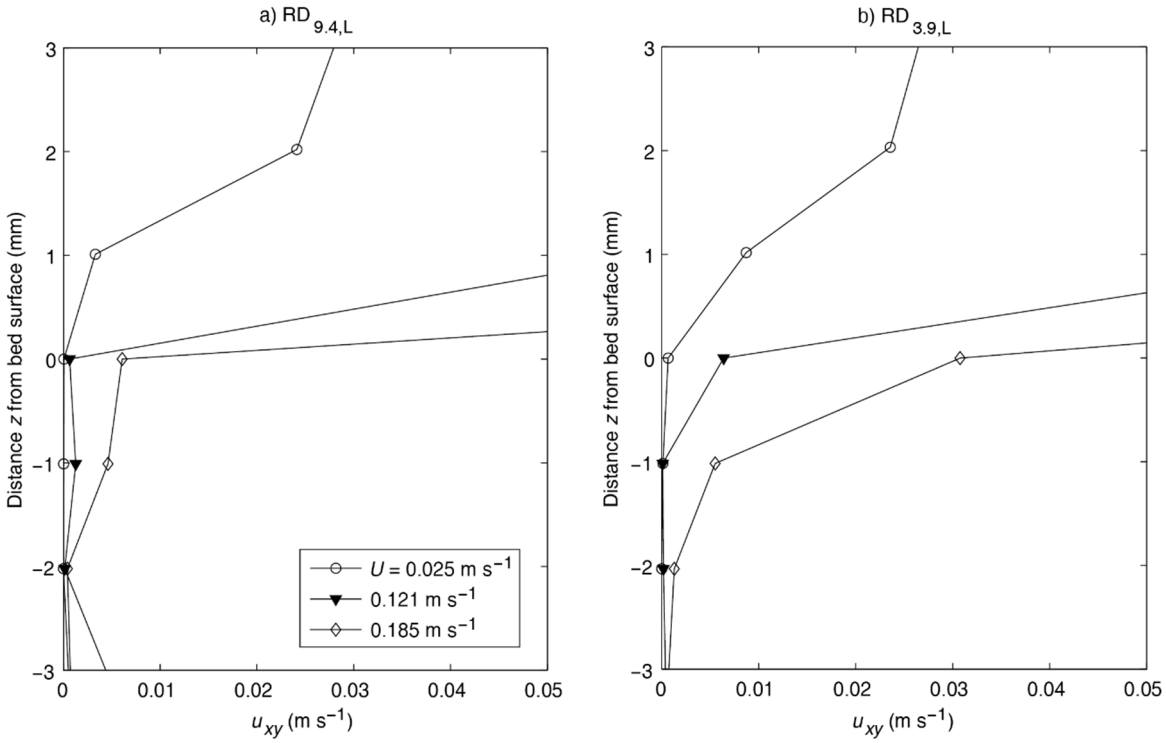

Figure 4.6: Detail of horizontal flow velocities at the bed surface of the two end members a) high grain-size ratio $RD_{9.4,L}$ (367/39 µm) with large fine-grained fraction and a low mobility of $\sigma^2_{b,norm}$ = 1.5 · 10^{-9} m and b) low grain-size ratio $RD_{3.9,L}$ (367/93 µm) with large fine-grained fraction and a high mobility of $\sigma^2_{b,norm}$ = 7.9 · 10^{-8} m. The profiles at low (U = 0.025 m s^{-1}), moderate (U = 0.121 m s^{-1}) and high (U = 0.185 m s^{-1}) free flows are shown.

4.4 Discussion

4.4.1 Bed mobility

From the results, it is apparent that the beds with medium and high grain-size ratios ($RD_{9.4}$ and $RD_{5.8}$) behave differently than the one with the lowest grain-size ratio ($RD_{3.9}$). The mobility of the different beds can be classified in two cases (Table 4.1, Figure 4.4, and Figure 4.7). In case 1, which covers $RD_{9.4}$ and $RD_{5.8}$, all beds (regardless of the amount of fines) were less mobile than the reference bed RD_0. Furthermore, the addition of fine material reduced particle movement at the bed surface and decreased the mobility of the bed (even though a slight increase is visible at a fine content of 40 %). While the beds with small and medium fine fractions ($RD_{9.4,S}$, $RD_{9.4,M}$, $RD_{5.8,S}$ and $RD_{5.8,M}$) still developed bed forms at high flow velocities, the beds with large fine fractions ($RD_{9.4,L}$, $RD_{5.8,L}$) remained flat. $RD_{5.8,L}$ with a fine-grained content of 38.4 % proved to be the most stable of all grain-size combinations used in this study with a very low normalized bottom variance of $\sigma^2_{b,norm}$ = 6.0 · 10^{-10} m. In case 2, which covers the $RD_{3.9}$-series with a low grain-size ratio, the bed was considerably more mobile than in RD_0, $RD_{9.4}$ and $RD_{5.8}$. Increasing the fine fraction in $RD_{3.9}$ from ≈ 10 % to ≈ 40 % led to increased changes of the bed level, i.e. mobilization of the bed. The bed failed and bed forms developed in all three scenarios, $RD_{3.9,S}$, $RD_{3.9,M}$ and $RD_{3.9,L}$. The most

mobile setup was $RD_{3.9,L}$ with a fine fraction of 43.2 % and a normalized bottom variance of $\sigma^2_{b,norm} = 7.9 \cdot 10^{-8}$ m.

The results demonstrate that the mobility of a mixed bed changes with the grain-size ratio and the amount of fines (Figure 4.7). Even at low fine contents (≈ 10 %), the beds with high *RD* experienced less bed-level changes than the reference bed, whereas the bed with the low *RD* experienced more changes (Figure 4.4). However, all beds became unstable, i.e. bed forms developed under the prevailing unidirectional flow conditions ($U \leq 0.19$ m s^{-1}). At higher fine contents (≥ 10 %), the effect of *RD* on the bed mobility is amplified (Figure 4.7): The increasing fine content can lead to opposing modes of erosion behaviour, i.e. a relative stabilization (high *RD*) or mobilization (low *RD*). Hence, the relative sizes of the coarse and fine grains govern the bed behaviour with an increase in fine content. The threshold grain-size ratio for glass beads was found between *RD* = 3.9 and *RD* = 5.8 (i.e. $RD_{cr} \approx 5$), where a transition in bed mobility occurred.

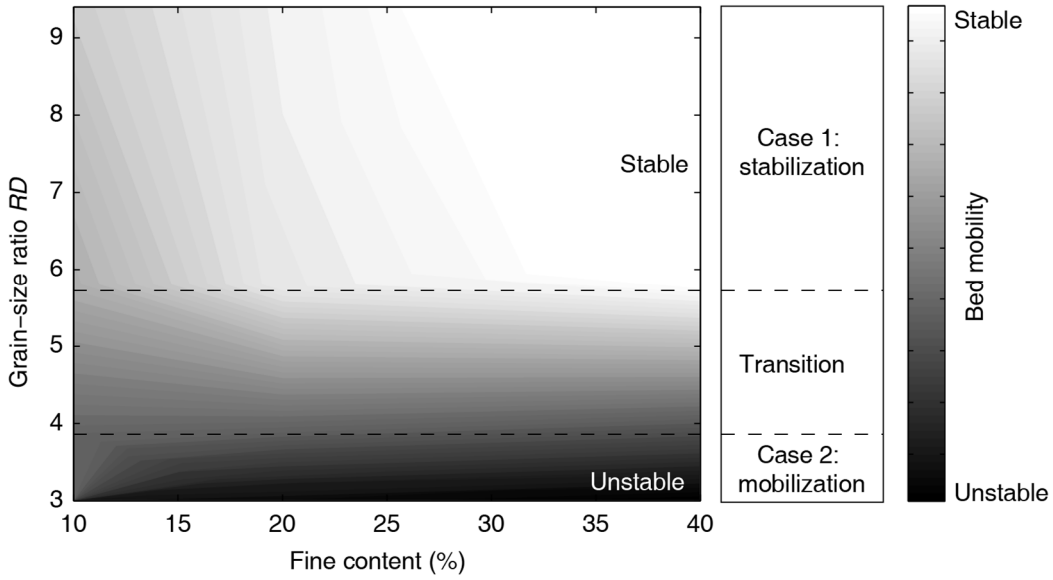

Figure 4.7: Bed mobility with varying grain-size ratio RD and fine fraction, at flow conditions $U \leq 0.19$ m s^{-1}. Bed with RD ≤ 3.9 become more mobile with increasing fine content, whereas beds with RD ≥ 5.8 become more stable. The transition between these two cases occurs at RD = 3.9–5.8.

4.4.2 Hydrodynamics

We postulate that the different grain-size ratios allow for variations in particle packing which affect the flow into and through the grain matrix. The surface of the unimodal bed (RD_0) had a higher roughness than that of the mixed beds because the pockets on the surface were not filled by fine particles (Figure 4.8a). This effect is indicated by the approximately logarithmic flow profile of RD_0: Owing to the high roughness and friction, the maximum flow velocity was reached at a larger distance *z* from the bed surface (Figure 4.5). Subsequently, the resulting drag forces and bed shear-stresses at the bed surface were much lower than in the mixed beds. However, without the fine particles filling the pore space, the reference bed also had a higher porosity than the mixed beds. The matrix of coarse grains was not blocked by fine grains, i.e. the flow could enter the matrix

unhindered. The reference bed eventually failed at high flow velocities, being more mobile than the beds in case 1 but less mobile than those in case 2.

With the addition of fine particles, the bed becomes smoother as the fines fill the pockets on the surface (Figure 4.8b and c). Similar to the results from other studies investigating the mobilization of mixed beds (e.g. Sambrook Smith and Nicholas, 2005; Venditti et al., 2010a), our flow profiles show an acceleration of near-bed flow occurring in all mixed experiments as fine particles were added to the bed (Figure 4.5). However, unlike e.g. Venditti et al. (2010a) observed in flume experiments with gravel and sand, we could not detect a clear reduction of *TKE* and the bed shear-stress with the addition of fine particles which could be due to differences in methodology and data quality (Buffington and Montgomery, 1997). The bed shear-stress in $RD_{9.4,M}$, $RD_{3.9,M}$ and $RD_{3.9,L}$ fluctuated slightly and exceeded the values of RD_0 during most periods of the experiment (Figure 4.2). A possible explanation for these differences in τ_0 could be micro-scale variations of the bed surface or bed-form development after particle erosion was initiated. In the case 1 experiments with a high grain-size ratio ($RD_{9.4}$ and $RD_{5.8}$) the addition of fine material led to an increased near-bed flow velocity and a decline of bed-level changes. At a high fine content (≈ 40 %) no bed forms developed under the tested flow conditions. In our case 2 experiments with a low grain-size ratio ($RD_{3.9}$), the addition of fine particles led to a similar flow acceleration, however, bed-level changes increased.

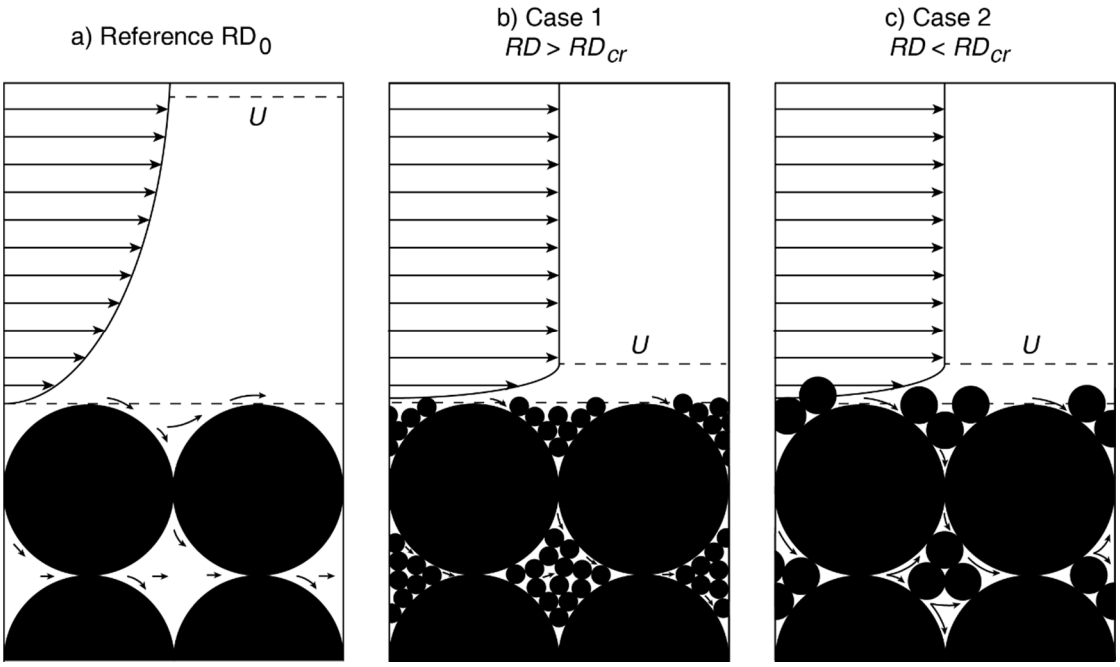

Figure 4.8: Conceptual model for the flow behaviour at the bed surface. a) Reference scenario RD_0. Development of a logarithmic boundary layer due to high bed roughness, resulting in low flow velocities at the bed surface. The higher porosity (relative to the mixed beds) allows unhindered inflow and discharge through the grain matrix, but the low flow velocities and larger particles result in little entrainment of material. b) High RD, large fine content: The pore space of the grain matrix is filled with fine particles and the bed roughness is reduced. The maximum flow velocity is reached close to the bed surface but the flow into and through the matrix is blocked by the high amount of fines. c) Low RD, large fine content: The fine particles fill the surface pockets, reducing the bed roughness. Again, the maximum flow is reached close to the bed surface. The higher near-bed flow velocities (than in the reference case) and the higher porosity (than in case 1 and the reference case) lead to higher inflow and particle entrainment.

The horizontal flow velocities for $RD_{9.4,L}$ and $RD_{3.9,L}$ show clear differences between the case 1 and case 2 (Figure 4.6). $RD_{9.4}$ represents an example of case 1 with $RD > RD_{cr}$: At low fine-grained content (e.g. in $RD_{9.4,S}$), the case 1 bed becomes unstable because the fines do not fill the pore space and flow can enter the particle matrix. At a high fine-grained fraction (e.g. in $RD_{9.4,L}$ with ≈ 40 % fines), the bed is densely packed and allows only little flow right at the bed surface (Figure 4.6a). The pore space between the coarse particles is blocked by fine grains. At this stage, the flow is not able to enter the upper layers of the bed and particle entrainment is inhibited (Figure 4.8b). This "stabilizing" behaviour is consistent with the experimental results of Bartzke et al. (2013) who used sand and silt with little cohesion and a grain-size ratio of RD = 5.5, and found that already small amounts of silt can cause an increase of the critical erosion threshold. In agreement with the theories by van Ledden et al. (2004) and Le Hir et al. (2008), we postulate that a network of fines has stabilized the coarse particles in our experiments. The results suggest that for a sandy bed a grain-size ratio of 5.8 and a threshold fine fraction of 20 % can lead to the formation of stabilizing network structures, even if cohesive forces are absent. We assume that the slight increase of bed mobility at 40 % is due to the higher abundance of mobile, fine particles that are washed out at increasing flow speeds. The increase in mobility could indicate sweeps of fine particles or a sheet flow of fines passing underneath the instrument. However, the development of bed forms is inhibited by the stabilizing network structures.

$RD_{3.9}$ represents an example of case 2 with $RD < RD_{cr}$: At a low fine-grained content, a case 2 bed is smoother than the reference bed, allowing higher near-bed flow velocities (Figure 4.5a) and increased drag forces. The fine particles cannot completely fill the pore space of the coarse-grained matrix, due to their size relative to the coarse particles. The larger pore space allows inflow into the upper bed layers, whereby particles can easily be entrained (Figure 4.8c). With increasing fine-grained content, the near-bed flow increases further (Figure 4.5b and c) and more flow can enter the matrix (Figure 4.6b), leading to more bed mobilization. The "mobilizing" behaviour as seen in case 2 agrees with studies describing the behaviour of coarse, mixed river sediments (e.g. Jackson and Beschta, 1984; Iseya and Ikeda, 1987; Wallbridge et al., 1999; Venditti et al., 2010a; Houssais and Lajeunesse, 2012). Similar to our findings, Sambrook Smith and Nicholas (2005) and Venditti (2010a) observed flow accelerations above the bed surface after fines were added to the bed. The results of case 2 also agree with the theoretical models describing the mobilization of coarse particles on a mixed bed (e.g. Komar and Li, 1986; Wiberg and Smith, 1987) and experimental studies based on these models (e.g. Wallbridge et al., 1999). The models indicate that coarse grains on a bed of finer grains are entrained at flow speeds below their critical erosion threshold. A grain that is larger than the roughness length of the bed protrudes into the flow, the pivoting angle is lower, and the grain has a lower resistance to erosion. In turn, a fine grain on a mixed bed hides in the roughness length of the coarse bed and is entrained at higher flow speeds. However, the theoretical and experimental studies mentioned above suggest that grains of the coarse fraction on a mixed bed are always entrained at a lower critical flow speed than the same grain size on a unimodal bed. Our experiments showed that the coarse fraction can be stabilized on a mixed bed

(i.e. no development of bed forms) if the ratio between coarse and fine grains is large enough (≥ 5.8). At a low grain-size ratio (3.9) however, no stabilizing network structures can be formed.

Our results agree with the geometrical approach to particle packing density proposed by McGeary (1961): He stated that a fine, spherical particle could fit through the triangular pore space of three coarse, spherical particles if the ratio between coarse and fine particles corresponds to $RD_{cr} \geq 6.5$. If *RD* lies at or above this threshold, the fine particles can percolate into the coarse matrix and fill the pore space, resulting in a tightly packed bed (= case 1). If *RD* lies below this threshold, i.e. D_{fine} is too large, the fine particles cannot percolate into the coarse-grained network and the particle packing is less dense (= case 2). In a random packing of spherical glass beads, the gaps between the coarse particles are wider than in a tightly packed triangular assemblage, i.e. even larger fines can percolate through the coarse particle matrix. For our glass-bead experiments, a slightly lower threshold ratio of $RD_{cr} \approx 5$ is therefore plausible. In addition, we assume that the porosity in case 1 is lower than in case 2. Although we have not measured the porosity of the glass-bead combinations, it is evident that very fine spherical particles are needed to completely fill a given pore space between larger spherical particles.

4.4.3 Hydraulic conductivity

A priori, it was assumed that the hydraulic conductivity (as presented in Figure 4.1) would act as a proxy for the ability of the bed to allow water flow into and through it (Bartzke et al., 2013). However, the hydraulic conductivities of the different grain-size combinations could not be related to the bed mobility (as presented in Figure 4.3 and Figure 4.4). The conductivity of the unstable bed $RD_{3.9}$ did not provide any indication for a different erosion behaviour than in $RD_{9.4}$ or $RD_{5.8}$. The hydraulic conductivity we measured with the permeameter represents the vertical percolation through a static porous medium, driven only by hydrostatic pressure and gravity, under no-flow conditions. In the flume experiments, the particles and the water inside the bed are subject to flow-driven drag forces, shear-stresses and turbulence. In addition, the bed packing might be influenced (i.e. compacted or loosened) by the flow through the matrix, a process which in turn again influences the flow. Therefore, the results from the permeameter measurements cannot be used to estimate or predict the water inflow and passage through a similar bed under flow conditions.

4.5 Conclusions

Erosion experiments with different mixtures of non-cohesive, fine glass beads with particle sizes similar to sand/silt were conducted in an annular flume. The mobility of the bed and the flow velocities in the vicinity of the bed surface were investigated. Under the range of the flow conditions tested here, we found:

- The addition of fine grains to a mixed bed leads to a reduction of the surface roughness and an acceleration of the near-bed flow compared to a unimodal bed, caused by the fine particles filling the pockets on the bed surface.
- Both the relative grain sizes of the coarse and fine grains and the abundance of fine material govern the stability of the bimodal bed. Depending on the grain-size ratio *RD*, a bimodal bed is either more mobile or more stable than the unimodal bed, and the bed behaviour changes at a critical grain-size ratio 5.8 > RD_{cr} > 3.9: The mixed beds with a grain-size ratio > RD_{cr} were less mobile than a unimodal bed. The mobility of these beds decreased with increasing fine-grained content and with a fine fraction of ≈ 40 %, they remained stable under the applied flow conditions (U_{max} = 0.19 m s^{-1}). The mixed beds with a grain-size ratio < RD_{cr} were more mobile than a unimodal bed. The mobility of these beds increased with increasing fine content, i.e. they could not be stabilized but erosion was facilitated by the addition of more fines. Thus, the grain-size ratio plays a primary role for bed mobility whereas the amount of fines has a supplementary effect.
- We postulate that the bed mobility is related to the flow into and through the grain matrix. In a bed with a large grain-size ratio (> RD_{cr}), a threshold fine fraction (≈ 20 % weight) can form a network structure around the coarse particles and plug the pore space of the coarse grain matrix. The accelerated near-bed flow cannot enter the matrix and the bed is stabilized. In our experiments, the optimal grain-size ratio for the stabilization of the bed was *RD* = 5.8 (at a fine-grained content of ≈ 17 %). In a bed with a low grain-size ratio (< RD_{cr}), the fine grains are too large to percolate into the pores of the coarse grain matrix. The accelerated near-bed flow can enter the matrix through the pore space, which leads to increasing bed mobility.
- For bimodal sediment in the sand-silt range, both the grain-size ratio and the fine-grained content are key characteristics for the bed mobility. For sediment mixtures with more than two size fractions, a factor similar to *RD* must be derived from the grain-size distribution.
- We suggest that further experiments should be conducted under a broader range of conditions (e.g. higher flow velocities, changing flow directions and wave loading) and a detailed investigation of the relationship between grain-size ratio *RD* and the porosity of a sediment should be undertaken. In addition, the mobility of natural, fine-grained sediment (sand/silt) with various *RD* should be tested to assess the applicability of the results found here to natural environments.

Acknowledgements

This study was carried out within the framework of the International Research Training Group INTERCOAST for Integrated Coastal Zone and Shelf-Sea Research of the University of Bremen, Germany, and the University of Waikato, Hamilton, New Zealand. The work has been funded through the German Research Foundation's (DFG) project GRK 1598 – INTERCOAST. CAP gratefully acknowledges the Walter and Andrée de Nottbeck Foundation, Prof A. Norkko and staff

at Tvärminne Zoological Station, University of Helsinki for support during manuscript preparation. The authors would like to thank Warrick Powrie and Dudley Bell for their assistance in the Benthic Flow Laboratory, as well as Gerhard Bartzke, Lina Podszun, Jannis Kuhlmann and Lars Lindner for their feedback on the manuscript.

References

Allen, J.R.L., 1985. Principles of physical sedimentology. George Allen & Unwin Ltd., London.

Bartzke, G., Bryan, K.R., Pilditch, C.A., Huhn, K., 2013. On the Stabilizing Influence of Silt On Sand Beds. J. Sediment. Res. 83, 691–703. doi:10.2110/jsr.2013.57

Buffington, J.M., Montgomery, D.R., 1997. A systematic analysis of eight decades of incipient motion studies, with special reference to gravel-bedded rivers. Water Resour. Res. 33, 1993–2029.

Chanson, H., Trevethan, M., Aoki, S., 2008. Acoustic Doppler velocimetry (ADV) in small estuary: Field experience and signal post-processing. Flow Meas. Instrum. 19, 307–313. doi:10.1016/j.flowmeasinst.2008.03.003

Einstein, H.A., 1950. The Bed-Load Function for Sediment Transportation in Open Channel Flows. US Dep. Agric. Tech. Bull. 1–71.

Goring, D.G., Nikora, V.I., 2002. Despiking Acoustic Doppler Velocimeter Data. J. Hydraul. Eng. 128, 117–126. doi:10.1061/(ASCE)0733-9429(2002)128:1(117)

Grant, J., Bathmann, U.V., Mills, E.L., 1986. The Interaction between Benthic Diatom Films and Sediment Transport. Estuar. Coast. Shelf Sci. 23, 225–238.

Guo, Y., Morgan, J.K., 2004. Influence of normal stress and grain shape on granular friction: Results of discrete element simulations. J. Geophys. Res. 109, B12305. doi:10.1029/2004JB003044

Houssais, M., Lajeunesse, E., 2012. Bedload transport of a bimodal sediment bed. J. Geophys. Res. 117, F04015. doi:10.1029/2012JF002490

Iseya, F., Ikeda, H., 1987. Pulsations in bedload transport rates induced by a longitudinal sediment sorting: A flume study using sand and gravel mixtures. Geogr. Ann. Ser. A, Phys. Geogr. 69, 15–27.

Jackson, W.L., Beschta, R.L., 1984. INFLUENCES OF INCREASED SAND DELIVERY ON THE MORPHOLOGY OF SAND AND GRAVEL CHANNELS. Water Resour. Bull. 20, 527–533.

Jacobs, W., Le Hir, P., Van Kesteren, W., Cann, P., 2011. Erosion threshold of sand-mud mixtures. Cont. Shelf Res. 31, 14–25.

Kim, S.-C., Friedrichs, C.T., Maa, J.P.-Y., Wright, L.D., 2000. Estimating bottom stress in tidal boundary layer from acoustic Doppler velocimeter data. J. Hydraul. Eng. 126, 399–406.

Kock, I., Huhn, K., 2007. Influence of particle shape on the frictional strength of sediments — A numerical case study. Sediment. Geol. 196, 217–233. doi:10.1016/j.sedgeo.2006.07.011

Komar, P.D., Li, Z., 1986. Pivoting analyses of the selective entrainment of sediments by shape and size with application to gravel threshold. Sedimentology 33, 425–436. doi:Doi 10.1111/J.1365-3091.1986.Tb00546.X

Kresic, N., 2006. Hydrogeology and Groundwater Modeling, Second Edi. ed. CRC Press, Taylor & Francis Group, Boca Raton, FL.

Le Hir, P., Cann, P., Waeles, B., Jestin, H., Bassoullet, P., 2008. Chapter 11 Erodibility of natural sediments: experiments on sand/mud mixtures from laboratory and field erosion tests, in: Kusada, T., Yamanishi, H., Spearman, J., Gailani, J.Z. (Eds.), Sediment and Ecohydraulics: INTERCOH 2005. Elsevier B.V., pp. 137–153. doi:10.1016/S1568-2692(08)80013-7

Leeder, M.R., 1982. Sedimentology: Process and Product. George Allen & Unwin Ltd., London.

Mair, K., Frye, K.M., Marone, C., 2002. Influence of grain characteristics on the friction of granular shear zones. J. Geophys. Res. 107, 2219. doi:10.1029/2001JB000516

McCave, I.N., 1984. Erosion, transport and deposition of fine-grained marine sediments. Geol. Soc. London, Spec. Publ. 15, 35–69. doi:10.1144/GSL.SP.1984.015.01.03

McGeary, R.K., 1961. Mechanical Packing of Spherical Grains. J. Am. Ceram. Soc. 44, 513–522.

Meadows, A., Meadows, P.S., Muir Wood, D., Murray, J.M.H., 1994. Microbiological effects on slope stability: an experimental analysis. Sedimentology 41, 423–435.

Mehta, A.J., Lee, S.-C., 1994. Problems in Linking the Threshold Condition for the Transport of Cohesionless and Cohesive Sediment Grain. J. Coast. Res. 10, 170–177.

Mehta, A.J., Letter, J. V., 2013. Comments on the transition between cohesive and cohesionless sediment bed exchange. Estuar. Coast. Shelf Sci. 131, 319–324. doi:10.1016/j.ecss.2013.07.001

Miller, M.C., McCave, I.N., Komar, P.D., 1977. Threshold of sediment motion under unidirectional currents. Sedimentology 24, 507–527. doi:10.1111/j.1365-3091.1977.tb00136.x

Mitchener, H., Torfs, H., 1996. Erosion of mud/sand mixtures. Coast. Eng. 29, 1–25. doi:10.1016/S0378-3839(96)00002-6

Panagiotopoulos, I., Voulgaris, G., Collins, M.B., 1997. The influence of clay on the threshold of movement of fine sandy beds. Coast. Eng. 32, 19–43.

Paterson, D.M., Crawford, R.M., Little, C., 1990. Subaerial Exposure and Changes in the Stability of Intertidal Estuarine Sediments. Estuar. Coast. Shelf Sci. 30, 541–556.

Sambrook Smith, G.H., Nicholas, A.P., 2005. Effect on flow structure of sand deposition on a gravel bed: Results from a two-dimensional flume experiment. Water Resour. Res. 41, W10405. doi:10.1029/2004WR003817

Shields, A., 1936. Anwendung der Aehnlichkeitsmechanik und der Turbulenzforschung auf die Geschiebebewegung. Mitteilungen der Preußischen Versuchsanstalt für Wasserbau und Schiffbau, Berlin 26.

Soulsby, R.L., 1983. The Bottom Boundary Layer of Shelf Seas, in: Johns, B. (Ed.), Physical Oceanography of Coastal and Shelf Seas. Elsevier, pp. 189–266.

Teisson, C., Ockenden, M., Le Hir, P., Kranenburg, C., Hamm, L., 1993. Cohesive sediment transport processes. Coast. Eng. 21, 129–162.

Torfs, H., Jiang, J., Mehta, A.J., 2001. Assessment of the erodibility of fine/coarse sediment mixtures, in: McAnally, W.H., Mehta, A.J. (Eds.), Coastal and Estuarine Fine Sediment Processes. Vol. 3. Proceedings in Marine Science. Elsevier, pp. 109–123. doi:10.1016/S1568-2692(00)80116-3

van Ledden, M., van Kesteren, W.G.. G.M., Winterwerp, J.. C., 2004. A conceptual framework for the erosion behaviour of sand–mud mixtures. Cont. Shelf Res. 24, 1–11. doi:10.1016/j.csr.2003.09.002

Venditti, J.G., Dietrich, W.E., Nelson, P.A., Wydzga, M.A., Fadde, J., Sklar, L., 2010a. Mobilization of coarse surface layers in gravel-bedded rivers by finer gravel bed load. Water Resour. Res. 46, W07506. doi:10.1029/2009WR008329

Venditti, J.G., Dietrich, W.E., Nelson, P.A., Wydzga, M.A., Fadde, J., Sklar, L., 2010b. Effect of sediment pulse grain size on sediment transport rates and bed mobility in gravel bed rivers. J. Geophys. Res. 115, F03039. doi:10.1029/2009JF001418

Wallbridge, S., Voulgaris, G., Tomlinson, B., Collins, M., 1999. Initial motion and pivoting characteristics of sand particles in uniform and heterogeneous beds: experiments and modelling. Sedimentology 46, 17–32. doi:10.1046/j.1365-3091.1999.00199.x

Whitehouse, R., Soulsby, R., Roberts, W., Mitchener, H., 2000. Dynamics of estuarine muds. HR Wallingford. Thomas Telford Publishing, London.

Wiberg, P.L., Smith, J.D., 1987. Calculations of the critical shear stress for motion of uniform and heterogeneous sediments. Water Resour. Res. 23, 1471. doi:10.1029/WR023i008p01471

Widdows, J., Brinsley, M.D., Bowley, N., Barrett, C., 1998. A Benthic Annular Flume for In Situ Measurement of Suspension Feeding/Biodeposition Rates and Erosion Potential of Intertidal Cohesive Sediments. Estuar. Coast. Shelf Sci. 46, 27–38. doi:10.1006/ecss.1997.0259

Widdows, J., Brinsley, M.D., Salkeld, P.N., Elliott, M., 1998. Use of Annular Flumes to Determine the Influence of Current Velocity and Bivalves on Material Flux at the Sediment-Water Interface. Estuaries 21, 552–559.

Wilcock, P.R., Kenworthy, S.T., Crowe, J.C., 2001. Experimental Study of the Transport of Mixed Sand and Gravel. Water Resour. Res. 37, 3349–3358.

Willows, R.I., Widdows, J., Wood, R.G., 1998. Influence of an infaunal bivalve on the erosion of an intertidal cohesive sediment: A flume and modeling study. Limnol. Oceanogr. 43, 1332–1343. doi:10.4319/lo.1998.43.6.1332

Table 4.1: Bed properties and changes in bottom morphology for all experiments. Two different modes of behaviour with an increase in fine content can be distinguished. See text for details.

Run	D_{50} (µm)	RD	Fine content (% dry weight)	Hydraulic conductivity k (cm s^{-1})	Critical velocity for fine grains $U_{cr,fine}$ (m s^{-1})	Critical velocity for bed failure $U_{cr,failure}$ (m s^{-1})	Normalized bottom variance (m)	Bed forms	Velocity u_{xy5} (m s^{-1}) at z = 5 mm, U = 0.17 m s^{-1}
Reference experiment (unimodal bed)									
RD_0	367	-	0	$7.38 \cdot 10^{-2}$	n.a.	0.06	$7.8 \cdot 10^{-9}$	Yes	0.11
					n.a.	0.15	$6.8 \cdot 10^{-10}$	Yes	0.09
					n.a.	0.14	$9.7 \cdot 10^{-9}$	Yes	n.a.
Case 1: Reduced mobility by increasing fine fraction									
$RD_{9.4,S}$	367/39	9.4	8.9	$6.29 \cdot 10^{-2}$	0.06	0.17	$3.0 \cdot 10^{-9}$	Yes	0.16
					0.06	0.17	$3.0 \cdot 10^{-9}$	Yes	0.17
$RD_{9.4,M}$	367/39	9.4	17.9	$6.66 \cdot 10^{-3}$	0.06	0.15	$1.0 \cdot 10^{-9}$	Yes	0.18
$RD_{9.4,L}$	367/39	9.4	38.1	$2.71 \cdot 10^{-4}$	0.10	> 0.19	$1.5 \cdot 10^{-9}$	No	0.18
$RD_{5.8,S}$	367/63	5.8	8.7	$4.54 \cdot 10^{-2}$	0.06	0.19	$4.3 \cdot 10^{-9}$	Yes	0.15
$RD_{5.8,M}$	367/63	5.8	17.0	$1.12 \cdot 10^{-2}$	0.04	0.17	$6.0 \cdot 10^{-10}$	Yes	n.a.
$RD_{5.8,L}$	367/63	5.8	38.4	$1.72 \cdot 10^{-3}$	0.06	> 0.19	$8.3 \cdot 10^{-10}$	No	0.13
Case 2: Increased mobility by increasing fine fraction									
$RD_{3.9,S}$	367/93	3.9	10.2	$3.27 \cdot 10^{-2}$	0.06	> 0.19	$6.5 \cdot 10^{-8}$	Yes	0.17
					0.07	0.19	$2.9 \cdot 10^{-8}$	Yes	n.a.
$RD_{3.9,M}$	367/93	3.9	20.7	$1.01 \cdot 10^{-2}$	0.06	0.15	$5.9 \cdot 10^{-8}$	Yes	0.17
					0.06	0.17	$3.2 \cdot 10^{-8}$	Yes	0.18
$RD_{3.9,L}$	367/93	3.9	43.2	$4.34 \cdot 10^{-3}$	0.03	0.09	$7.9 \cdot 10^{-8}$	Yes	0.19

5. A numerical micro-scale model of the flow inside a sediment matrix

Franziska Staudt, Gerhard Bartzke and Katrin Huhn

MARUM Center for Marine Environmental Sciences, Universität Bremen, Leobener Straße, 28359 Bremen, Germany

From laboratory studies with marine and fluvial sediment it is known that the sediment texture has an influence on the flow regime at the bed surface and subsequently, on the sediment stability. It has been assumed that besides the relative amounts of coarse and fine fraction, the ratio between coarse and fine particle diameter, i.e. the grain-size ratio, plays an important role for the bed's stability. However, laboratory experiments are restricted in the quantification of the fluid-sediment interaction at the bed surface and within the upper layers of the bed. To mimic these micro-scale processes, we used a high-resolution 3D numerical model which couples a particle simulation with a fluid simulation. Four different particle compositions – one unimodal reference and three bimodal beds – were used to study the relation between the grain-size ratio and the flow through the particle matrix. The 3D flow velocities in the numerical bed were investigated at various free flow velocities. It could be observed that the cross-stream and vertical flow components within the particle matrix vary significantly with the grain-size ratio. The results suggest that the flow through the particle matrix changes at a critical grain-size ratio. With decreasing grain-size ratio, higher cross-stream and vertical flow deflections occurred within the bed. We assume that especially the increased vertical flow velocities can facilitate the destabilization and entrainment of particles from the surface of a mixed bed.

5.1 Introduction

Sediment transport plays an important role for the coastal marine environment. Sediment erosion or deposition can impact structural integrity, the benthic flora and fauna as well as maritime traffic. Unwanted deposition, e.g. in estuaries or harbour inlets, can cause immense costs, whereas unwanted erosion around industrial developments or along populated coastlines can endanger the stability of coastal structures (jetties, harbours, seawalls, offshore plants etc.) and residential buildings. For the stability of a mixed sediment bed, the sediment texture, i.e. the interaction of particle sizes and particle-size fractions, is a main factor next to cohesion or bioactivity (e.g. Mitchener and Torfs 1996, van Ledden et al. 2004).

In marine sciences it is commonly understood that an increase in the fine-grained content leads to the stabilization of a sediment bed. Van Ledden et al. (2004) described this concept of stabilization through network formation where a critical fine-grained fraction is able to encompass the coarse

grains, e.g. a sand-dominated network transforms to a mud-dominated network. In past studies (e.g. Mitchener and Torfs 1996, Le Hir et al. 2008), the formation of such caging structures could be shown in laboratory experiments with sand-mud mixtures (with $D_{50,mud} \leq 63$ µm). Obviously, in these experiments the stabilizing cohesive forces increased with increasing clay content. However it has been shown that also sand-silt mixtures with little cohesion become stable with increasing fine content (Bartzke et al. 2013).

In contrast to the stabilization of a bed through the addition of fine material, flume experiments with river sediments (gravel-sand) have investigated how the addition of fine material leads to the destabilization of the bed, i.e. an increase in erosion (e.g. Venditti et al. 2010a, Houssais and Lajeunesse 2012). These laboratory studies observed that the fine particles fill the surface pockets of the coarse bed, thus reducing the bed roughness. A subsequent increase of the near-bed flow leads to increased drag force and subsequent erosion of coarse particles that protrude into the flow. Here, the mixed bed is mobilized with increasing fine content.

However, common in both scientific fields, it has been presumed that the erosion behaviour of mixed beds does not only depend on the amount of fines but also on the ratio between the particle diameters (Le Hir et al. 2008, Venditti et al. 2010a). In the following, this ratio will be called the grain-size ratio $RD = D_{(50)coarse}/D_{(50)fine}$.

In the experiments analysing the stabilization of a mixed bed, Torfs et al. (2001) used sand and mud (clay-silt or pure clay) with $RD \approx 9.2$ to $RD \approx 115$, and Bartzke et al. (2013) used sand and silt with $RD = 5.5$. In the experiments investigating the mobilization of a mixed bed, Venditti et al. (2010a) used a gravel and sand mixture with a grain-size ratio of $RD = 2.7$, Houssais and Lajeunesse (2012) used gravel and sand with $RD = 3.1$. Based on these previous studies using marine and river sediment, we assume that the critical grain-size ratio for the transition from stabilizing to mobilizing behaviour is $5.5 > RD_{crit} > 3.1$, and that a change of the micro-scale flow processes at the sediment-fluid interface occurs at this threshold. In laboratory experiments and field measurements however, the *in-situ* quantification of the controlling parameters (such as flow speed, porosity, sediment properties etc.) proves to be difficult. To close this gap, small-scale numerical models have gained importance in the simulation of near-bed flow processes and particle entrainment (e.g. Drake and Calantoni 2001, Schmeeckle and Nelson 2003, Bartzke and Huhn 2015). The water flow above and through the sediment bed can be simulated to investigate processes inside the sediment matrix (i.e. the flow around the single grains) on a micro-scale (i.e. grain scale). In contrast to the analogue experiment, a numerical model can provide detailed, continuous data collection of the critical parameters (e.g. flow velocities and resulting hydrodynamic forces). The results form the basis for larger scale sediment movement and erosion models. Using a numerical model of a mixed bed ($D_{coarse} = 600$ µm, $D_{fine} = 80$ µm), Bartzke and Huhn (2015) showed that the fine particles percolate into the pore space in between the large particles and thus flatten the bed surface. Based on velocity profiles and porosity changes, the authors have suggested that the fine particles block the water inflow into the pores of the coarse particle matrix, and subsequently stabilize the bed. However, Bartzke and Huhn (2015) did not modify the texture

(i.e. *RD*) of the numerical bed.

For the following study we used a numerical model to investigate the micro-scale 3D flow processes in the upper layers of a mixed bed in relation to *RD*. In addition to the flow profiles we analysed the cross-stream and vertical flow components and the flow deflections from the streamwise path. Eventually we drew the connection between the grain-size ratio *RD* and the flow field in the upper layer of the bed and evaluated the importance of the near-bed flow processes for the bed stability.

5.2 Methods

5.2.1 Modelling method

A high-resolution 3D numerical model (Figure 5.1) was used to simulate the interaction between particles and fluid flow in the upper 1.8 mm of a sediment bed. The numerical model coupled a particle simulation (discrete element method, DEM) with a flow simulation (finite difference method, FDM). The particle interactions were simulated using the commercial software PFC3D (3D Particle Flow Code, Itasca Consulting Group, Inc. 2005) and the flow simulations were conducted using FLAC3D (Fast Lagrangian Analysis of Continua in Three Dimensions, Itasca Consulting Group, Inc. 2006).

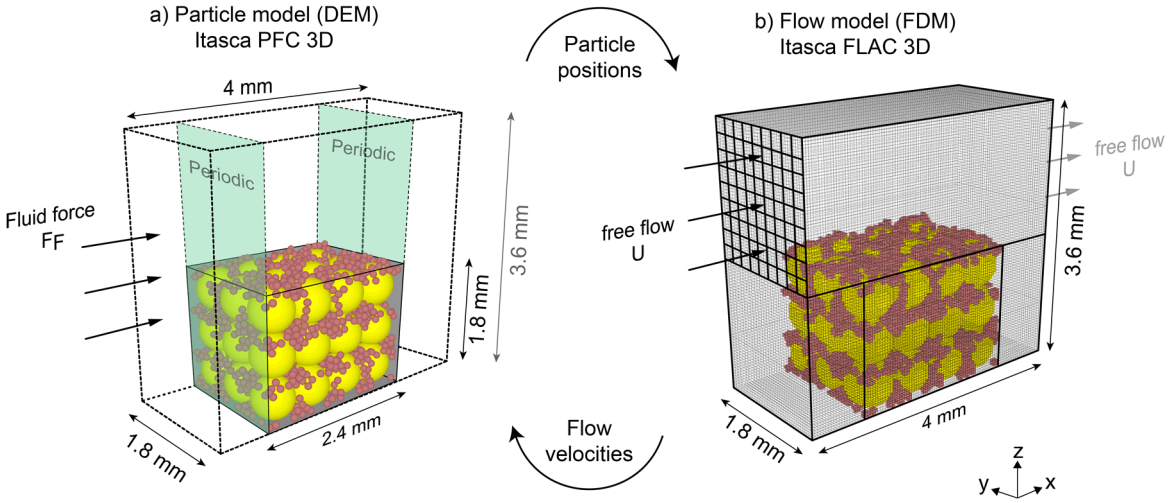

Figure 5.1: Schematic of the coupled particle-flow model.

The box encompassing the numerical particles (Figure 5.1a) had a size of 2.4 x 1.8 x 1.8 mm (length x height x width), yielding a volume of 7.776 mm^3. The left- and right-hand walls of this particle model (corresponding to the in- and outflow) were periodic boundaries, i.e. particles that exited the modelling domain on the right-hand side, re-entered the box on the left-hand side, mimicking a recirculation flume. The “sediment grains” in our particle model were represented by ideal spherical particles. For comparative reasons, a simplified cubic assemblage of 4 x 3 x 3 = 36 coarse particles (D_{coarse} = 600 µm) was used in each simulation (Figure 5.2). One reference bed (Figure 5.2.I) was simulated with coarse particles only, whereas the pore space of the other particle packages (Figure 5.2.II–IV) was filled with a similar amount of fine particles with different diameters

(Table 5.1). For every experiment, the coarse particles were generated first, then the according fine particles were generated within the pore space and the bed was allowed to settle until a steady state was reached. The particle packing was cut off above the height of the box (1.8 mm). Depending on the particle sizes of the fines, different grain-size ratios were produced (Table 5.1).

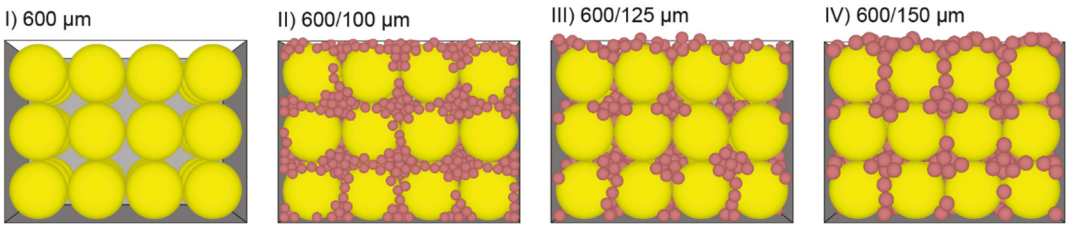

Figure 5.2: Grain-size combinations (side view).

Table 5.1: Simulation outline.

Simulation series	Particle-size distribution (µm)	Grain-size ratio *RD* (-)	Fine content (vol %)	Number of coarse particles	Number of fine particles
I	600	-	-	36	-
II	600/100	6	17.4	36	1642
III	600/125	4.8	13.8	36	636
IV	600/150	4	17.6	36	493

The coupling process was started by transferring the particle sizes and positions from the particle model to the flow model, where the particle matrix was discretized and the fluid flow around the (now rigid) particles was simulated. The flow model (Figure 5.1b) had an extent of 4.0 x 3.6 x 1.8 mm (length x height x width), covering a volume of 25.92 mm^3. The model was discretized into 100 x 90 x 45 = 405,000 cubic cells with an edge length of 0.04 mm each. The smallest used particles, having a diameter of D = 100 µm (Figure 5.2), filled at least 2 x 2 x 2 cells (and in some cases, were represented by cubes). To simulate the free flow above the bed as a driver for the flow through the sediment matrix, the flow model was twice as high as the particle model. In addition, in order to minimize the influence of boundary effects on the particle motion and to allow the development of a smooth flow field above the bed, the flow model exceeded the particle model by 0.8 mm on either side (in flow direction). The flow velocities in each cell of the flow model were simulated at various free flow velocities (U = 0.08; 0.15; 0.23; 0.31 m s^{-1}). The coupling process was finished by transferring the flow velocities back to the particle model where the resulting fluid forces were applied on the particles' centres of gravity, causing particle movements. The fluid force moving the particles in horizontal (x- and y-) direction was calculated using the equation for the drag force:

$$F_D = \frac{1}{2} \cdot \rho \cdot u^2 \cdot C_D \cdot A \qquad [5.1]$$

where F_D is the drag (N), ρ is the density of the fluid (ρ = 1000 kg m^{-1}), u is the velocity of the particle relative to the fluid (m s^{-1}), C_D is the drag coefficient ($C_{D,\text{sphere}}$ = 0.47), and A is the cross sectional area of the particle (m^2).

The particle movement in vertical (z-) direction was calculated using Stokes' law for the movement and settling of small spheres under low Reynold's numbers:

$$F = 6\pi \cdot \mu \cdot u \cdot r \qquad [5.2]$$

where F is the Stokes' drag (N), μ is the dynamic viscosity of the fluid (μ = 1.002 · 10^{-3} Pa s), u is the particle's relative velocity (m s^{-1}) and r is the particle radius (m).

The described coupling between the two models was repeated 100 times. Depending on the number of particles, our coupled simulations took several days to three weeks each, and after 100 steps a simulated time of t = 0.006–0.098 s had passed. The data from all simulations was compared at the common time t = 0.006 s.

The used fluid model describes a laminar flow both above and inside the discretized particle matrix (Itasca Consulting Group, Inc., 2006). As the flow inside a sediment bed is assumed to be laminar (i.e. Darcy flow), the result of our simulation is an accurate representation of the flow through the particle matrix. For the flow processes above the numerical sediment bed, the applied fluid model depicts a significant simplification compared to nature, due to the absence of turbulences.

5.2.2 Data analysis

From the particle simulation, the x-y-z coordinates of the particles, particle velocities and resulting particle interactions (i.e. contact forces) and displacements were logged. From the fluid simulations, we extracted values of specific discharge in every cell of the model. For comparison of the flow through the different particle matrices, we analysed the 3D flow velocities at two sampling locations situated halfway through the particle model in x-direction (Figure 5.3). To highlight the influence of *RD* on the flow through the particle matrix, the two sampling volumes were located in the pore space between the coarse particles. Each sampling volume had a crosswise cross-section covering 12 cells and a vertical extent of 85 cells (3.4 mm). Due to possible boundary effects, the data within 0.2 mm (5 cells) distance from the bottom of the fluid model was neglected.

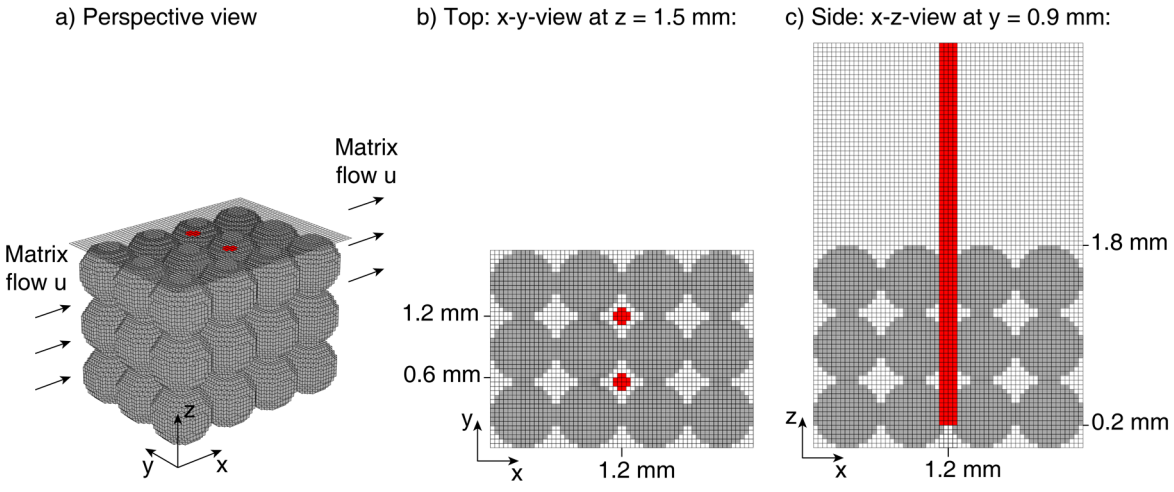

Figure 5.3: Position of sampling volume (red) in the grid of the flow model.

For each experiment, the flow magnitude u_{xyz} was averaged over the two sampling volumes to receive one flow profile. In the following, the flow below z = 1.5 mm, i.e. the flow through the particle matrix, will be referred to as "matrix flow". In addition, the flow deflections in cross-stream and vertical direction, the y- and z-velocity components of the flow (u_y and u_z) were analysed separately. The maximum matrix flows were related to the free flow velocity U above the bed to quantify the deceleration of the flow within the particle matrix. As an absolute measure for the degree of flow deflections in cross-stream and vertical direction, the spatial variances σ_y^2 and σ_z^2 of u_y and u_z over depth z were determined using the following equations:

$$\sigma_y^2 = \frac{1}{N-1}\sum\left(u_{yi} - \overline{u_y}\right)^2 \quad \text{and} \quad \sigma_z^2 = \frac{1}{N-1}\sum(u_{zi} - \overline{u_z})^2 \qquad [5.3]$$

where σ_y^2 and σ_z^2 are the variances of the respective y- and z-velocity components (m^2 s^{-2}), N is the number of velocity measurement (N = 85), u_{yi} and u_{zi} are the respective velocity components (m s^{-1}), and $\overline{u_y}$ and $\overline{u_z}$ are the respective average velocities (m s^{-1}).

5.3 Results

5.3.1 Flow profiles

The flow profiles for all grain-size combinations at different inflow velocities are presented in Figure 5.4. For U = 0.15 and 0.31 m s^{-1}, the maximum matrix flows ($u_{xyz,max}$) are indicated by vertical dashed lines in Figure 5.4. The maximum matrix flows relative to the according free flow velocities (% of U) are shown in Table 5.2.

With identical in- and outflow boundary conditions, the flow velocity U at the top of the model (z = 3.6 mm) varied marginally between experiments (Table 5.2, Figure 5.4). All profiles showed a logarithmic decrease in velocity in the vicinity of the bed surface. Within the particle matrix, u_{xyz} decreased visibly at z = 0.3; 0.9 and 1.5 mm, i.e. on the levels of the three coarse particle layers (Figure 5.4). In the pore space between these layers, i.e. at $z \approx$ 0.6 and 1.2 mm, the flow accelerated and the maximum occurring matrix flow velocity ($u_{xyz,max}$) was reached (Table 5.2, Figure 5.4).

Table 5.2: Maximum occurring matrix flow velocities (at z < 1.5 mm) in percentage (%) of the according free flow velocity U.

Flow component	Magnitude (x-y-z) $u_{xyz,max}$		Cross-stream (y) $u_{y,max}$		Vertical (z) $u_{z,max}$			
					Upwards		Downwards	
U (m s^{-1})	0.15	0.31	0.15	0.31	0.15	0.31	0.15	0.31
I	50.4	50.4	0.3	0.7	0.1	0.7	0.0	0.7
II	52.9	52.0	4.3	4.5	5.8	5.1	7.3	9.1
III	59.7	57.5	6.2	8.3	9.1	10.3	5.3	6.8
IV	63.3	58.9	6.6	7.0	10.0	15.5	12.8	13.7

In the profiles of reference experiment I (Figure 5.4.I), the sole effect of the coarse particles on the matrix flow is visible. In between the upper two particle layers (z = 1.2 mm), $u_{xyz,max}$ still reached about half of the free flow velocity (Table 5.2). For beds II (RD = 6), III (RD = 4.8) and IV (RD = 4), $u_{xyz,max}$ became higher with decreasing grain-size ratio. The velocity magnitude within the particle matrix was highest in experiment IV with RD = 4 (≈ 60 % of U). We can summarize that with increasing particle size D_{fine} (i.e. decreasing RD) higher flow velocity magnitudes were reached within the particle matrix in all experiments (Figure 5.4.I–IV).

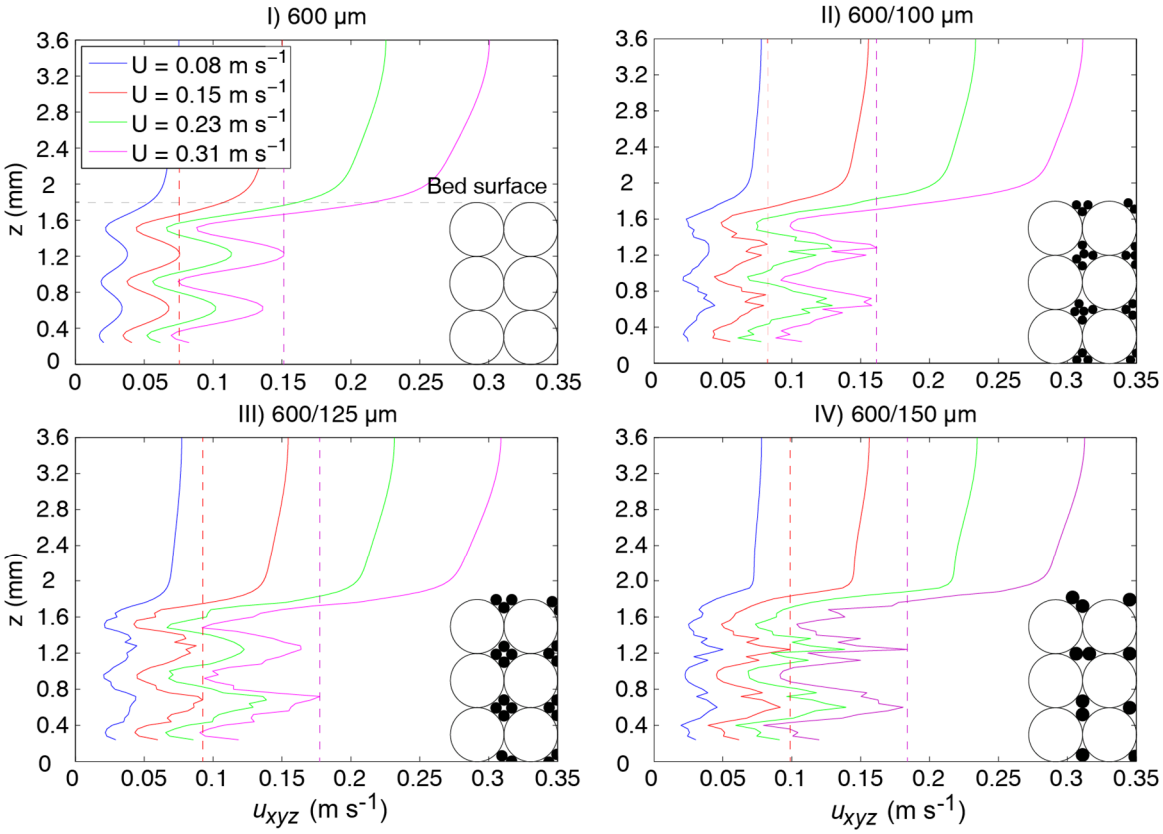

Figure 5.4: Velocity magnitude u_{xyz}.

5.3.2 Flow deflections

The cross-stream (u_y) and vertical (u_z) flow components indicate the flow deflection from the streamwise (x-) flow path. The cross-stream flow describes the horizontal flow deflection around the particles (i.e. flow to the left and right), whereas the vertical flow describes the up- and downwards flow deflection. The maximum cross-stream and vertical matrix flows relative to U are shown in Table 5.2. In the following figures we present the flow deflections that occur at U = 0.15 m s^{-1} (Figure 5.5a, Figure 5.6a) and U = 0.31 m s^{-1} (Figure 5.5b, Figure 5.6b) depending on the grain-size combinations.

The cross-stream velocities (u_y) are shown in Figure 5.5. A positive velocity denotes flow deflection to the left (when looking in streamwise direction), whereas a negative velocity denotes flow to the

right. In particle model I (reference), a cross-stream flow deflection was only marginally visible at low free flow velocities (Figure 5.5a, black line). At the highest free flow (U = 0.31 m s^{-1}), a slight cross-stream deflection to the right occurred (Figure 5.5b, black line). With the addition of very fine particles to the model (II with RD = 6), a deflection of the flow in cross-stream direction became visible (Figure 5.5a–b, red line). As expected, $u_{y,max}$ within the sediment matrix increased with increasing U. In relation to the free flow velocity U, the cross-stream component accounted for only 4.5 % (Table 5.2). With further decreasing RD in experiments III (RD = 4.8) and IV (RD = 4), the cross-stream velocities increased, i.e. the deflections became stronger (Figure 5.5a–b, green and blue line), and depicted 7–8 % of U at the highest free flow velocity (Table 5.2).

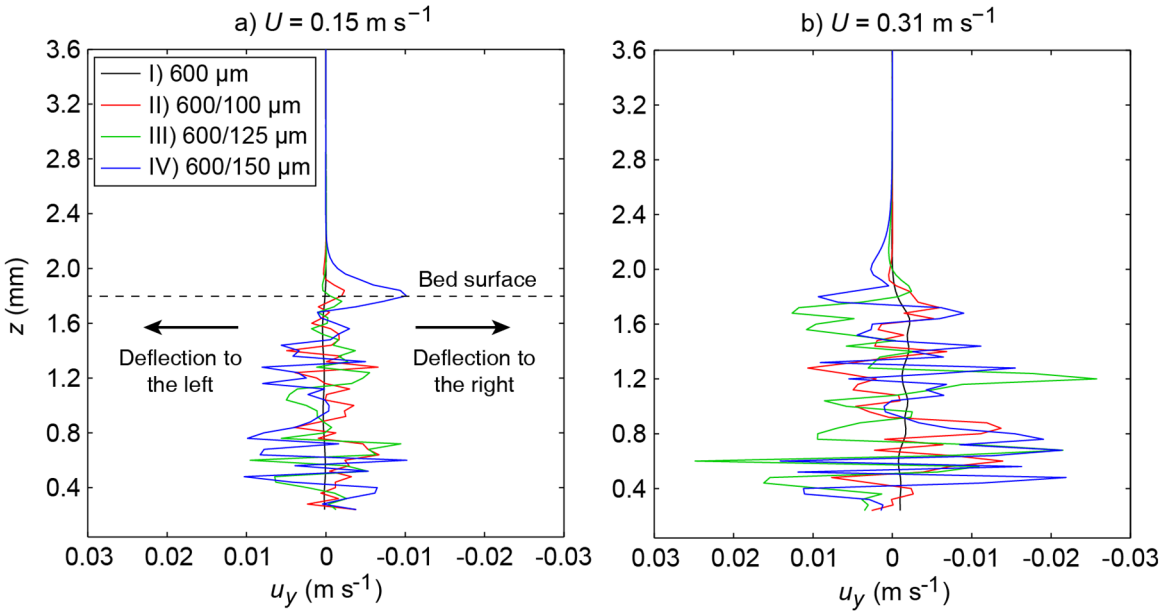

Figure 5.5: Cross-stream velocity components (u_y).

The vertical velocities (u_z) at U = 0.15 and 0.31 m s^{-1} depending on the grain-size combination are presented in Figure 5.6. Note that the graphs were rotated counter clockwise to represent up- and downwards flow on the ordinate. A positive value denotes upwards flow, whereas a negative value denotes downwards flow. The model height z is now represented on the abscissa. In the reference experiment (I), u_z remained low compared to the other experiments, i.e. only very little vertical flow deflection was observed (Figure 5.6, black line). Slight up- and downward deflection around the coarse particles in the two upper layers could be seen at the highest U (Figure 5.6b). In experiment II with fine particles filling the pore space, we observed an increase in flow deflection in vertical direction (Figure 5.6, red line). The maximum downwards flow velocities outweighed the upwards velocities (Table 5.2). In experiment III (Figure 5.6, green line), the absolute $u_{z,max}$ was similar to bed II, however, the maximum upwards flow in bed III clearly exceeded the maximum downwards flow (Table 5.2). The vertical velocity curve of bed IV (Figure 5.6, blue line) looks significantly different from II and III, with $u_{z,max}$ a lot higher than in the previous experiments. We can summarize that the maximum vertical flow velocity $u_{z,max}$ (especially in upwards direction) increased with decreasing RD. From all experiments, it was observed that the flow is predominantly deflected into

the vertical direction, with vertical matrix flows reaching up to 15.5 % of *U*, whereas the cross-stream matrix flows accounted for only 8.3 % of *U* (Table 5.2).

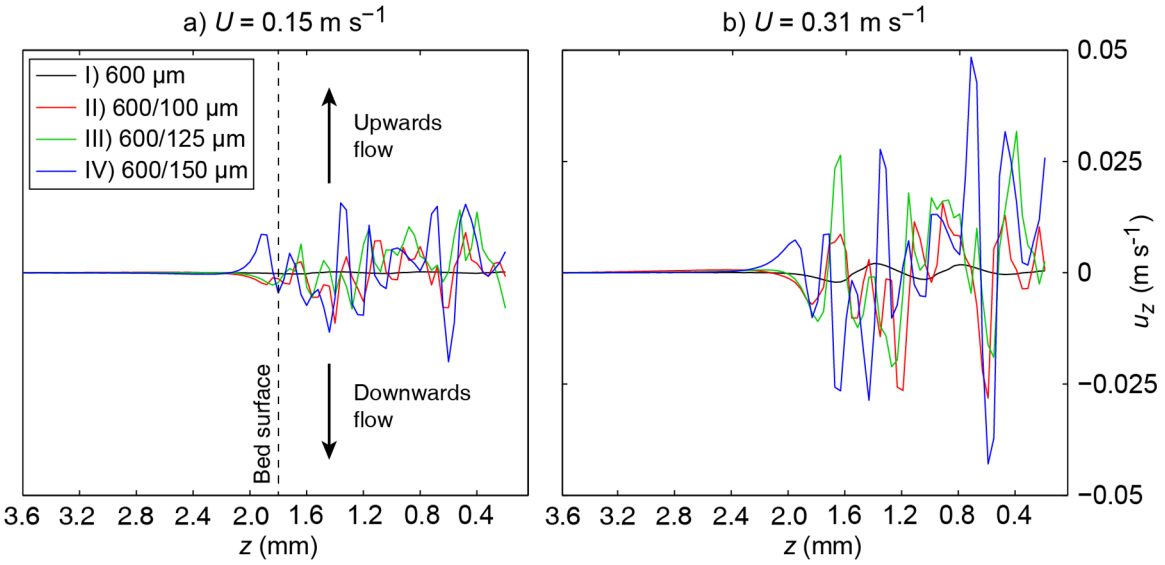

Figure 5.6: Vertical velocity components (u_z).

The cross-stream and vertical flow components indicate the differences between the grain-size combinations, but do not present the flow deflections as comparable quantities. To obtain one absolute degree of flow deflections, we calculated the variances over model depth *z* of both cross-stream (Figure 5.7a) and vertical flow components (Figure 5.7b) for every simulation. In the unimodal reference simulation (I), the variances of both u_y (Figure 5.7a, black line) and u_z (Figure 5.7b, black line) were negligible, as the flow in the space between the particles was rarely deflected from its streamwise direction (Figure 5.5, Figure 5.6). The mixed beds (II–IV) experienced higher cross-stream and vertical variances than the reference at all free flow velocities (Figure 5.7). With increasing *U*, the cross-stream velocity variance σ_y^2 increased almost exponentially for II (*RD* = 6, red) and III (*RD* = 4.8, green), and linearly for IV (*RD* = 4, blue). The maximum variance of the cross-stream flow occurred in simulation III (*RD* = 4.8, green) at *U* = 0.31 m s^{-1}, closely followed by IV (*RD* = 4, blue). In all simulations, the flow experienced stronger deflection in vertical than in cross-stream direction, indicated by a vertical variance σ_z^2 that was about two to four times higher than the cross-stream variance (note the different y-axis scaling in Figure 5.7a and b). At the lowest *U*, the vertical flow variances for the mixed simulations II, III and IV were similarly small. With increasing flow speed, σ_z^2 increased exponentially (Figure 5.7b). In experiment IV (*RD* = 4, blue) it reached a clear maximum which was more than twice the variance of experiment III (*RD* = 4.8, green).

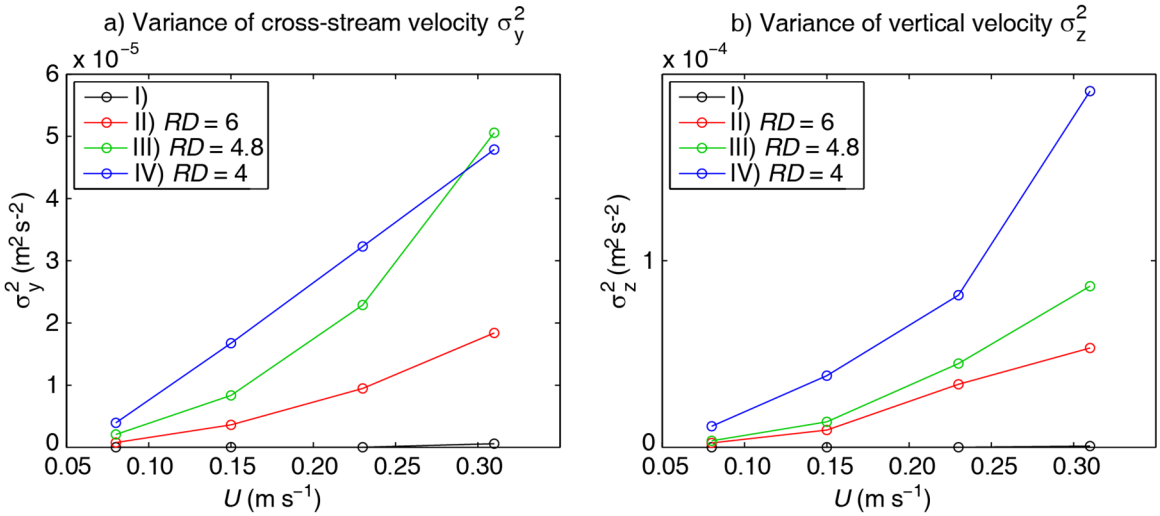

Figure 5.7: Velocity variances over model depth z of a) cross-stream y-velocities and b) vertical z-velocities, in relation to U and RD.

The simulation results show a clear relation between the texture, i.e. the grain-size ratio *RD*, and the cross-stream and vertical components of the matrix flow. With decreasing grain-size ratio *RD*, the flow diversion inside the particle matrix increased, indicated by the higher degree of velocity deflections (variance). The vertical flow variance was about 2–4 times higher than the cross-stream flow variance. The lowest, thereby negligible flow deflections occurred within the unimodal bed I (*D* = 600 µm). The maximum cross-stream flow deflections occurred inside bed III (*RD* = 4.8), if only slightly higher than the values in IV (*RD* = 4). The maximum vertical flow deflections occurred inside bed IV (with *RD* = 4). It can be summarized that at the same free flow velocity, the vertical flows in bed IV (with a low *RD*) were significantly higher and fluctuated between up- and downwards flow more extensively than in beds II–III (with a high *RD*).

5.4 Discussion

5.4.1 Model performance

Our numerical model presents a useful tool to simulate the laminar flow through the upper layers of a sediment bed. It can be applied to visualize the micro-scale flow processes at the sediment surface and thus contribute to the understanding of larger-scale sediment entrainment processes. As the fluid model was based on purely laminar flow (Itasca Consulting Group, 2006c), the flow profile in the water column showed a similar velocity decrease towards the bed surface for all grain-size combinations. In contrast to laboratory studies that observed a significant acceleration of the near-bed flow and a condensed boundary layer with the addition of fine particles to an initially unimodal bed (e.g. Venditti et al. 2010a), our numerical model did not show a considerable change of the boundary layer with the addition of fines. For the flow above the bed the applied equations denoted a strong simplification and could not represent a change in turbulences and a resulting change of the flow boundary layer. However, this limitation of the model did not affect the

interpretation of the laminar matrix flow. On the contrary, the model could show that the laminar flow in the upper bed layers is influenced significantly by the bed texture, even if turbulences are excluded. For the analysis of the matrix flow it is important to remember that we are looking at a snap-shot at t = 0.006 s only. The model simulates short-term processes, i.e. the velocities are instantaneous. Nevertheless, the observed flow deflections could subsequently influence the entrainment of particles.

The flow strongly depends on the particle assemblage in the sampling volume. The cubic assemblage of coarse particles should yield a higher comparability between the different beds. However, if the flow forces from the fluid model are large enough to entrain particles in the particle model, these move relative to the fixed sampling points for the flow data analysis. This could be observed in the reference scenario (I) at the highest free flow velocity U: at t = 0.006 s, coarse particles in the two upper layers had moved into the sampling volume. Subsequently the influence of the particles on the flow field became visible in the graphs of cross-stream and vertical velocities, which showed slight deflections for U = 0.31 m s^{-1} (Figure 5.5, Figure 5.6).

As the spherical particles from the DEM model are discretized into the grid of the FDM model, the flow through the (discretized) particle matrix depends significantly on the resolution of the grid. Due to the discretization, the porosity and cross-sections that are used for the flow calculation in the fluid model (FLAC) are slightly different from the particle model (PFC). We used the maximum number of grid cells that still allowed the coupling between particle and fluid model.

5.4.2 Matrix flow and flow deflections as trigger for particle mobilization

With a constant discharge through the bed, the streamwise flow velocity within the particle matrix increased with the addition of fine particles. This acceleration is based on the continuity of flow of an incompressible medium. At a constant discharge Q, a decrease of the flow cross-section A leads to an increase of the flow velocity u. In our simulations, the horizontal flow through the particle matrix was forced by the free flow above the bed, i.e. it was constant as long as the free flow velocity U was constant. In a natural environment, the (tidal or wind-induced) currents above the sediment force a micro-flow into and through the upper layers of the bed. Thus, similar to our numerical model, the flow through the sediment matrix is induced by the free flow above the bed. In the model, the pore space of a coarse particle matrix was filled with fine particles, the porosity and the flow cross-section A were reduced and the flow was accelerated, as could be seen in the flow profiles of the mixed experiments II–IV (Figure 5.4.II–IV). Analogue to this, the slightly faster free flow (at z = 3.6 mm) in the mixed simulations (II–IV) was a result of the reduction in total flow cross-section. In our simulations, the fine particles in the pore space of the coarse particle matrix did not cause a significant reduction of the inflow into the bed. We assume that the inflow reduction observed by Bartzke and Huhn (2015) was amplified by the confinement of the flow model which, unlike the flow model used in this study, did not allow flow development in the deeper bed layers. In nature, an inflow reduction could however occur if fine particles filled the surface pockets of the mixed bed and

reduced the bed's roughness, resulting in a decrease in turbulences above the bed (Venditti et al. 2010a).

In addition to the streamwise flow acceleration, the particles in the flow path deflected the flow in cross-stream (Figure 5.5) and vertical (Figure 5.6) direction. Larger particles (i.e. in experiments III and IV with lower *RD*) led to stronger deflection, i.e. to higher vertical and cross-stream velocities. Higher flow velocities lead to a higher drag that is exerted on a single particle, as can be seen in equation 5.1. We hypothesize that in a long-term simulation, the observed increased flow velocities could contribute to the mobilization of particles in the upper layers of the bed. In scenarios with high upwards flow velocities, such as in simulation IV with $RD = 4$, these could facilitate the uplift of single particles at the bed surface. Looking at the vertical flow deflections in I, II ($RD = 6$) and III ($RD = 4.8$) on one hand, and IV ($RD = 4$) on the other hand, there was a clear distinction in the highest occurring flow velocities (Figure 5.6, Figure 5.7b). Thus, we suggest that the critical grain-size ratio for the mobilization of the upper bed layer is $RD_{crit} = 4$. This agrees with the critical ratio $5.5 > RD_{crit} > 3.1$ assumed from literature. The high flow velocities in vertical direction could explain why mixed sediment beds with $RD < 4$ become mobilized easily (e.g. Venditti et al. 2010a, Houssais and Lajeunesse 2012), whereas beds with $RD > 4$ usually remain stable (e.g. Mitchener and Torfs 1996, Le Hir et al. 2008, Bartzke et al. 2013).

In marine geosciences, it is understood that a mixed bed is generally more stable than a unimodal bed. In our simulations, all mixed beds – also those with a high *RD* (i.e. usually stable) – experienced increased vertical flow velocities compared to a unimodal bed. However, it is important to note that most empirically tested (marine) sediments with a high *RD* contained very fine, muddy sediment which, in addition to high particle complexity, is subject to cohesive forces and bioactivity (e.g. Le Hir et al. 2008). These factors contribute significantly to the stability of the bed, and can easily outweigh the increased flow forces within the particle matrix.

5.5 Conclusion and outlook

The used model presented a promising approach to the understanding of small-scale processes at the fluid-sediment interface and how these can affect sediment stability. We could show that the short-term laminar flow processes within a simplified, cubic sediment matrix are influenced by the grain-size ratio *RD*. Merely through differences in particle sizes, the laminar flow is modified in a way that could subsequently influence the particle entrainment. Compared to a unimodal bed, the fine particles in the pore space of a coarse particle matrix led to increased flow deflection in cross-stream and vertical direction. With decreasing *RD*, the cross-stream and vertical flow velocities increased. At $RD = 4$, the vertical flow velocities were significantly higher than in beds with larger *RD*. We suggest that bimodal beds with $RD < 4$ can be easily mobilized, whereas bimodal beds with $RD > 4$ remain stable, which agrees with laboratory studies investigating the stabilization and mobilization of mixed beds. A more time-efficient micro-scale model is required to simulate longer-

term processes like erosion (and erosion rates), and to verify if the vertical flow deflections inside the particle matrix will subsequently contribute to the particle entrainment.

We are currently working on the implementation of a turbulent flow model into a coupled modelling approach to investigate possible near-bed flow acceleration depending on the sediment texture, and the micro-scale effects of varying turbulences on the particle entrainment.

References

Bartzke, G., Bryan, K.R., Pilditch, C.A., Huhn, K., 2013. On the Stabilizing Influence of Silt On Sand Beds. J. Sediment. Res. 83, 691–703. doi:10.2110/jsr.2013.57

Bartzke, G., Huhn, K., 2015. A conceptual model of pore-space blockage in mixed sediments using a new numerical approach, with implications for sediment bed stabilization. Geo-Marine Lett. 35. doi:10.1007/s00367-015-0399-1

Drake, T.G., Calantoni, J., 2001. Discrete particle model for sheet flow sediment transport in the nearshore. J. Geophys. Res. 106, 19859–19868. doi:10.1029/2000JC000611

Houssais, M., Lajeunesse, E., 2012. Bedload transport of a bimodal sediment bed. J. Geophys. Res. 117, F04015. doi:10.1029/2012JF002490

Itasca Consulting Group, I., 2006. Fast Lagrangian Analysis of Continua in 3 Dimensions. User's Guide, Third Edit. ed. Itasca Consulting Group, Inc., Minneapolis, MN.

Le Hir, P., Cann, P., Waeles, B., Jestin, H., Bassoullet, P., 2008. Chapter 11 Erodibility of natural sediments: experiments on sand/mud mixtures from laboratory and field erosion tests, in: Kusada, T., Yamanishi, H., Spearman, J., Gailani, J.Z. (Eds.), Sediment and Ecohydraulics: INTERCOH 2005. Elsevier B.V., pp. 137–153. doi:10.1016/S1568-2692(08)80013-7

Mitchener, H., Torfs, H., 1996. Erosion of mud/sand mixtures. Coast. Eng. 29, 1–25. doi:10.1016/S0378-3839(96)00002-6

Schmeeckle, M.W., Nelson, J.M., 2003. Direct numerical simulation of bedload transport using a local, dynamic boundary condition. Sedimentology 50, 279–301. doi:10.1046/j.1365-3091.2003.00555.x

Torfs, H., Jiang, J., Mehta, A.J., 2001. Assessment of the erodibility of fine/coarse sediment mixtures, in: McAnally, W.H., Mehta, A.J. (Eds.), Coastal and Estuarine Fine Sediment Processes. Vol. 3. Proceedings in Marine Science. Elsevier, pp. 109–123. doi:10.1016/S1568-2692(00)80116-3

van Ledden, M., van Kesteren, W.G.. G.M., Winterwerp, J.. C., 2004. A conceptual framework for the erosion behaviour of sand–mud mixtures. Cont. Shelf Res. 24, 1–11. doi:10.1016/j.csr.2003.09.002

Venditti, J.G., Dietrich, W.E., Nelson, P.A., Wydzga, M.A., Fadde, J., Sklar, L., 2010a. Mobilization of coarse surface layers in gravel-bedded rivers by finer gravel bed load. Water Resour. Res. 46, W07506. doi:10.1029/2009WR008329

6. Stabilization and mobilization of a mixed sandy sediment bed through the addition of fines with various grain sizes

Franziska Staudt [a], Julia C. Mullarney [b], Conrad A. Pilditch [b], Katrin Huhn [a]

[a] MARUM Center for Marine Environmental Sciences, Universität Bremen, Leobener Straße, 28359 Bremen, Germany
[b] School of Science, Faculty of Science and Engineering, University of Waikato, Private Bag 3105 Hamilton, New Zealand

Flume experiments were conducted with natural, bimodal sediment. Medium sand ($D_{50,coarse}$ ≈ 400 µm) was mixed with 40 % fine material ($D_{50,fine}$ = 53; 111; 193 µm) and subjected to increasing flow velocities (U = 1.6–23.0 cm s^{-1}). The aim of the study was to investigate how the grain-size ratio $RD = D_{50,coarse}/D_{50,fine}$ between the coarse and fine grain diameters influences the mobility of a natural sediment bed. The bed mobility, derived from the variance of the bed level over time, as well as turbidity and near-bed hydrodynamics were analysed. The results were compared with similar experiments with spherical glass beads. The findings indicate that the fine fraction can either stabilize or mobilize a bed depending on *RD*: Whereas a mixed bed with a low *RD* = 2 behaved like a unimodal bed, the mixed beds with *RD* between 2 and 4 were considerably more mobile (i.e. the bottom variance was one magnitude higher). The beds with *RD* higher than 5 were more stable than the reference bed (i.e. the bottom variance was one magnitude lower). The trend in mobility with changing *RD* is comparable to the behaviour of glass beads, however, due to the complex grain shapes of sand and silt, the natural beds were generally more stable than the smooth, spherical beads. In addition, *RD* and the grain shape influenced the bed shear-stress and the near-bed flow. For a sandy, bimodal bed (D_{50} ≤ 410 µm), the grain-size ratio can serve as a key parameter for the bed stability. While it is already known for gravel-bedded rivers that the addition of fine material can trigger bed mobilization, our results show that this concept is transferrable to finer, sandy material with low *RD*. Further experiments with a wider range of conditions are recommended.

Keywords: sediment, stability, mobility, texture, laboratory experiments, fluvial, marine

6.1 Introduction

Knowledge about sediment stability is a critical component of understanding sediment dynamics and geomorphological processes in fluvial and coastal environments. A broader understanding of sediment dynamics is also required e.g. for the protection, sustainable development, successful ecosystem management or renaturation of rivers, estuaries and coastlines. The stability of aquatic sediments is known to be influenced by several factors. Next to stabilizing cohesive forces between very fine clay particles (e.g. Teisson et al., 1993; Mehta and Lee, 1994; Panagiotopoulos et al.,

1997; Torfs et al., 2001; Le Hir et al., 2008; Jacobs et al., 2011), micro- or macrofauna stabilizing or disrupting the sediment matrix (e.g. Grant, 1986; Paterson et al., 1990; Meadows et al., 1994; Willows et al., 1998; Widdows et al., 2000), and the grain complexity increasing the intergranular friction (e.g. Mair et al., 2002; Guo and Morgan, 2004; Kock and Huhn, 2007), the interaction between grain sizes and grain-size fractions (sediment texture) plays an important role for the sediment stability. It is commonly known that the amount of fine grains influences the behaviour of a sediment matrix. However, experiments from different research areas have yielded different results: Studies investigating the marine or estuarine environment concluded that an increase in fine-grained fraction leads to the stabilization of a bimodal sediment (e.g. Mitchener and Torfs, 1996; Torfs et al., 2001; Le Hir et al., 2008; Bartzke et al., 2013). Even if cohesive forces are absent, fine grains fill the pores between the coarse grains, and at a threshold fine content, a “network” of fines develops, breaking up the contacts between the coarse grains (van Ledden et al., 2004). This process inhibits movement of the coarse grains and can also reduce water flow into the bed (Bartzke and Huhn, 2015), thus increasing the erosion resistance of the bed. In contrast, in fluvial environments, an increase in (or input of a pulse of) fine material has been found to mobilize the bed (e.g. Jackson and Beschta, 1984; Iseya and Ikeda, 1987; Wilcock et al., 2001; Houssais and Lajeunesse, 2012). While it had long been observed that the addition of sand to a coarser gravel bed triggers the mobilization of the bed, only recent technical development, such as acoustic Doppler velocimetry (ADV) or particle image velocimetry (PIV), has allowed measurements of the near-bed hydrodynamics accompanying this effect. Using these techniques, several laboratory studies (e.g. Sambrook Smith and Nicholas, 2005; Venditti et al., 2010a; Wren et al., 2011) could show that the addition of fine material reduces the roughness of the bed surface, leading to a decrease of the bed shear-stress and an acceleration of the near-bed flow, which in these scenarios results in more particle entrainment.

In both cases (stabilization and mobilization), the effects of the fine fraction on the sediment stability is attributed to small-scale processes. It has been suggested that not only the amount of fines but also the ratio between the coarse and fine grain sizes influences the near-bed flow processes and subsequently the erosion behaviour (Le Hir et al., 2008; Venditti et al., 2010a).

In flume experiments with bimodal glass-bead mixtures (chapter 4), we showed that the erosion behaviour and mobility of a bimodal, artificial bed of glass beads (D_{50} = 39–367 µm) can be controlled using the sediment texture only, especially through the grain-size ratio $RD = D_{50,coarse}/D_{50,fine}$ between the diameters of the coarse and the fine grains. Mixed glass bead with a high grain-size ratio ($RD \geq 5.8$) and a fine fraction of ≈ 10 % (dry weight) are more stable than a unimodal reference bed and are further stabilized by an increase in the fine fraction to ≈ 40 %. The mobility of these beds (as analysed through the variance of the bottom level as a proxy for the bed movement during the experiment) is at least one magnitude lower than in the unimodal case. The near-bed flow accelerates with the addition of fine particles. However, the beds with a high *RD* are tightly packed and do not allow high flow velocities at the bed surface. In contrast, beds with a low grain-size ratio ($RD \leq 3.9$) and ≈ 10 % fines are less stable than the reference bed, and

are further mobilized by an increase of the fine fraction to ≈ 40 % (at flow speeds up to U = 19 cm s^{-1}). The mobility of these beds with low *RD* is one magnitude higher than the mobility of the unimodal reference bed. It was found that the near-bed flow field changes with the grain-size ratio, allowing higher velocities at the bed surface with lower *RD*, subsequently leading to more particle movement at the bed. The experiments with glass beads could show that even at low fine-grained contents (10 %), the grain-size ratio alone leads to differences in sediment stability, and the stabilizing or mobilizing effect is amplified with an increase in fine-grained fraction.

However, due to the uniformity and sphericity of the glass beads, the applicability of the developed concept is limited for natural processes, as natural sediment grains can have more complex shapes and a rough, jagged surface. Based on this restriction, in the study at hand we focus on the grain-size ratio *RD* and investigate the mobility of natural sediment, comparing the results to the end members (large fine fraction, various *RD*) of the glass-bead experiments. In the following text, the natural sediment treatments are denoted N_{RD} (i.e. N_0 for the unimodal reference experiment, N_2 for the treatment with *RD* = 2 etc.), whereas the glass-bead mixtures are denoted GB_{RD} (i.e. GB_0 for the reference, $GB_{3.5}$ for the treatment with *RD* = 3.5 etc.). We conducted new erosion experiments with natural sediment in an annular flume, using flow velocities ranging from U = 1.6 to 23.0 cm s^{-1}. Medium to fine sand and silt was used to create one coarse, unimodal reference bed and three bimodal beds with *RD* ranging from 2 to 7.7. In the experiments, we analysed the bed mobility, reflected by the variance of the bottom level (σ_b^2) and suspended particulate matter concentration (*SPM*), and the near-bed hydrodynamics, illustrated by flow profiles and changes in bed shear-stress (τ_0). The paper addresses the relation between *RD* and the bed mobility for natural sediment under laboratory flume conditions. Based on the comparison between the results for glass beads and natural sediment, we can also draw conclusions about the effect of the particle shape on sediment stability.

6.2 Methods

6.2.1 Material

The used sediment consisted of quarried and sampled medium sand (D_{50} = 389–410 µm), fine sand (D_{50} = 193 µm), very fine sand (D_{50} = 111 µm) and silt (D_{50} = 53 µm). For the erosion experiments, one unimodal sediment bed (N_0) with only coarse grains and three mixed sediment beds (N_2, $N_{3.5}$ and $N_{7.7}$) with coarse and fine grains were created. The grain sizes and grain-size ratios of the different treatments can be seen in Table 6.1. Every mixed bed contained 40 % (dry weight) fine material. Although a fine fraction of 40 % is far more than what can be found in natural sediment, it allowed us to compare the results with the end-members (low *RD*, 40 % fines vs. high *RD*, 40 % fines) of the glass-bead mixtures from our previous study (chapter 4).

A saturated sediment bed of 5 cm height was created in the flume and seawater was added to a height of 25 cm above the flume base. Every experimental run except for $N_{7.7}$ was replicated three

times with the sediment bed being taken out of the flume and remixed between runs. In this paper we will show selected results from one experiment of every series, the supplementary data from the replications is shown in Table 6.1.

6.2.2 Annular flume

We used an annular flume similar to the one developed by Widdows et al. (1998b) for the erosion experiments. The flume consisted of two concentric cylinders of 63 and 43 cm, respectively, which formed a flow channel with a width of 10 cm. A motor-driven rotating lid with a diameter of 53 cm was placed on top of the flume and was submerged in the water column at a depth of 3 cm. The rotation of the lid induced a current of U = 1.6–23.0 cm s^{-1} in the flume. The rotational speed of the flume lid was accelerated in 12 steps of 5 rpm from 5 rpm to 60 rpm. Every flow speed was maintained for 15 min to obtain an equilibrium between flow field and sediment transport, yielding a duration of 180 min for the complete experiment. The resulting flow velocity at a height of z = 1 cm above the sediment surface can be described by the following equation:

$$U \mathrel{\widehat{=}} 0.0039 \cdot \omega - 0.004 \qquad [6.1]$$

where U (m s^{-1}) is the horizontal flow velocity, and ω (rpm) is the rotational speed of the flume lid. The flow during the experiment can be described as fully turbulent in terms of the Reynolds number ($Re = \frac{UD}{\nu} \approx 2500 \text{ to } 37000$, where U is the flow velocity, D is the hydraulic diameter and ν is the kinematic viscosity of water).

A profiling acoustic Doppler velocimeter (ADV) was used to record the flow velocities, the changes of the bed level and the turbidity of the water column. The ADV was positioned at a height of 5.5 cm above the bed to ensure that the near-bed velocities fell in the middle of the profile, where the signal-to-noise ratio (and thus the data quality) is highest. The flow profile above the bed was sampled at a frequency of 50 Hz, the bed level below the instrument at a frequency of 10 Hz. The acoustic backscatter intensity of the ADV was used to derive the turbidity and changes in the *SPM* concentration. Water samples (200–250 ml) were taken during the experiments to calibrate the turbidity measurements. The samples were filtered through pre-weighed glass microfiber filters, oven-dried at 105 °C for 15 h and weighed. The *SPM* concentration could be determined from the sediment mass trapped on the filter and the volume of the water sample. For every experiment, an exponential fit of the form *SPM = a * exp(b * BS)* was obtained to relate the backscatter intensity *BS* (dB) at 1.0 cm above the bed to the *SPM* concentration (mg l^{-1}), with an average fit of R^2 = 0.91.

6.2.3 Data analysis

When the erosion threshold is exceeded, medium to fine sand starts moving as bedload, whereas silty particles are mostly suspended directly. Measuring the bedload transport using sediment samplers or traps or the tracking of individual particles is not practicable in the narrow annular flume. Hence, in addition to *SPM* (indicating particle transport in suspension at a height of 1.0 cm above

the bed), a method was developed to evaluate the "bed mobility" from the ADV data (indicating bed movement underneath the ADV).
When interpreting the bed level data from the ADV, we can distinguish two different boundaries: 1. The sediment-fluid interface or bed surface and 2. the "bottom" as detected by the instrument.

1. The sediment-fluid interface is located at the depth with the maximum change in acoustic backscatter ($\partial BS/\partial z$ = max), i.e. where a clear boundary between the water column (low backscatter) and the sediment bed (high backscatter) is visible. As this boundary is derived from the flow velocity data, it is similarly sampled at 50 Hz. In the velocity profiles presented in this study, the location of the sediment-fluid interface is defined as datum (z = 0).

2. The "bottom", as sampled by the profiling ADV at a rate of 10 Hz, is the depth with the strongest acoustic backscatter (BS = max), i.e. the location of the maximum bulk density, within the predefined measurement range. The bottom distance, i.e. the distance between the instrument's central transmitter and the bottom, can be used to determine changes of the sediment bed during the experiment. As a proxy for the bed mobility, the (moving) variance of the bottom was calculated:

$$\sigma_b^2 = \frac{1}{N-1}\sum_{i=1}^{N}(d_{bi} - \overline{d_b})^2 \qquad [6.2]$$

where σ_b^2 (m^2) is the bottom variance, N (-) is the number of measurements, d_{bi} (m) is the bottom distance and $\overline{d_b}$ (m) is the mean bottom distance averaged over the entire duration of the experiment.
To exemplify the onset of particle mobilization during the experimental run and the critical velocity U_{cr} for the initiation of sediment motion, the *moving* variance of the bottom distance ($\sigma_{b,mov}^2$) was calculated over a span of N = 20 values (i.e. a sampling time of 2 s). The critical velocity U_{cr} is defined as the minimum velocity that is required for the moving variance to exceed 0.025 mm^2. Using the moving variance, we classified the mobility of the sediment in two types: minor movement ($\sigma_{b,mov}^2 \leq$ 0.1 mm^2) and major movement ($\sigma_{b,mov}^2 >$ 0.1 mm^2).
As an absolute measure of the bed mobility, a *normalized* variance was determined that is independent of the flow velocity or the duration of the experiment. For each velocity interval, the bottom variance $\sigma_{b,int}^2$ was calculated according to equation 6.2 using the bottom distance record over a time span of 15 min (i.e. N = 9000). The mobility from each interval was then normalized, dividing it by the average flow speed of the respective interval, and the time span covered. The resulting mobility values from each interval were averaged to receive one normalized value for the mobility of the bed:

$$\sigma_{b,norm}^2 = \frac{1}{n_{int}}\sum\frac{\sigma_{b,int}^2}{U_{int}\cdot t} \qquad [6.3]$$

where $\sigma_{b,norm}^2$ (m) is the normalized bottom variance as a proxy for the bed mobility, n_{int} (-) is the number of flow speed intervals covered, $\sigma_{b,int}^2$ (m^2) is the bottom variance calculated over one flow speed interval, U_{int} (m s^{-1}) is the average flow speed in the respective interval, and t (s) is the

duration of the interval (i.e. 900 s). This method allows adequate comparison of our data with experiments in different flow environments.

The velocity data was despiked using the phase-space thresholding method developed by Goring and Nikora (2002) and poor quality data (beam correlations < 60 %, signal-to-noise ratios SNR < 12) were discarded. The velocities were averaged over the last 10 min of each 15-min interval to obtain one velocity profile for every flow velocity *U*. The bed shear-stress was calculated from the averaged velocity data from the boundary layer using the turbulent kinetic energy (*TKE*) method after Kim et al. (2000):

$$TKE = \frac{1}{2}\rho \cdot \left(\overline{u_x{}'^2} + \overline{u_y{}'^2} + \overline{u_z{}'^2}\right) \quad [6.4]$$

$$\tau_0 = C_1 \cdot TKE \quad [6.5]$$

where *TKE* (N m^{-2}) is the turbulent kinetic energy, ρ (kg m^{-3}) is water density, u_x', u_y' and u_z' (m s^{-1}) are the flow velocity fluctuations in stream-wise, cross-stream and vertical directions, respectively, and τ_0 (N m^{-2}) is the bed shear-stress. The bed shear-stress is related to *TKE* through a constant C_1 = 0.19 (Soulsby, 1983).

6.3 Results

6.3.1 Bed mobility

The mobility of the sediment bed differed significantly between experimental runs with various *RD*. The moving variance of the bottom level (Figure 6.1) indicates that in experiment N_0 with a unimodal sediment bed, minor bed movement ($\sigma^2_{b,mov} \leq 0.1$ mm^2) occurred during the first 10 velocity intervals of the experiment with larger peaks at *U* = 15.2 m s^{-1}. Major movement ($\sigma^2_{b,mov} > 0.1$ mm^2) started at *U* = 21.1 cm s^{-1} and continued until the end of the experiment (Figure 6.1a). In experiment N_2 with a low grain-size ratio, we see minor movement during the whole experimental run, with some separate peaks at *U* = 5.5 cm s^{-1} and *U* = 17.2–21.1 cm s^{-1} (Figure 6.1b). At *U* = 23.0 cm s^{-1} further erosion occurred and movement persisted throughout the interval. The mixed bed $N_{3.5}$ with *RD* = 3.5 experienced bed movements throughout the whole experimental run, with major changes in bottom level starting at flow speeds of *U* = 7.4 cm s^{-1} and continuing up to *U* = 21.1 cm s^{-1} (Figure 6.1c). Bed movement declined again during the interval with the largest flow speed. $N_{7.7}$ did barely show any considerable bed movement during large parts of the experiment but only minor changes of the bottom level at very high flow speeds (*U* = 21.1–23.0 cm s^{-1}, Figure 6.1d).

Analogue to the moving variance, the normalized variance of the bottom level shows that the mobility of the mixed N_2 treatments was similar to the mobility of the unimodal bed N_0, even though slightly lower (Figure 6.2): While the normalized bottom variance in N_0 ranged from $1.2 \cdot 10^{-10}$ m to $3.8 \cdot 10^{-10}$ m, the values in N_2 ranged from $7.8 \cdot 10^{-11}$ m to $2.4 \cdot 10^{-10}$ m (Table 6.1). All mixed $N_{3.5}$ treatments were considerably more mobile than the unimodal bed, with variances ranging from $8.8 \cdot 10^{-10}$ up to $1.3 \cdot 10^{-8}$ m (Table 6.1). $N_{7.7}$ was the most stable sediment: the bottom variance of

$1.4 \cdot 10^{-11}$ m is about one magnitude lower than in the reference case N_0 and two magnitudes below that of $N_{3.5}$ (Figure 6.2, Table 6.1).

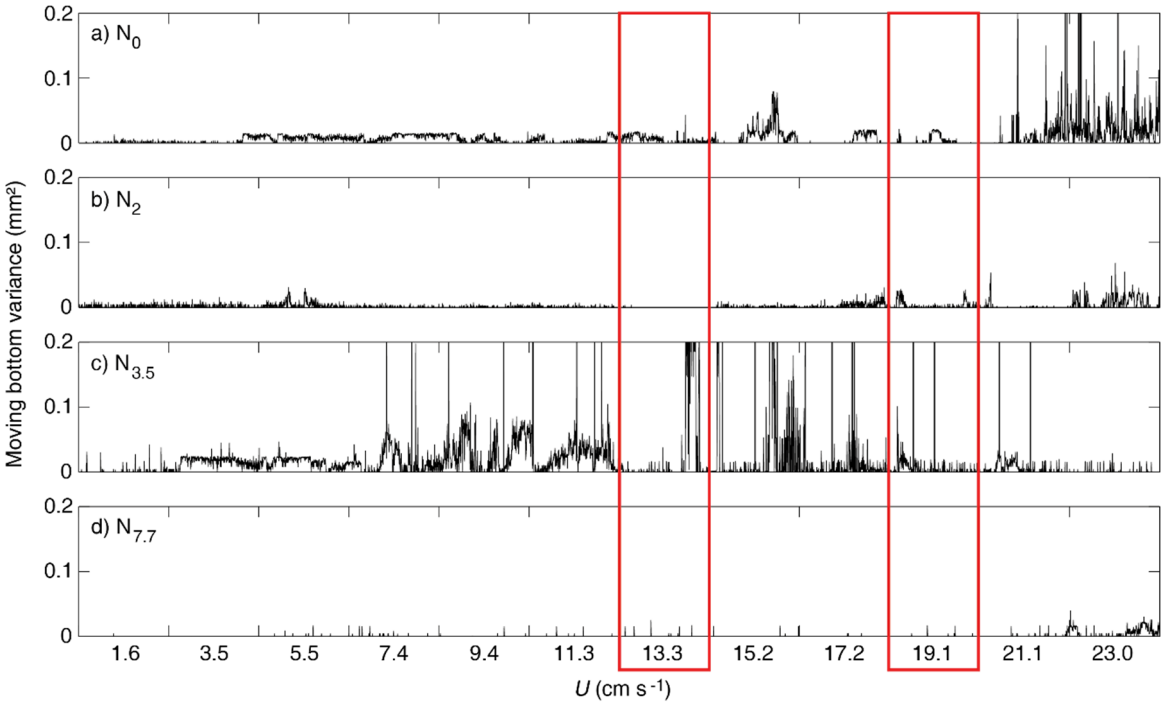

Figure 6.1: Moving bottom variance as a proxy for the onset of bed mobilization, for a) the unimodal reference bed N_0 (389 µm) and the three mixed beds: b) N_2 (393/193 µm), c) $N_{3.5}$ (387/111 µm) and d) $N_{7.7}$ (410/53 µm). The red boxes mark the two intervals from which the velocity profiles (Figure 6.4) were extracted. More information on the different sediment treatments is summarized in Table 6.1.

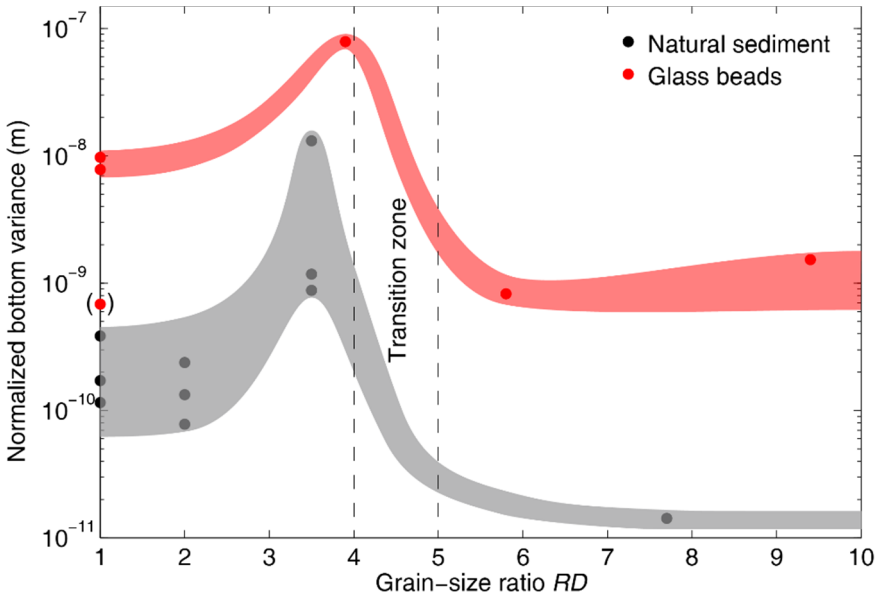

Figure 6.2: Normalized bottom variance (logarithmic scale), i.e. bed mobility, with varying grain-size ratio. Shown are the values for natural sediment in black and for glass beads in red. The shaded grey and red areas indicate the proposed trend of mobility with changing RD for natural and artificial sediment. The value in brackets is regarded as an outlier, as the glass beads were not remixed properly before this experiment. The transition between mobilization and stabilization (relative to the stability of the unimodal bed) occurs at RD = 4 – 5.

The results presented in the bottom level records (Figure 6.1 and 6.2) are to a certain extent reflected in the *SPM* data (Figure 6.3). The curve for the unimodal reference experiment N_0 shows a slight, stepwise growth in *SPM* with every increase of the flow speed starting at U = 7.4 cm s^{-1}. A significant rise occurs at U = 21.1 cm s^{-1}, followed by a decline at U = 23.0 cm s^{-1}. The sudden increase in *SPM* indicates bed failure and entrainment of coarse particles with subsequent transport in suspension, analogue to the major bed movement at U = 21.1 cm s^{-1} as seen in Figure 6.1a. The *SPM* concentration in the mixed treatment N_2 increased with a similar, stepwise slope as N_0, but only rose steeply at the end of the last interval, coinciding with the particle movement at U = 23.0 cm s^{-1} in Figure 6.1b. The data from experiment $N_{3.5}$ shows a stepwise *SPM* growth starting at U = 7.4 cm s^{-1} which is analogue to the major changes in bottom level during the experiment (Figure 6.1c). The maximum *SPM* concentration stayed below the values from N_0 and N_2. Although $N_{7.7}$ had a very low bottom variance and only a minor onset of bedload transport in the last two flow speed intervals (Figure 6.1d), the *SPM* record of $N_{7.7}$ shows an almost exponential increase during the second half of the experiment ($U \geq$ 7.4 cm s^{-1}). The maximum *SPM* concentration exceeded the values from experiments N_0 and $N_{3.5}$ and was similar to the maximum concentration in N_2.

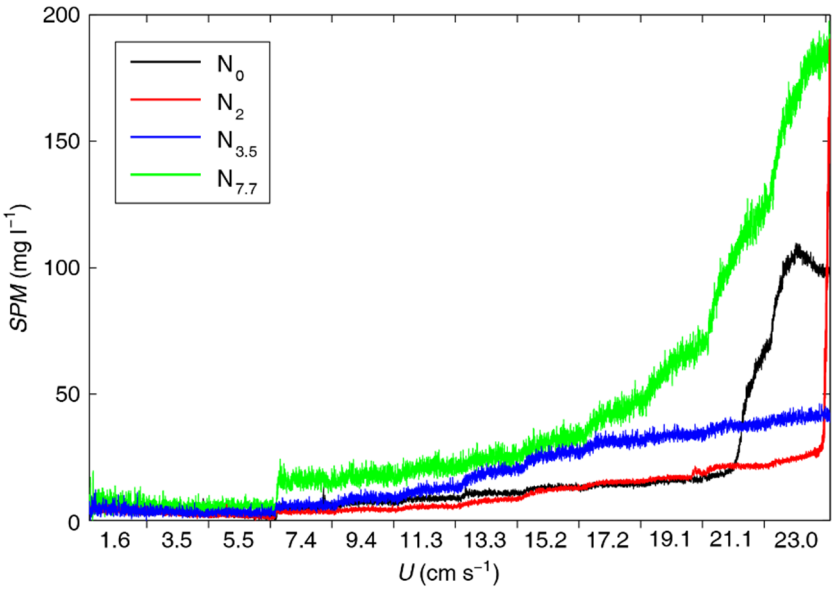

Figure 6.3: SPM concentration with increasing flow velocity U for the different sediment treatments.

6.3.2 Hydrodynamics

For two flow velocities ($U \approx$ 13 cm s^{-1} and $U \approx$ 19 cm s^{-1}, as indicated by red boxes in Figure 6.1), the near-bed hydrodynamics above the different grain-size combinations are compared (Figure 6.4a and b). At $U \approx$ 13 cm s^{-1} (Figure 6.4a), the profiles above the unimodal N_0 and the mixed bed N_2 resemble each other in the lower 2-3 mm, indicating a higher roughness than in the other experiments $N_{3.5}$ and $N_{7.7}$. The flow velocity at the bed surface (z = 0) was approximately zero in both experiments (Table 6.1). In the water column at z > 3 mm, the flow in N_0 exceeded the flow from N_2 by about 5 %. In the mixed experiment $N_{3.5}$, *u(z=0)* was visibly higher than in the other

experiments (Table 6.1) and at a height of z = 3 mm above the bed, the profile converges with that of N_2. At the bed surface of treatment $N_{7.7}$, the flow velocity was very low (comparable to N_0 and N_2, Table 6.1). Above the bed, the velocity increased sharply (u = 5.9 cm s^{-1} at z = 1 mm) but only reached $u \approx$ 12.7 cm s^{-1} in the water column.

At the higher flow velocity $U \approx$ 19 cm s^{-1} (Figure 6.4b) we obtained profiles with a comparable shape: The curves of N_0 and N_2 indicate a slightly higher roughness and a boundary layer of 2-3 mm. At the bed surface of $N_{3.5}$, a flow of $u(z=0)$ = 1.5 cm s^{-1} was measured. For $N_{3.5}$ at $U \approx$ 13 cm s^{-1} this trend of $u(z=0) > 0$ is visible in 1 out of 3 replications, at $U \approx$ 19 cm s^{-1}, it is visible in 2 out of 3 replications (Table 6.1). At $U \approx$ 19 cm s^{-1}, the flow profile of $N_{7.7}$ shows an increased flow velocity of $u(z=0)$ = 2 cm s^{-1} at the bed surface as well.

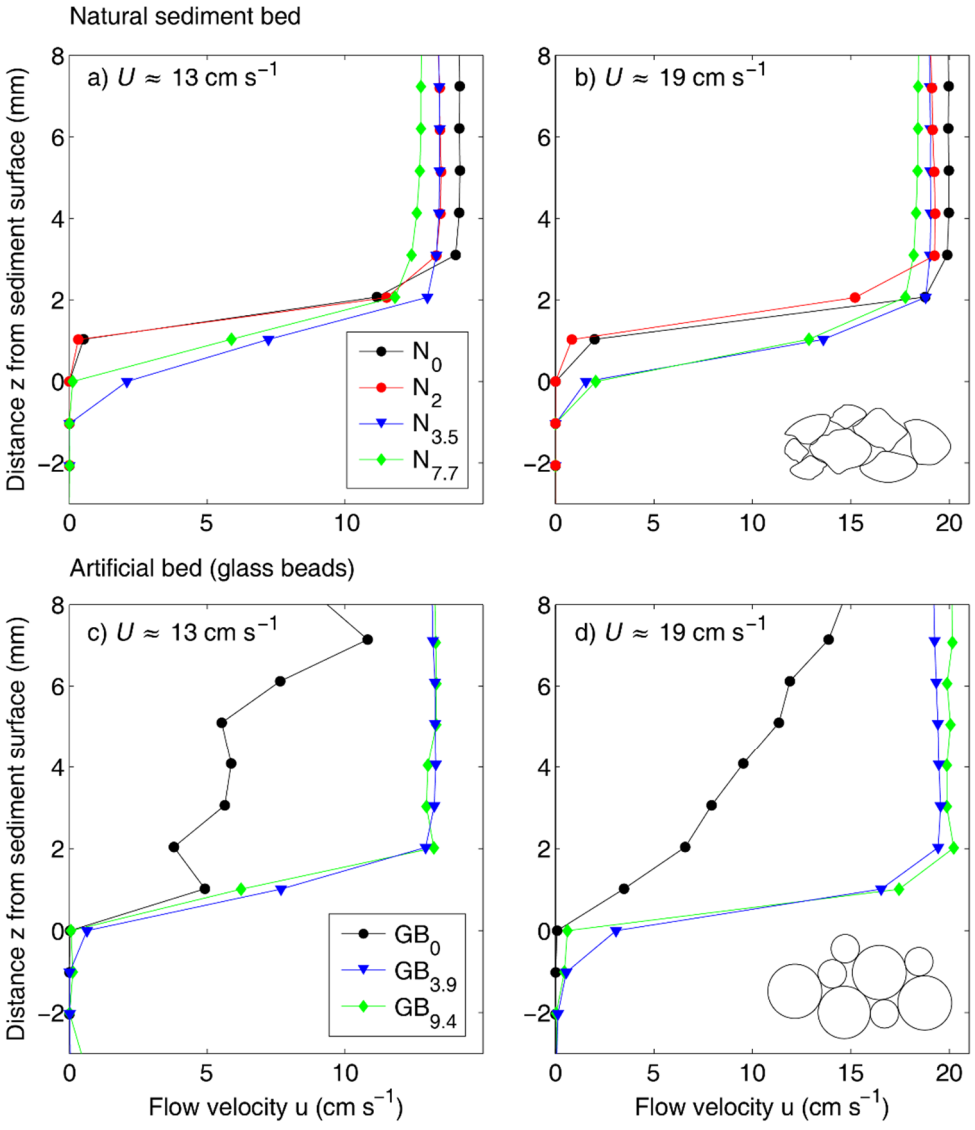

Figure 6.4: Near-bed flow profiles above beds comprised of different materials with different RD, at two flow velocities: a) Flow profile at U ≈ 13 cm s^{-1} above the natural sediment beds, b) flow profile at U ≈ 19 cm s^{-1} above the natural sediment beds, c) flow profile at U ≈ 13 cm s^{-1} above the glass beads and d) flow profile at U ≈ 19 cm s^{-1} above the glass beads.

The bed shear-stress τ_0 in relation to the flow velocity is presented in Figure 6.5. In the unimodal reference case N_0, τ_0 increased approximately linearly with increasing flow velocity up to U = 19.1 cm s^{-1}, then rose abruptly to τ_0 = 0.22 N m^{-2}. The bed shear-stress in N_2 had a similar trend but no steep increase at high flow velocities, instead τ_0 levelled off at about 0.05 N m^{-2} at the highest flow speed. For the other mixed experiments $N_{3.5}$ and $N_{7.7}$, the bed shear-stress was similar to N_0 and N_2 at flow velocities up to $U \approx$ 10 cm s^{-1}. At $U >$ 10 cm s^{-1}, both curves slightly deviate from the other experiments and show lower slopes than N_0 and N_2. Similar to N_2, a stepwise increase in τ_0 is visible at U = 21.1 cm s^{-1} in both $N_{3.5}$ and $N_{7.7}$, before the curve stabilizes at about τ_0 = 0.04 N m^{-2} ($N_{3.5}$) or slightly declines ($N_{7.7}$) at the highest flow speed. In $N_{7.7}$, the bed shear-stress remained below the values from all other experiments.

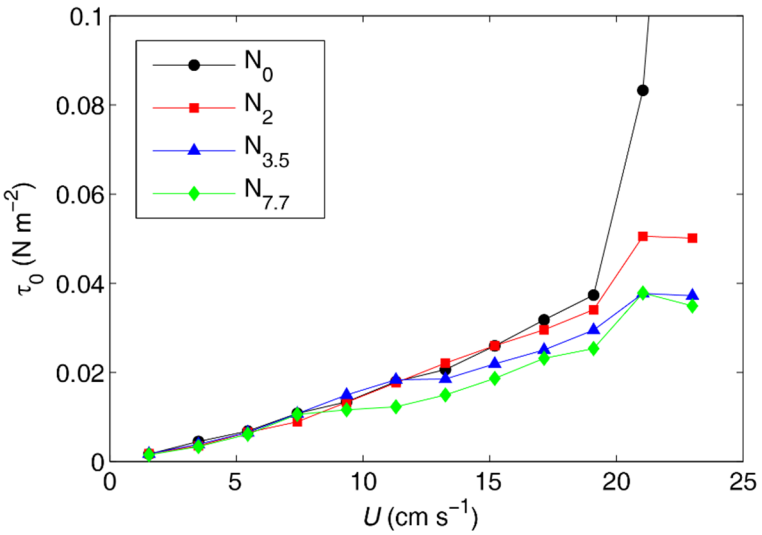

Figure 6.5: Bed shear-stress τ_0 for the different sediment treatments with increasing flow velocity U.

6.3.3 Comparison with spherical glass beads

In this section, we compare the mobility (i.e. normalized variance of the bottom level) and hydrodynamics from the experiments with glass beads with the data from the experiments with natural sediment (as presented in 6.3.1 and 6.3.2). The grain size of the coarse fraction was similar in both experimental series (367–410 µm), whereas the grain size of the fines (and thus, the grain-size ratios of the mixed beds) varied slightly (Table 6.1). With regard to the hydrodynamic regime, we focus on the unimodal reference experiments (natural sediment N_0 with D_{50} = 389 µm and glass beads GB_0 with D_{50} = 367 µm), the beds with a low grain-size ratio ($N_{3.5}$ with D_{50} = 387/111 µm and $GB_{3.9}$ with D_{50} = 367/93 µm) and the beds with a high grain-size ratio ($N_{7.7}$ with D_{50} = 410/53 µm and $GB_{9.4}$ with D_{50} = 367/39 µm). A direct analogue to the natural bed N_2 with RD = 2 is not available in the glass-bead experiments. A full description of the results of the mobility experiments with glass beads can be found in chapter 4.

The mobility of the glass beads, as represented by the normalized bottom variance, showed a trend that is similar to the mobility of the natural sediment (Figure 6.2). Relative to the unimodal reference bed GB_0, the first glass-bead mixture with a low grain-size ratio ($GB_{3.9}$ with *RD* = 3.9) was more mobile, analogue to the natural bed $N_{3.5}$. A further increase of *RD* ($GB_{5.8}$ and $GB_{9.4}$) led to a higher bed stability than in the reference case, analogue to $N_{7.7}$. In general, the artificial sediment consisting of glass beads was more mobile ($\sigma^2_{b,norm}$ is ≈ 2 magnitudes higher) than the natural sediment, indicated by the vertical offset of the mobility curve in Figure 6.2.

Examining the flow profiles at $U \approx 13$ and 19 cm s^{-1}, we can see that especially the velocities above the unimodal, natural sediment N_0 (Figure 6.4a–b) were different from those above the unimodal glass beads GB_0 (Figure 6.4c–d). The flow profiles of N_0 indicate a confined boundary layer, similar to N_2 and only slightly higher than the boundary layers of the mixed treatments $N_{3.5}$ and $N_{7.7}$ (Figure 6.4a–b). In contrast, the flow profile above the unimodal glass-bead bed GB_0 is approximately logarithmic (although some velocity fluctuations with height are visible in the profile at $U \approx 13$ cm s^{-1}), and the boundary layer has a height of more than 8 mm (Figure 6.4c–d). The boundary layer above the mixed experiments $GB_{3.9}$ and $GB_{9.4}$ is considerably thinner (≈ 2 mm) and the flow velocities in the water column are very similar to each other. At the bed surface however, the mobile bed $GB_{3.9}$ experienced higher flow velocities than the stable bed $GB_{9.4}$ (Table 6.1).

6.4 Discussion

6.4.1 Bed mobility

In our flume experiments, the unimodal reference bed N_0 and the mixed bed N_2 with *RD* = 2 behaved similarly, showing erosion especially at higher flow velocities ($U \geq 15$ cm s^{-1}). Treatment $N_{3.5}$ was one magnitude more mobile than N_0 and N_2, whereas the mobility of $N_{7.7}$ was one magnitude lower than the mobility of the reference bed. Based on the results we hypothesize that at a small grain-size ratio (*RD* ≤ 2), a mixed sediment bed composed of two major grain-size fractions behaves like a unimodal bed (N_2 and N_0). We call this the *unimodal case*. Starting at a grain-size ratio of *RD* > 2, the mobility of a natural bed changes with the grain-size ratio. A mixed bed with a grain-size ratio larger than 2 but smaller than approximately 4 is more mobile than a unimodal bed ($N_{3.5}$), this is named the *mobilizing case*. At this grain-size ratio, the fines facilitate particle entrainment and more bedload transport. Although we lack information for the mobility of the natural bed at *RD* = 4–7, we assume that the mobility declines rapidly at *RD* = 4–5, analogue to the mobility of glass beads (Figure 6.2), and that the bed behaviour changes from mobilization to stabilization. The mixed bed with a high *RD* is more stable than a unimodal bed, representing the *stabilizing case* ($N_{7.7}$). In this scenario, the presence of fines leads to the stabilization of the bed, i.e. less entrainment and bedload transport. These hypotheses agree with the trend we found in glass-bead mixtures with a similar fine-grained content of ≈ 40 %, as shown in Figure 6.2.

The bottom level records from the unimodal experiment N_0 and the mixed experiment N_2 with the lowest grain-size ratio show comparable periods of (minor) bed movement (Figure 6.1) and similar values for the normalized mobility (Figure 6.2). With an increase in grain-size ratio to *RD* = 3.5 in $N_{3.5}$, the moving variance (Figure 6.1) indicates considerable particle movement during the complete duration of the experiment, as the bed became more mobile. This behaviour is comparable to the glass-bead experiments with low *RD* (3.9) and observations from other laboratory experiments with gravel and sand (e.g. Venditti et al., 2010a; Houssais and Lajeunesse, 2012) with low *RD* (2.7–3.1), where a mixed bed was more mobile than a unimodal bed, or a pulse of fine sediment facilitated entrainment of a coarser bed. It has to be noted that in the studies of Venditti et al. (2010a) and Houssais and Lajeunesse (2012), the grain sizes were in the mm range and flow characteristics were similar to flow over a riverbed, with a shallow flow depth, high flow velocities ($U_{max} \approx 1$ m s^{-1}) and fully turbulent flow, i.e. bed shear-stresses were significantly higher than in our flume experiments.

Treatment $N_{7.7}$ with the highest grain-size ratio was the most stable bed, comparable to the glass-bead experiments with a high grain-size ratio of *RD* = 5.8 and 9.4. A similar behaviour was also observed in experiments with sand-silt mixtures (e.g. Bartzke et al., 2013) with little to no cohesion and *RD* = 5.5. Bartzke et al. (2013) hypothesized that the fines form stabilizing network structures around the coarse grains, in agreement with the concept developed by van Ledden et al. (2004). Similar to our flume experiments, the median grain sizes in the study of Bartzke et al. (2013) were below 0.5 mm. The flow characteristics were comparable to our flume environment, with a large water depth relative to grain size, relatively low flow velocities, and bed shear-stresses ranging from about 0.01 to 1 N m^{-2}.

The described concept of bed mobility applies for sediment mixtures with small grain sizes (≤ 410 µm) and 40 % fines in a flume environment with unidirectional flow ($U \leq 23$ cm s^{-1}). The previous experimental series with glass beads had shown that even with a lower fine content (10-20 %), a clear difference in bed mobility between beds with various *RD* can be observed (chapter 4).

Our results prove that non-cohesive sand-silt beds with high *RD* can be stabilized through texture-induced network structures between fine and coarse grains, as hypothesized by van Ledden et al. (2004). In addition, we could show that the mobilization of coarse bed material through the addition of fines, as observed e.g. in gravel-bedded rivers, can occur in finer, sandy beds with low *RD*. However, coarse gravel beds cannot be stabilized through the addition of fine material. In shallow river streams, i.e. under fully turbulent, near critical or supercritical flow conditions, the fine material will be winnowed out almost immediately, resulting in the development of a coarse bed armouring (Andrews and Parker, 1987), or will lead to increased mobilization of coarser bed material (as shown by Jackson and Beschta, 1984; Iseya and Ikeda, 1987; Wilcock et al., 2001 and others).

6.4.2 Bed shear-stresses and near-bed hydrodynamics

The addition of fine material to the unimodal bed led to a decrease in bed shear-stress (Figure 6.5). It is noticeable that the smaller the added fine grains, the lower the bed shear-stress became (experiment $N_{7.7}$ with 40 % of 53 µm fines shows the lowest bed shear-stress). The fine particles fill the gaps between the coarser particles (if they are small enough relative to the coarse particles, i.e. if *RD* is high enough), thus reducing the bed surface roughness. This process leads to a reduction of *TKE* and bed shear-stress. A similar decrease of *TKE* with decreasing surface roughness was observed in laboratory studies that analysed turbulences and flow velocities above a gravel bed after the input of (a pulse of) fine sediment (e.g. Sambrook Smith and Nicholas, 2005; Venditti et al., 2010a; Wren et al., 2011). Sambrook Smith and Nicholas (2005) described in detail how the infilling of pockets on a gravel bed leads to a reduction in vertical flow, turbulent kinetic energy and near-bed velocity downstream of "peaks" in the bed topography.

Along with the reduction of the bed shear-stress in $N_{3.5}$ and $N_{7.7}$, the flow velocities at and just above the bed surface (z = 0–1 mm) were higher than in N_0 and N_2 (Figure 6.4a–b, Table 6.1). The similar mobility of the unimodal bed N_0 and treatment N_2 with a low *RD* (Figure 6.2) is reflected in the hydrodynamic data: The flow profiles (especially at $U \approx 13$ cm s^{-1}, Figure 6.4a) and the higher bed shear-stresses (Figure 6.5) indicate the higher roughness of N_0 and N_2 relative to the other mixed beds. In $N_{3.5}$ and $N_{7.7}$ the fine 111 µm- and 53 µm-grains were small enough to "hide" in the gaps between the coarse grains on the bed surface, decreasing the roughness. Although the beds behaved contrarily, only a slight difference in the flow profiles above the very stable ($N_{7.7}$) and the very mobile bed ($N_{3.5}$) is visible. The sediment bed in $N_{3.5}$ was very mobile during the complete experiment with major movement starting at low flow velocities (Figure 6.1). The high flow velocities at the bed surface at $U \approx 13$ cm s^{-1} and $U \approx 19$ cm s^{-1} (Figure 6.4a–b) support the mobility result. Flow was able to enter the bed at moderate flow velocities, leading to early particle entrainment and erosion. This indicates that the blocking of the pore space (Bartzke and Huhn, 2015; Bartzke et al., 2013) is not possible if *RD* is too low. A similar correlation is visible in the data of the glass-bead experiments, where the mobile bed $GB_{3.9}$ experienced the highest bed surface flow velocity *u(z=0)* (Figure 6.4c–d, Table 6.1). $N_{7.7}$ remained comparatively stable during the whole experiment. Analogue to the records of bed movement (Figure 6.1) which show no major peaks up to a flow of U = 21.1 cm s^{-1}, no flow at the bed surface was measured at $U \approx 13$ cm s^{-1} (Figure 6.4a). Minor bottom level changes occur at U = 21.1–23.0 cm s^{-1} (Figure 6.1) which coincides with an increase in *u(z=0)* at $U \approx 19$ cm^{-1} (Figure 6.4b): The flow entered the upper bed layers and shortly thereafter the sediment bed started moving slightly (Figure 6.1). At lower flow velocities however, the fine particles stabilized the coarse particle matrix and inhibited inflow into the bed, agreeing with the concept of van Ledden et al. (2004) and the hypotheses of pore-space blocking by Bartzke et al. (2013) and Bartzke and Huhn (2015).

Although the addition of fine material seems to have an influence on the bed shear-stress and the flow velocity at the bed surface of the natural sediment, the flow velocities at larger distances from

the bed (z = 5 mm) do not follow the expected pattern: the flow above the unimodal bed N_0 is faster than above the mixed beds, whereas the flow above $N_{7.7}$ is lowest (Figure 6.4a–b, Table 6.1).

6.4.3 Effects of particle shape

Irrespective of the grain-size ratio, the natural sediment was more stable than the spherical glass beads. We hypothesize that this difference in mobility arises from the different particle sphericity and angularity, in agreement with several studies investigating the frictional strength of sediment in relation to the particle shapes (e.g. Mair et al., 2002; Guo and Morgan, 2004; Kock and Huhn, 2007). Mair et al. (2002) used shear tests to investigate the frictional strength of both spherical glass beads and angular quartz grains, concluding that the angularity and roughness of the quartz grains significantly increased the frictional strength of the bed. These findings can be transferred to flow conditions: The smooth, spherical glass beads have a very low friction and start sliding or rolling easily when the drag force outweighs the particle's resisting force. In contrast, beds consisting of more complex particles with a jagged, rough surface, like the sand and silt used in this study, have a higher intergranular friction (particle interlocking) that has to be overcome to initiate particle motion. We conclude that the gap between the two mobility curves in Figure 6.2 accounts for this difference in particle complexity and intergranular friction.

The comparison of the flow profiles of both the glass-bead experiments and the experiments with natural sediment suggests that the particle shape also has an influence on the near-bed flow velocity (Figure 6.4). The flow velocity above the unimodal bed GB_0 increased logarithmically, indicating a higher roughness compared to the mixed glass bead and the natural sediment beds. The bed roughness results in higher turbulences above the bed and the development of a logarithmic boundary layer. Only with the addition of a sufficient amount of fine particles – that are small enough to fill the pockets between the coarse particles (high RD) – the bed roughness decreases and the near-bed flow velocities increase.
In contrast, the flow above the unimodal bed N_0 consisting of complex, angular grains is faster than the flow above the coarse, spherical particles. Based on this, we assume that although the individual sand and silt grains are more complex than the smooth glass beads, the bed surface of N_0 has a lower roughness than GB_0: The angular sand grains form a relatively smooth bottom compared to the spherical glass beads, thus *TKE* and bed shear-stress are reduced and the near-bed flow is relatively fast. We therefore postulate that, in addition to *RD*, the shape of individual particles influences the micro-scale turbulence above the bed. However, the small-scale investigation of the bed roughness is beyond the scope of this study. Further high-resolution laboratory measurements or the development of a small-scale numerical model of turbulent flow are necessary to assess the bed roughness and to further elucidate its effects on the flow above a sediment bed.

6.4.4 Assessment of the bed mobility using the variance of the bottom level

The moving variance and the normalized variance of the bottom level served as useful proxies for bed mobility. For mixed beds containing a variety of grain sizes that are not directly transported in

suspension but at least partly move as bedload, this method can be a useful addition for the assessment of erosion. However, the method requires further development, e.g. the calibration with bedload samples to obtain a volumetric transport rate.

In studies investigating the behaviour of a variety of grain sizes, e.g. mixed sand-silt beds, a combination of *SPM* and changes of the sediment bed is beneficial to assess the onset of bed mobilization. In contrast to *SPM* concentration (and erosion rate derived from *SPM*) which is used as an indicator for the erosion of fine sediment in many studies (e.g. Amos et al., 1992; Widdows et al., 1998b; Andersen, 2001; Andersen et al., 2005), the onset of mobilization of sandy particles can be determined more accurately using changes of the sediment bed. In our experiments both measurements were combined to draw plausible conclusions for the stability of the bed. The *SPM* concentration alone can be misleading when trying to define an erosion event from our data: While $N_{7.7}$ was the most stable bed (low variance of the bottom level, Figure 6.1 and 6.2), the final *SPM* concentration was much higher (≈ 200 mg l^{-1}) than in the other experiments (Figure 6.3). We assume that the reason for the high turbidity was the early entrainment and dispersion of a small quantity of very fine 53 µm-particles from the bed surface. However, the mixed bed of coarse and very fine particles remained stable up to high flow velocities (only minor bed movement, Figure 6.1). In contrast to this, the final *SPM* concentration of the very mobile experiment $N_{3.5}$ was comparatively low. Although the bed experienced extensive bed-level changes (particles moving visibly, high variance of the bottom level, Figures 6.1 and 6.2), the *SPM* concentration did not exceed 50 mg l^{-1} because the entrained 111 µm-particles moved as bedload mostly.

6.5 Conclusion

In this paper we describe erosion experiments with natural, bimodal sediment (D_{50} ≤ 410 µm) that were conducted in an annular flume under unidirectional flow (U ≤ 23.0 cm s^{-1}). Based on the results, we can draw the following conclusions:

- The behaviour of bimodal beds consisting of natural sediment with a large fine fraction (40 %) changed considerably depending on the grain-size ratio $RD = D_{50,coarse}/D_{50,fine}$. The sediment behaviour can be classified in three cases: The *unimodal* case: The behaviour of a bed with a low grain-size ratio (RD ≤ 2) is similar to that of a unimodal reference bed. The *mobilizing* case: At RD > 2 the mobility of the bed increases with the grain-size ratio, until at RD = 3.5 it is one magnitude higher than the mobility of the unimodal bed, i.e. the bed is more mobile. At RD > 3.5 the mobility of the bed declines steeply and we hypothesize that a transition between the mobilizing and the stabilizing case occurs at RD = 4–5. The *stabilizing* case: At a grain-size ratio RD > 4.5 the bed becomes more stable and at RD = 7.7 the mobility is one magnitude lower than the unimodal bed. These findings are similar to the behaviour of spherical glass beads with comparable grain sizes and RD, although the glass beads are generally more mobile. For glass beads the transition between mobilizing and stabilizing behaviour was found at RD ≈ 5.

- The near-bed flow velocities at different stages during the experiment could be connected to the bed mobility. High flow velocities at the bed surface (z = 0) indicate that flow is entering the sediment matrix and subsequently particles are entrained. We propose that the relative size of the grains on the bed surface leads to differences in near-bed hydrodynamics. A unimodal sediment bed or a mixed bed with a low *RD* is comparatively rough. Flow above the bed is turbulent, bed shear-stress high, and grains exposed to the flow can be entrained easily. The addition of finer material to the bed leads to a reduction of the bed roughness length and the bed shear-stress. The higher the *RD* is, the lower the bed shear-stress becomes, as fine particles fill the surface gaps in between the coarse particles. At a high *RD* less flow is entering the sediment matrix and erosion is reduced.
- The shape of the individual particles of a bed plays an additional role for the bed stability. With increasing particle complexity and roughness, the bed has a higher intergranular friction and stability than a bed made up of smooth, spherical particles.
- Differences in the flow profiles suggest that a bed comprised of spherical particles has a higher roughness than a bed comprised of angular sand grains with similar D_{50}. Further research is necessary to investigate possible small-scale processes in the near-bed hydrodynamics depending on the particle shape.
- The results of this study can help to understand erosion and transport of non-cohesive sediment in aquatic environments. The findings can be used to evaluate the stability or mobility of bimodal sediment using information on the grain-size distribution and the particle complexity. Additional research is required to narrow down the critical *RD* for the transition between mobilization and stabilization. To verify the main findings for a wider range of conditions, similar experiments should be conducted with larger grain sizes (> 400 µm) and under different flow conditions.

Acknowledgements

This study was carried out within the framework of the International Research Training Group INTERCOAST for Integrated Coastal Zone and Shelf-Sea Research, which is funded by the German Research Foundation – DFG (project GRK 1598 – INTERCOAST). The authors would like to thank the staff at the Benthic Flow Laboratory at the University of Waikato for their assistance during the flume experiments, as well as Gerhard Bartzke for his feedback on the manuscript.

References

Amos, C.L., Grant, J., Daborn, G.R., Black, K., 1992. Sea Carousel - A Benthic, Annular Flume. Estuar. Coast. Shelf Sci. 34, 557–577.

Andersen, T.J., 2001. Seasonal variation in erodibility of two temperate, microtidal mudflats. Estuar. Coast. Shelf Sci. 53, 1–12. doi:10.1006/ecss.2001.0790

Andersen, T.J., Lund-Hansen, L.C., Pejrup, M., Jensen, K.T., Mouritsen, K.N., 2005. Biologically induced differences in erodibility and aggregation of subtidal and intertidal sediments: A possible cause for seasonal changes in sediment deposition. J. Mar. Syst. 55, 123–138. doi:10.1016/j.jmarsys.2004.09.004

Andrews, E.D., Parker, G., 1987. Formation of a Coarse Surface Layer as the Response to Gravel Mobility, in: Thorne, C.R., Bathurst, J.C., Hey, R.D. (Eds.), Sediment Transport in Gravel-Bed Rivers. John Wiley & Sons, Ltd, Chichester, p. 995.

Bartzke, G., Bryan, K.R., Pilditch, C.A., Huhn, K., 2013. On the Stabilizing Influence of Silt On Sand Beds. J. Sediment. Res. 83, 691–703. doi:10.2110/jsr.2013.57

Bartzke, G., Huhn, K., 2015. A conceptual model of pore-space blockage in mixed sediments using a new numerical approach, with implications for sediment bed stabilization. Geo-Marine Lett. 35. doi:10.1007/s00367-015-0399-1

Goring, D.G., Nikora, V.I., 2002. Despiking Acoustic Doppler Velocimeter Data. J. Hydraul. Eng. 128, 117–126. doi:10.1061/(ASCE)0733-9429(2002)128:1(117)

Grant, J., Bathmann, U.V., Mills, E.L., 1986. The Interaction between Benthic Diatom Films and Sediment Transport. Estuar. Coast. Shelf Sci. 23, 225–238.

Guo, Y., Morgan, J.K., 2004. Influence of normal stress and grain shape on granular friction: Results of discrete element simulations. J. Geophys. Res. 109, B12305. doi:10.1029/2004JB003044

Houssais, M., Lajeunesse, E., 2012. Bedload transport of a bimodal sediment bed. J. Geophys. Res. 117, F04015. doi:10.1029/2012JF002490

Iseya, F., Ikeda, H., 1987. Pulsations in bedload transport rates induced by a longitudinal sediment sorting: A flume study using sand and gravel mixtures. Geogr. Ann. Ser. A, Phys. Geogr. 69, 15–27.

Jackson, W.L., Beschta, R.L., 1984. INFLUENCES OF INCREASED SAND DELIVERY ON THE MORPHOLOGY OF SAND AND GRAVEL CHANNELS. Water Resour. Bull. 20, 527–533.

Jacobs, W., Le Hir, P., Van Kesteren, W., Cann, P., 2011. Erosion threshold of sand-mud mixtures. Cont. Shelf Res. 31, 14–25.

Kim, S.-C., Friedrichs, C.T., Maa, J.P.-Y., Wright, L.D., 2000. Estimating bottom stress in tidal boundary layer from acoustic Doppler velocimeter data. J. Hydraul. Eng. 126, 399–406.

Kock, I., Huhn, K., 2007. Influence of particle shape on the frictional strength of sediments — A numerical case study. Sediment. Geol. 196, 217–233. doi:10.1016/j.sedgeo.2006.07.011

Le Hir, P., Cann, P., Waeles, B., Jestin, H., Bassoullet, P., 2008. Chapter 11 Erodibility of natural sediments: experiments on sand/mud mixtures from laboratory and field erosion tests, in: Kusada, T., Yamanishi, H., Spearman, J., Gailani, J.Z. (Eds.), Sediment and Ecohydraulics: INTERCOH 2005. Elsevier B.V., pp. 137–153. doi:10.1016/S1568-2692(08)80013-7

Mair, K., Frye, K.M., Marone, C., 2002. Influence of grain characteristics on the friction of granular shear zones. J. Geophys. Res. 107, 2219. doi:10.1029/2001JB000516

Meadows, A., Meadows, P.S., Muir Wood, D., Murray, J.M.H., 1994. Microbiological effects on slope stability: an experimental analysis. Sedimentology 41, 423–435.

Mehta, A.J., Lee, S.-C., 1994. Problems in Linking the Threshold Condition for the Transport of Cohesionless and Cohesive Sediment Grain. J. Coast. Res. 10, 170–177.

Mitchener, H., Torfs, H., 1996. Erosion of mud/sand mixtures. Coast. Eng. 29, 1–25. doi:10.1016/S0378-3839(96)00002-6

Panagiotopoulos, I., Voulgaris, G., Collins, M.B., 1997. The influence of clay on the threshold of movement of fine sandy beds. Coast. Eng. 32, 19–43.

Paterson, D.M., Crawford, R.M., Little, C., 1990. Subaerial Exposure and Changes in the Stability of Intertidal Estuarine Sediments. Estuar. Coast. Shelf Sci. 30, 541–556.

Sambrook Smith, G.H., Nicholas, A.P., 2005. Effect on flow structure of sand deposition on a gravel bed: Results from a two-dimensional flume experiment. Water Resour. Res. 41, W10405. doi:10.1029/2004WR003817

Soulsby, R.L., 1983. The Bottom Boundary Layer of Shelf Seas, in: Johns, B. (Ed.), Physical Oceanography of Coastal and Shelf Seas. Elsevier, pp. 189–266.

Teisson, C., Ockenden, M., Le Hir, P., Kranenburg, C., Hamm, L., 1993. Cohesive sediment transport processes. Coast. Eng. 21, 129–162.

Torfs, H., Jiang, J., Mehta, A.J., 2001. Assessment of the erodibility of fine/coarse sediment mixtures, in: McAnally, W.H., Mehta, A.J. (Eds.), Coastal and Estuarine Fine Sediment Processes. Vol. 3. Proceedings in Marine Science. Elsevier, pp. 109–123. doi:10.1016/S1568-2692(00)80116-3

van Ledden, M., van Kesteren, W.G.. G.M., Winterwerp, J.. C., 2004. A conceptual framework for the erosion behaviour of sand–mud mixtures. Cont. Shelf Res. 24, 1–11. doi:10.1016/j.csr.2003.09.002

Venditti, J.G., Dietrich, W.E., Nelson, P.A., Wydzga, M.A., Fadde, J., Sklar, L., 2010a. Mobilization of coarse surface layers in gravel-bedded rivers by finer gravel bed load. Water Resour. Res. 46, W07506. doi:10.1029/2009WR008329

Widdows, J., Brinsley, M.D., Bowley, N., Barrett, C., 1998. A Benthic Annular Flume for In Situ Measurement of Suspension Feeding/Biodeposition Rates and Erosion Potential of Intertidal Cohesive Sediments. Estuar. Coast. Shelf Sci. 46, 27–38. doi:10.1006/ecss.1997.0259

Widdows, J., Brinsley, M.D., Salkeld, P.N., Lucas, C.H., 2000. Influence of biota on spatial and temporal variation in sediment erodability and material flux on a tidal flat (Westerschelde, The Netherlands). Mar. Ecol. Prog. Ser. 194, 23–37. doi:10.3354/meps194023

Wilcock, P.R., Kenworthy, S.T., Crowe, J.C., 2001. Experimental Study of the Transport of Mixed Sand and Gravel. Water Resour. Res. 37, 3349–3358.

Willows, R.I., Widdows, J., Wood, R.G., 1998. Influence of an infaunal bivalve on the erosion of an intertidal cohesive sediment: A flume and modeling study. Limnol. Oceanogr. 43, 1332–1343. doi:10.4319/lo.1998.43.6.1332

Wren, D.G., Langendoen, E.J., Kuhnle, R.A., 2011. Effects of sand addition on turbulent flow over an immobile gravel bed. J. Geophys. Res. Earth Surf. 116, 1–12. doi:10.1029/2010JF001859

Table 6.1: Bed properties, changes in bed morphology and near-bed flow velocities for all treatments.

		$D_{50,coarse}$ (µm)	$D_{50,fine}$ (µm)	Grain-size ratio	Fine-grained fraction (% dry weight)	Critical velocity U_{cr} (cm s^{-1}) for bed movement (i.e. moving variance ≥ 0.025 mm^2)	Normalized bottom variance $\sigma_{b,norm}^2$ (m)	Flow at bed surface *u(z=0)* (cm s^{-1}) at $U \approx 13$ cm s^{-1}	Flow at bed surface *u(z=0)* (cm s^{-1}) at $U \approx 19$ cm s^{-1}	Flow *u(z=5)* (cm s^{-1}) at control height z = 5 mm at $U = 19.1$ cm s^{-1}
Natural sediment										
N_0	1	389	-	-	-	15.2	1.16e-10	0.09	0.91	n.a.
	2					11.3	1.72e-10	0.26	0.02	16.13
	3					13.3	3.84e-10	0.00	0.01	19.97
N_2	1	393	193	2.0	40	9.4	1.33e-10	0.06	0.13	19.13
	2					5.5	2.38e-10	0.01	0.11	19.16
	3					5.5	7.80e-11	0.00	0.00	19.23
$N_{3.5}$	1	387	111	3.5	40	1.6	1.31e-08	0.06	0.13	19.59
	2					1.6	1.18e-09	0.09	0.76	18.78
	3					1.6	8.78e-10	2.09	1.55	19.03
$N_{7.7}$		410	53	7.7	40	23.0	1.42e-11	0.12	2.04	18.39
Glass beads										
GB_0	1	367	-	-	-	n.a.	7.81e-09	0.03	0.09	11.35
	2					n.a.	6.83e-10	1.98	0.04	10.69
	3					n.a.	9.72e-09	0.02	0.12	n.a.
$GB_{3.9}$		367	93	3.9	40	n.a.	7.88e-08	0.64	3.08	19.42
$GB_{5.8}$		367	63	5.8	40	n.a.	8.25e-10	n.a.	n.a.	n.a.
$GB_{9.4}$		367	39	9.4	40	n.a.	1.53e-09	0.06	0.61	20.05

7. Summary

7.1 Conclusions

In the following, the research questions from each chapter are addressed and answered.

Chapter 4 focused on the following research objective:

- What are the influences of a) the fine-grained fraction and b) the grain-size ratio $RD = D_{50,coarse}/D_{50,fine}$ on the near-bed flow and the mobility of a mixed bed composed of spherical particles?

The chapter described laboratory flume experiments with spherical glass beads. The erosion behaviour of mixed beds with different grain-size ratios (RD = 3.9, 5.8, 9.4) and various fine-grained fractions (10; 20; 40 % dry weight) was tested and compared with a unimodal reference bed. The experiments were successful in illustrating the influences of both the grain-size ratio and the fine fraction on the near-bed flow regime and the bed mobility.
The addition of fine material led to the acceleration of the flow above the mixed beds, indicating a decrease of bed roughness compared to the unimodal bed. The grain-size ratio controlled the further effects of the fine fraction on the bed mobility: The mixed beds with a similar amount of fine sediment behaved contrarily depending on RD. The beds with a low grain-size ratio ($RD \leq 3.9$) were *more mobile* than the unimodal bed, and a further rise in mobility occurred as the fine content was increased. Flow velocities right at the bed surface ($z = 0$) were relatively high, indicating inflow into the bed. It was hypothesized that the fine particles are too large in relation to the coarse particles (low RD), and thus cannot completely fill the pore space. Hence, the accelerated near-bed flow can enter the bed which leads to an increase in particle entrainment. The mixed beds with a high grain-size ratio ($RD \geq 5.8$) were *less mobile* than the unimodal reference bed, and the mobility declined as the fine content was increased. The flow velocities at the bed surface ($z = 0$) were relatively low, indicating that the inflow into the bed is inhibited. It was postulated that, if the fine particles are small enough in relation to the coarse particles (i.e. if RD is high), the pores between the coarser particles can be completely filled with fines, which leads to the reduction of the bed surface roughness, less inflow into the bed and thus a decrease of particle entrainment.
The results of chapter 4 suggest that the grain-size ratio governs the particle packing, subsequently controlling the inflow into the sediment bed and the resulting particle entrainment. However, although the development of flow instrumentation has advanced considerably and flow profiling is possible in the millimetre range, the flow data from chapter 4 is relatively coarse (resolution: 1 mm) in comparison to the used grain sizes (< 500 µm).

Based on the indications of small-scale processes at the bed surface governing the bed mobility (chapter 4), **chapter 5** aimed to answer the following research question:

- What is the influence of the grain-size ratio *RD* on micro-scale flow processes at the bed surface?

A high resolution numerical model was set up to investigate the small-scale processes at the surface and in the upper layers of a bed consisting of spherical particles, comparable to the glass beads used in chapter 4. In a series of numerical simulations with one unimodal and four mixed (*RD* = 4; 4.8; 6) particle packings, the flow through the numerical particle matrix was investigated. The model could successfully highlight the different micro-scale flow patterns in the various particle packings.
The model results indicate that the laminar flow in the upper millimetres of a bed changes with the grain-size ratio. A constant discharge through the upper layers of a packed particle bed, induced by the constant free stream current in the water column, is deflected around the particles, i.e. in cross-stream and vertical direction. If the flow cross section inside the bed is reduced, e.g. through the addition of fine particles, the flow velocities in the pore space (i.e. the matrix flow) increase. Subsequently, the flow velocities inside the mixed beds were higher than inside the unimodal bed. Furthermore, the flow through the mixed beds depended on the grain-size ratio: High cross-stream and vertical flow velocities were observed inside the bed with a low *RD* = 4 (i.e. larger D_{fine}), whereas lower cross-stream and vertical flow velocities occurred inside the bed with higher *RD* (i.e. smaller D_{fine}).
Based on the analysis of the 3D flow velocities, it was hypothesized that the high cross-stream and vertical flow velocities within a bed with a low $RD \leq 4$ could contribute to particle entrainment. This outcome supports the results from chapter 4, where a transition between stabilization and mobilization of a bed through the addition of fine material was found at *RD* = 3.9–5.8.

To validate the developed hypotheses of chapter 4 and chapter 5 for natural sediment, further flume experiments were conducted with sediment in the sand-silt range. **Chapter 6** answered the following research questions:

- What is the influence of the grain-size ratio *RD* on the near-bed flow and the mobility of a mixed bed composed of natural sediment?
- How does the particle shape affect the mobility of a mixed bed and the near-bed flow?

In the second experimental series the erosion behaviour of natural sand-sand and sand-silt mixtures with a large fine fraction (40 %) and various grain-size ratios (*RD* = 2; 3.5; 7.7) was tested and compared with a unimodal reference bed. The experiments showed that the mobility of natural, bimodal sediment beds with various grain-size ratios is similar to the behaviour of spherical glass beads. The mixed beds with a very low grain-size ratio (*RD* = 2) behaved similar to the unimodal beds. The mixed beds with a low grain-size ratio (*RD* = 3.5) were about one magnitude more mobile than the unimodal beds, whereas the bed with a high grain-size ratio (*RD* = 7.7) was significantly more stable than the other beds. It was postulated that the transition between mobilizing and

stabilizing behaviour of the bed occurs at $RD \approx 4.5$, analogue to the behaviour of the glass beads in chapter 4. High flow velocities at the bed surface at different stages during the experiment could be connected to events of bed mobilization. In addition, a decrease in bed shear-stress was observed with an increase in grain-size ratio. The changes in near-bed hydrodynamics indicate that the bed surface flattens with the addition of fine material that fills the gaps between the coarse grains, leading to a decrease of turbulences and an increase of the near-bed flow velocity.
In direct comparison with the mobility of the glass beads with 40 % fines, the natural beds with similar grain sizes and grain-size ratios were more stable. As suggested by other laboratory and numerical studies, it was assumed that the particle complexity, i.e. the higher angularity of the natural sediment grains, leads to increased intergranular friction and a higher bed stability.
In addition, it was assumed that the particle shape influences the bed roughness and the boundary layer: In comparison to the unimodal glass-bead bed, the flow boundary layer above the unimodal sand bed was confined, and the free flow velocity was reached closer to the bed surface. These results indicated a change of the bed roughness that was induced by the angularity of the individual grains.

7.2 Synthesis

The main aim of the dissertation was to analyse the influences of sediment texture (*RD* and fine content) on the mobility of a mixed bed and the near-bed flow. A secondary aim was to investigate the influence of the particle complexity on the bed mobility and the near-bed flow. The research questions could be answered using a combination of physical laboratory experiments and numerical modelling on different spatial and temporal scales. While laboratory flume experiments were used to investigate the near-bed hydrodynamics and the mobility of a variety of different beds (various grain sizes, grain-size ratios, grain shapes and fine fractions) over the course of several hours, a numerical model was developed to analyse short-term grain-scale flow processes at the bed surface depending on the bed texture.
The results presented in this dissertation prove the relevance of the sediment texture in the mobility of a fine-grained, bimodal sediment bed. For the range of tested grain sizes (laboratory: $D_{50} \leq 410$ µm; numerical model: $D_{50} \leq 600$ µm) and flow velocities (laboratory: $U \leq 0.23$ m s^{-1}; numerical model $U \leq 0.31$ m s^{-1}), it was found that the grain-size ratio between coarse and fine grain diameter controls the mobility of a mixed bed through small-scale processes at the bed surface. The grain-size ratio influences the flow above the bed surface (through changes of the bed roughness), the particle packing density, the flow at the bed surface and inside the upper bed layers, and thus the bed mobility. Based on the grain-size ratio, the amount of fine material has a supplementary effect on the bed mobility (see below).

Due to the relatively rough surface of a unimodal bed, the turbulent kinetic energy above the bed is high and the flow velocity increases approximately logarithmic with distance from the bed. The mobility of the unimodal bed served as reference scenario for the mobility assessment of the mixed

beds. If the grain-size ratio is high (*RD* = 5.8 for glass beads, *RD* = 7.7 for natural sediment), the addition of fine material reduces the mobility of the mixed bed (chapters 4 and 6). In comparison to the unimodal scenario, the flow at and above the bed surface accelerates because the fine particles fill the surface gaps between the coarse particles, reducing the bed roughness and near-bed turbulences. However, the flow velocities directly at the bed surface are very low. It is postulated that the fine particles fill the pores between the coarse particles, reducing water inflow into the bed. For spherical glass beads, a threshold amount of ≈ 40 % is required to completely fill the pore space and to prevent the development of bed forms at velocities of up to $U \approx 0.2$ m s^{-1} (chapter 4). Inside the bed, the addition of fine particles to the coarse particle matrix reduces the flow cross-sectional area (chapter 5). If a constant matrix flow is assumed, the flow velocities inside the particle matrix rise with an increase in fine material. In addition, the streamwise flow is deflected around the particles, leading to slight cross-stream and vertical flows inside the particle matrix. In a bed with *RD* = 6, these flow deflections are low compared to beds with lower *RD*. Although the flow above the bed is accelerated (due to the reduced bed roughness, chapters 4 and 6) and slight flow deflections occur inside the particle matrix (chapter 5), it is assumed that the inflow from the water column into the bed is largely inhibited, because the fine particles block the pore space. This leads to the stabilization of the bed (chapters 4 and 6).

If the grain-size ratio of a mixed bed is low (*RD* = 3.9 for glass beads, *RD* = 3.5 for natural sediment), the addition of fine material causes bed mobilization (chapters 4 and 6). Again the fines leads to a lower bed roughness, a decrease of near-bed turbulence and an acceleration of the flow above the bed (chapters 4 and 6). However, due to the size of the fine particles relative to the coarse particles, the bed surface is not as smooth as in the stable scenario described above, as indicated by the flow velocities at the bed surface. Furthermore, the fine particles in the pore space of the coarse particle matrix reduce the flow cross-sectional area and the flow velocities in the pores increase (chapter 5). At a constant discharge through the bed, the presence of the fines in the pore space leads to higher 3D flow velocities, as the fine particles are larger than in the stable scenario. However, the pores between the coarse particles cannot be fully filled, i.e. the pore space cannot be blocked, and water inflow from the water column is not inhibited. Consequently, the increased flow velocities inside the particle matrix (due to the larger size of the fines, chapter 5), in combination with the increased flow velocities above the bed (due to the reduced bed roughness, chapters 4 and 6), lead to the destabilization. If the difference between coarse and fine grain diameter is almost negligible (e.g. at *RD* = 2), the addition of fines does not have a major effect on the near-bed hydrodynamics and the mobility of the mixed bed is similar to that of the unimodal bed (chapter 6).

The findings apply to both spherical, smooth particles and natural, more complex and angular particles in the sand-silt range. The particle complexity (i.e. angularity) has an overall stabilizing effect: A mixed sand-silt bed is more stable than a glass-bead mixture with similar D_{50} and *RD*. In addition, the flow above the unimodal sand bed is faster than the flow above the unimodal glass beads of similar particle size, indicating a lower surface roughness of the natural bed consisting of angular sand grains (chapter 6).

The studies comprising this dissertation present an important contribution to the research of texture-induced stability and dynamics of non-cohesive beds. The findings can be used to further elucidate the stabilizing effect of non-cohesive fines through the blocking of inflow into the bed and the formation of network structures. The laboratory results provide empirical proof for a transition between texture-induced bed stabilization and mobilization. The critical *RD* for the transition between the two modes of behaviour could be narrowed down to 3.9–5.8 for glass beads and 3.5–7.7 for natural sediment. The results of the micro-scale numerical model underline that not only processes above but also inside the bed have to be considered when analysing the bed stability. The texture, characterized by the grain-size ratio, plays a key role for these small-scale processes. The study results can contribute to the better understanding and the prediction of sediment transport processes in fluvial and marine environments. Within the range of the tested grain sizes, the findings are valuable for engineering applications, such as river training, damming, coastal protection, offshore structures etc., and can be used to prevent or to facilitate sediment transport in the vicinity of man-made structures. However, it has to be noted that additional factors affect the sediment stability in a natural environment, e.g. the presence of cohesive clay minerals or benthic organisms.

The numerical model used in this dissertation offers new insight into three-dimensional processes at the sediment-fluid interface on a scale that cannot be examined in laboratory experiments. The model can be further extended and incorporated into, or serve as a base for, larger scale models to understand and predict sediment transport.
The developed approach for the evaluation of bed mobility presents an innovative method for laboratory and field studies. In contrast to other methods like sediment samplers or traps, the in-situ measurement of the bed-level changes does not require the removal of material from the system and can be applied in confined flume environments. As the bottom data can be acquired using an ADV, only one instrument is necessary to measure hydrodynamics, suspended sediment concentration (using the acoustic backscatter intensity) and bed mobility. The normalized method (3.1.3) can be applied in any other laboratory or field setting to evaluate and compare the mobility of a bed under steady flow.

7.3 Outlook

The approach using the grain-size ratio as the main factor to evaluate bed mobility requires a grain-size distribution with two main modes. The more distinct the modes are, the more accurate the *RD*-based evaluation of the bed mobility will be. However, in many scenarios natural sediment does not comprise two main modes but a normal distribution with a wider range of grain sizes. Future research should focus on the influence of more than two grain-size fractions on the processes controlling bed mobility.

The laboratory experiments presented here were restricted in the flow conditions that could be applied (unidirectional flow, $U \leq 0.23$ m s^{-1}) and subsequently in the range of grain sizes ($D_{50} \leq 410$ µm) that were erodible in the annular flume. Future studies should investigate the behaviour of mixed beds under a wider range of conditions, e.g. higher flow velocities, cyclic loading (tides, waves), and larger grain sizes. Additional measurements of sediment properties like porosity, pore pressure, and shear strength could be conducted to further explain the stabilizing behaviour of non-cohesive silt and sand depending on the texture.
The method for the evaluation of bed mobility should be further tested and developed, e.g. calibrated with collected bedload samples to derive a volumetric bedload transport rate.

Future numerical studies should optimize the numerical model setup for small-scale sediment-fluid interactions. As the presented model only simulated short-term processes (and the investigated flow velocities were transient), it is recommended to develop a more time-efficient modelling approach to yield a longer simulated time. More powerful processors could be used to simulate longer (and also larger-scaled) processes without sacrificing model resolution. Subsequently, such a model could be used to evaluate if the high cross-stream and vertical flow velocities inside the bed persist and whether these flow patterns, which are a result of the different *RD* alone, could facilitate particle entrainment from the surface. It is suggested to incorporate turbulent flow into the model to evaluate the contribution of turbulences to particle entrainment. Based on that, the contribution of turbulences should be compared to the effects of the increased matrix flow velocities on particle entrainment. In addition, different particle shapes and packings should be simulated to investigate the micro-scale processes in a more realistic model of a sediment bed.

Figure Index

Figure 4.1: Hydraulic conductivity (k*)* as a function of increasing fine fraction in the different glass-bead combinations (fitted with an arctangent fit): Reference bed RD_0 with coarse particles only (D_{50} = 367 µm), mixed bed $RD_{9.4}$ with large grain-size ratio RD = 9.4 (D_{50} = 367/39 µm), mixed bed $RD_{5.8}$ with medium grain-size ratio RD = 5.8 (D_{50} = 367/63 µm) and mixed bed $RD_{3.9}$ with low grain-size ratio RD = 3.9 (D_{50} = 367/93 µm). Insets show the relative coarse and fine grain sizes (*RD* to scale).

Figure 4.2: Development of bed shear-stresses (τ_0) with increasing flow velocity *U* for the different glass-bead treatments. The indices S, M and L refer to the different treatments with small (≈ 10 % dry weight), medium (≈ 20 %), and large (≈ 40 %) fine-grained fraction. See Table 4.1 for further information on the different treatments.

Figure 4.3: Changes in suspended particulate matter (*SPM*) concentration with increasing flow velocity *U*: a) Unimodal reference bed RD_0, b) mixed bed $RD_{9.4}$, c) mixed bed $RD_{5.8}$, d) mixed bed $RD_{3.9}$. S, M and L in the panels of the mixed experiment (b, c, d) refer to the different treatments with small (≈ 10 %), medium (≈ 20 %) and large (≈ 40 %) fine-grained fraction. See Table 4.1 for the different grain sizes.

Figure 4.4: Normalized bottom variance (logarithmic scale), as a proxy for bed mobility, with varying grain-size ratio *RD* and fine fraction. The mobility of the unimodal treatment RD_0 (solid horizontal line) serves as the reference for the mobility of the mixed beds $RD_{9.4}$, $RD_{5.8}$ and $RD_{3.9}$.

Figure 4.5: Flow profiles from all experiments at flow velocity U = 0.17 m s^{-1}. z = 0 indicates the bed surface or bed-water interface. The horizontal lines at z < 0 indicate the “bottom” detected by the profiling ADV in each experiment (see 4.2.1 for details). At the reference height z = 5 mm the velocity u_{xy5} is measured. Note the gaps in the profiles where data was excluded due to poor quality.

Figure 4.6: Detail of horizontal flow velocities at the bed surface of the two end members a) high grain-size ratio $RD_{9.4,L}$ (367/39 µm) with large fine-grained fraction and a low mobility of $\sigma^2_{b,norm}$ = 1.5 · 10^{-9} m and b) low grain-size ratio $RD_{3.9,L}$ (367/93 µm) with large fine-grained fraction and a high mobility of $\sigma^2_{b,norm}$ = 7.9 · 10^{-8} m. The profiles at low (U = 0.025 m s^{-1}), moderate (U = 0.121 m s^{-1}) and high (U = 0.185 m s^{-1}) free flows are shown.

Figure 4.7: Bed mobility with varying grain-size ratio *RD* and fine fraction, at flow conditions $U \leq 0.19$ m s^{-1}. Bed with $RD \leq 3.9$ become more mobile with increasing fine content, whereas beds with $RD \geq 5.8$ become more stable. The transition between these two cases occurs at RD = 3.9–5.8.

Figure 4.8: Conceptual model for the flow behaviour at the bed surface. a) Reference scenario RD_0. Development of a logarithmic boundary layer due to high bed roughness, resulting in low flow velocities at the bed surface. The higher porosity (relative to the mixed beds) allows unhindered inflow and discharge through the grain matrix, but the low flow velocities and larger particles result in little entrainment of material. b) High *RD*, large fine content: The pore space of the grain matrix is filled with fine particles and the bed roughness is reduced. The maximum flow velocity is reached close to the bed surface but the flow into and through the matrix is blocked by the high amount of fines. c) Low *RD*, large fine content: The fine particles fill the surface pockets, reducing the bed roughness. Again, the maximum flow is reached close to the bed surface. The higher near-bed flow velocities (than in the reference case) and the higher porosity (than in case 1 and the reference case) lead to higher inflow and particle entrainment.

Figure 5.1: Schematic of the coupled particle-flow model.

Figure 5.2: Grain-size combinations (side view).

Table Index

References

Allen, J.R.L., 1985. Principles of physical sedimentology. George Allen & Unwin Ltd., London.

Allen, P.A., 2009. Earth Surface Processes. Wiley-Blackwell, Hoboken, NJ.

Amos, C.L., Grant, J., Daborn, G.R., Black, K., 1992. Sea Carousel - A Benthic, Annular Flume. Estuar. Coast. Shelf Sci. 34, 557–577.

Andersen, T.J., 2001. Seasonal variation in erodibility of two temperate, microtidal mudflats. Estuar. Coast. Shelf Sci. 53, 1–12. doi:10.1006/ecss.2001.0790

Andersen, T.J., Lund-Hansen, L.C., Pejrup, M., Jensen, K.T., Mouritsen, K.N., 2005. Biologically induced differences in erodibility and aggregation of subtidal and intertidal sediments: A possible cause for seasonal changes in sediment deposition. J. Mar. Syst. 55, 123–138. doi:10.1016/j.jmarsys.2004.09.004

Andrews, E.D., Parker, G., 1987. Formation of a Coarse Surface Layer as the Response to Gravel Mobility, in: Thorne, C.R., Bathurst, J.C., Hey, R.D. (Eds.), Sediment Transport in Gravel-Bed Rivers. John Wiley & Sons, Ltd, Chichester, p. 995.

Bartzke, G., Bryan, K.R., Pilditch, C.A., Huhn, K., 2013. On the Stabilizing Influence of Silt On Sand Beds. J. Sediment. Res. 83, 691–703. doi:10.2110/jsr.2013.57

Bartzke, G., Huhn, K., 2015. A conceptual model of pore-space blockage in mixed sediments using a new numerical approach, with implications for sediment bed stabilization. Geo-Marine Lett. 35. doi:10.1007/s00367-015-0399-1

Bridge, J.S., Bennett, S.J., 1992. A Model for the Entrainment and Transport of Sediment Grains of Mixed Sizes, Shapes, and Densities. Water Resour. Res. 28, 337–363.

Buffington, J.M., Montgomery, D.R., 1997. A systematic analysis of eight decades of incipient motion studies, with special reference to gravel-bedded rivers. Water Resour. Res. 33, 1993–2029.

Chanson, H., Trevethan, M., Aoki, S., 2008. Acoustic Doppler velocimetry (ADV) in small estuary: Field experience and signal post-processing. Flow Meas. Instrum. 19, 307–313. doi:10.1016/j.flowmeasinst.2008.03.003

Cohen, Y., 1981. Wall Effects in Laminar Flow of Fluids through Packed Beds. AIChE J. 27, 705–715. doi:10.1002/aic.690270502

Cundall, P.A., Strack, O.D.L., 1979. A Discrete Numerical Model for Granular Assemblies. Géotechnique 29, 47–65.

Dey, S., 2014. Fluvial Hydrodynamics, GeoPlanet: Earth and Planetary Sciences. Springer, Berlin, Heidelberg.

Drake, T.G., Calantoni, J., 2001. Discrete particle model for sheet flow sediment transport in the nearshore. J. Geophys. Res. 106, 19859–19868. doi:10.1029/2000JC000611

Einstein, H.A., 1950. The Bed-Load Function for Sediment Transportation in Open Channel Flows. US Dep. Agric. Tech. Bull. 1–71.

Engel, P., Lau, Y.L., 1980. Computation of Bed Load Using Bathymetric Data. J. Hydraul. Div. ASCE HY 3.

Goring, D.G., Nikora, V.I., 2002. Despiking Acoustic Doppler Velocimeter Data. J. Hydraul. Eng. 128, 117–126. doi:10.1061/(ASCE)0733-9429(2002)128:1(117)

Grant, J., Bathmann, U.V., Mills, E.L., 1986. The Interaction between Benthic Diatom Films and Sediment Transport. Estuar. Coast. Shelf Sci. 23, 225–238.

Guo, Y., Morgan, J.K., 2004. Influence of normal stress and grain shape on granular friction: Results of discrete element simulations. J. Geophys. Res. 109, B12305. doi:10.1029/2004JB003044

Hillel, D., 2004. Introduction to Environmental Soil Physics. Elsevier Academic Press, San Diego, London, Burlington.

Hjulström, F., 1935. Studies in the morphological activity of rivers as illustrated by the River Fyris. Geol. Inst. Univ. Upsala Bull. 25, 221–528.

Houssais, M., Lajeunesse, E., 2012. Bedload transport of a bimodal sediment bed. J. Geophys. Res. 117, F04015. doi:10.1029/2012JF002490

Inoue, T., Glud, R.N., Stahl, H., Hume, A., 2011. Comparison of three different methods for assessing in situ friction velocity: A case study from Loch Etive, Scotland. Limnol. Oceanogr. Methods 9, 275–287.

Iseya, F., Ikeda, H., 1987. Pulsations in bedload transport rates induced by a longitudinal sediment sorting: A flume study using sand and gravel mixtures. Geogr. Ann. Ser. A, Phys. Geogr. 69, 15–27.

Itasca Consulting Group, I., 2006a. Particle Flow Code in 3 Dimensions. Theory and Background, First Revi. ed. Itasca Consulting Group, Inc., Minneapolis, MN.

Itasca Consulting Group, I., 2006b. Fast Lagrangian Analysis of Continua in 3 Dimensions. Fluid-Mechanical Interaction, Third Edit. ed. Itasca Consulting Group, Inc., Minneapolis, MN.

Itasca Consulting Group, I., 2006c. Fast Lagrangian Analysis of Continua in 3 Dimensions. User's Guide, Third Edit. ed. Itasca Consulting Group, Inc., Minneapolis, MN.

Jackson, W.L., Beschta, R.L., 1984. INFLUENCES OF INCREASED SAND DELIVERY ON THE MORPHOLOGY OF SAND AND GRAVEL CHANNELS. Water Resour. Bull. 20, 527–533.

Jacobs, W., Le Hir, P., Van Kesteren, W., Cann, P., 2011. Erosion threshold of sand-mud mixtures. Cont. Shelf Res. 31, 14–25.

Julien, P.Y., 1998. Erosion and Sedimentation. Cambridge University Press, Cambridge.

Kestin, J., Sokolov, M., Wakeham, W.A., 1978. Viscosity of liquid water in the range of -8 °C to 150 °C. J. Phys. Chem. 7, 941–948. doi:10.1063/1.555581

Kim, S.-C., Friedrichs, C.T., Maa, J.P.-Y., Wright, L.D., 2000. Estimating bottom stress in tidal boundary layer from acoustic Doppler velocimeter data. J. Hydraul. Eng. 126, 399–406.

Kock, I., Huhn, K., 2007. Influence of particle shape on the frictional strength of sediments — A numerical case study. Sediment. Geol. 196, 217–233. doi:10.1016/j.sedgeo.2006.07.011

Komar, P.D., Li, Z., 1986. Pivoting analyses of the selective entrainment of sediments by shape and size with application to gravel threshold. Sedimentology 33, 425–436. doi:Doi 10.1111/J.1365-3091.1986.Tb00546.X

Kresic, N., 2006. Hydrogeology and Groundwater Modeling, Second Edi. ed. CRC Press, Taylor & Francis Group, Boca Raton, FL.

Le Hir, P., Cann, P., Waeles, B., Jestin, H., Bassoullet, P., 2008. Chapter 11 Erodibility of natural sediments: experiments on sand/mud mixtures from laboratory and field erosion tests, in: Kusada, T., Yamanishi, H., Spearman, J., Gailani, J.Z. (Eds.), Sediment and Ecohydraulics: INTERCOH 2005. Elsevier B.V., pp. 137–153. doi:10.1016/S1568-2692(08)80013-7

Leeder, M., 1999. Sedimentology and Sedimentary Basis: From Turbulence to Tectonics. Blackwell Publishing, Malden, Oxford, Carlton.

Leeder, M.R., 1982. Sedimentology: Process and Product. George Allen & Unwin Ltd., London.

Loveland, P.J., Whalley, W.R., 2001. 7 Particle Size Analysis, in: Smith, K.A., Mullins, C.E. (Eds.), Soil and Environmental Analysis: Physical Methods. Marcel Dekker, Inc., New York, pp. 281–314.

Mair, K., Frye, K.M., Marone, C., 2002. Influence of grain characteristics on the friction of granular shear zones. J. Geophys. Res. 107, 2219. doi:10.1029/2001JB000516

McCave, I.N., 1984. Erosion, transport and deposition of fine-grained marine sediments. Geol. Soc. London, Spec. Publ. 15, 35–69. doi:10.1144/GSL.SP.1984.015.01.03

McGeary, R.K., 1961. Mechanical Packing of Spherical Grains. J. Am. Ceram. Soc. 44, 513–522.

Meadows, A., Meadows, P.S., Muir Wood, D., Murray, J.M.H., 1994. Microbiological effects on slope stability: an experimental analysis. Sedimentology 41, 423–435.

Mehta, A.J., Lee, S.-C., 1994. Problems in Linking the Threshold Condition for the Transport of Cohesionless and Cohesive Sediment Grain. J. Coast. Res. 10, 170–177.

Mehta, A.J., Letter, J. V., 2013. Comments on the transition between cohesive and cohesionless sediment bed exchange. Estuar. Coast. Shelf Sci. 131, 319–324. doi:10.1016/j.ecss.2013.07.001

Miller, M.C., McCave, I.N., Komar, P.D., 1977. Threshold of sediment motion under unidirectional currents. Sedimentology 24, 507–527. doi:10.1111/j.1365-3091.1977.tb00136.x

Mitchener, H., Torfs, H., 1996. Erosion of mud/sand mixtures. Coast. Eng. 29, 1–25. doi:10.1016/S0378-3839(96)00002-6

Morgan, J.K., 1999. Numerical simulations of granular shear zones using the distinct element method 2. Effects of particle size distribution and interparticle friction on mechanical behavior. J. Geophys. Res. 104, 2721–2732.

Nortek Inc., 2012. Vectrino Profiler: Profiling Velocimeter. User Guide. Boston.

Panagiotopoulos, I., Voulgaris, G., Collins, M.B., 1997. The influence of clay on the threshold of movement of fine sandy beds. Coast. Eng. 32, 19–43.

Paterson, D.M., Crawford, R.M., Little, C., 1990. Subaerial Exposure and Changes in the Stability of Intertidal Estuarine Sediments. Estuar. Coast. Shelf Sci. 30, 541–556.

Randle, T.J., Bountry, J.A., Makar, P.W., Fotherby, L.M., Bauer, T.R., Murphy, P.J., 2006. Chapter 7: River Processes and Restoration, in: Yang, C.T. (Ed.), Erosion and Sedimentation Manual. U.S. Department of the Interior, Bureau of Reclamation, Technical Service Center, Sedimentation and River Hydraulics Group, Denver, CO, pp. 7–1 – 7–64.

Reeve, D., Chadwick, A., Fleming, C., 2004. Coastal Engineering: Processes, theory and design practice. Spon Press. Taylor & Francis Group, London, New York.

Rhodes, M., 2008. Introduction to Particle Technology, Second Edi. ed. John Wiley & Sons, Ltd, Chichester.

Robert, A., 2003. River Processes. Arnold, Hodder Headline Group, London.

Sambrook Smith, G.H., Nicholas, A.P., 2005. Effect on flow structure of sand deposition on a gravel bed: Results from a two-dimensional flume experiment. Water Resour. Res. 41, W10405. doi:10.1029/2004WR003817

Schmeeckle, M.W., Nelson, J.M., 2003. Direct numerical simulation of bedload transport using a local, dynamic boundary condition. Sedimentology 50, 279–301. doi:10.1046/j.1365-3091.2003.00555.x

Seymour, R.J., 2005. Cross-shore transport. Encycl. Coast. Sci.

Shields, A., 1936. Anwendung der Aehnlichkeitsmechanik und der Turbulenzforschung auf die Geschiebebewegung. Mitteilungen der Preußischen Versuchsanstalt für Wasserbau und Schiffbau, Berlin 26.

Siekmann, H.E., Thamsen, P.U., 2008. Strömungslehre, 2. Auflage. ed. Springer, Berlin, Heidelberg, New York. doi:10.1007/978-3-540-73727-8

Simons, D.B., Richardson, E. V., Nordin, C.F., 1965. Bedload equation for ripples and dunes. US Geol. Surv. Prof. Pap. 462-H, 1–9.

Small, C., Nicholls, R.J., 2003. A Global Analysis of Human Settlement in Coastal Zones. J. Coast. Res. 19, 584–599.

Soulsby, R.L., 1983. The Bottom Boundary Layer of Shelf Seas, in: Johns, B. (Ed.), Physical Oceanography of Coastal and Shelf Seas. Elsevier, pp. 189–266.

Soulsby, R.L., 1997. Dynamics of marine sands: a manual for practical applications. HR Wallingford, Thomas Telford Publishing, London.

Spork, V., 1997. Erosionsverhalten feiner Sedimente und ihre biogene Stabilisierung. Mitteilungen des Lehrstuhls und Instituts für Wasserbau und Wasserwirtschaft der RWTH Aachen 114.

Stanley, D.J., Swift, D.J.P. (Eds.), 1976. Marine sediment transport and environmental management. John Wiley & Sons, Inc., New York, London, Sydney, Toronto.

Teisson, C., Ockenden, M., Le Hir, P., Kranenburg, C., Hamm, L., 1993. Cohesive sediment transport processes. Coast. Eng. 21, 129–162.

Thorne, P.D., Bell, P.S., 2009. Acoustic measurement of near-bed sediment transport processes, in: Steele, J.H., Thorpe, S.A., Turekian, K.K. (Eds.), Measurement Techniques, Platforms and Sensors. A Derivative of Encyclopedia of Ocean Sciences, 2nd Edition. Elsevier Academic Press, London, p. 652.

Torfs, H., Jiang, J., Mehta, A.J., 2001. Assessment of the erodibility of fine/coarse sediment mixtures, in: McAnally, W.H., Mehta, A.J. (Eds.), Coastal and Estuarine Fine Sediment Processes. Vol. 3. Proceedings in Marine Science. Elsevier, pp. 109–123. doi:10.1016/S1568-2692(00)80116-3

van Ledden, M., van Kesteren, W.G.. G.M., Winterwerp, J.. C., 2004. A conceptual framework for the erosion behaviour of sand–mud mixtures. Cont. Shelf Res. 24, 1–11. doi:10.1016/j.csr.2003.09.002

Venditti, J.G., Dietrich, W.E., Nelson, P.A., Wydzga, M.A., Fadde, J., Sklar, L., 2010a. Mobilization of coarse surface layers in gravel-bedded rivers by finer gravel bed load. Water Resour. Res. 46, W07506. doi:10.1029/2009WR008329

Venditti, J.G., Dietrich, W.E., Nelson, P.A., Wydzga, M.A., Fadde, J., Sklar, L., 2010b. Effect of sediment pulse grain size on sediment transport rates and bed mobility in gravel bed rivers. J. Geophys. Res. 115, F03039. doi:10.1029/2009JF001418

Wallbridge, S., Voulgaris, G., Tomlinson, B., Collins, M., 1999. Initial motion and pivoting characteristics of sand particles in uniform and heterogeneous beds: experiments and modelling. Sedimentology 46, 17–32. doi:10.1046/j.1365-3091.1999.00199.x

Wentworth, C.K., 1922. A Scale of Grade and Class Terms for Clastic Sediments. J. Geol. 30, 377–392.

Whitehouse, R., Soulsby, R., Roberts, W., Mitchener, H., 2000. Dynamics of estuarine muds, HR Wallingford. Thomas Telford Publishing, London.

Wiberg, P.L., Smith, J.D., 1987. Calculations of the critical shear stress for motion of uniform and heterogeneous sediments. Water Resour. Res. 23, 1471. doi:10.1029/WR023i008p01471

Widdows, J., Brinsley, M., Elliott, M., 1998a. Use of in situ flume to quantify particle flux (biodeposition rates and sediment erosion) for an intertidal mudflat in relation to changes in current velocity and benthic macrofauna. Geol. Soc. London, Spec. Publ. 139, 85–97. doi:10.1144/GSL.SP.1998.139.01.07

Widdows, J., Brinsley, M.D., Bowley, N., Barrett, C., 1998b. A Benthic Annular Flume for In Situ Measurement of Suspension Feeding/Biodeposition Rates and Erosion Potential of Intertidal Cohesive Sediments. Estuar. Coast. Shelf Sci. 46, 27–38. doi:10.1006/ecss.1997.0259

Widdows, J., Brinsley, M.D., Salkeld, P.N., Elliott, M., 1998. Use of Annular Flumes to Determine the Influence of Current Velocity and Bivalves on Material Flux at the Sediment-Water Interface. Estuaries 21, 552–559.

Widdows, J., Brinsley, M.D., Salkeld, P.N., Lucas, C.H., 2000. Influence of biota on spatial and temporal variation in sediment erodability and material flux on a tidal flat (Westerschelde, The Netherlands). Mar. Ecol. Prog. Ser. 194, 23–37. doi:10.3354/meps194023

Wilcock, P.R., Kenworthy, S.T., 2002. A two-fraction model for the transport of sand/gravel mixtures. Water Resour. Res. 38, 1194. doi:10.1029/2001WR000684

Wilcock, P.R., Kenworthy, S.T., Crowe, J.C., 2001. Experimental Study of the Transport of Mixed Sand and Gravel. Water Resour. Res. 37, 3349–3358.

Willows, R.I., Widdows, J., Wood, R.G., 1998. Influence of an infaunal bivalve on the erosion of an intertidal cohesive sediment: A flume and modeling study. Limnol. Oceanogr. 43, 1332–1343. doi:10.4319/lo.1998.43.6.1332

Wren, D.G., Langendoen, E.J., Kuhnle, R.A., 2011. Effects of sand addition on turbulent flow over an immobile gravel bed. J. Geophys. Res. Earth Surf. 116, 1–12. doi:10.1029/2010JF001859

Wright, J., Colling, A., Park, D., 1999. Waves, Tides and Shallow Water Processes. Butterworth-Heinemann, in association with the Open University, Oxford.

Yang, C.T., 2006. Chapter 6: Sustainable Development and Use of Reservoirs, in: Yang, C.T. (Ed.), Erosion and Sedimentation Manual. U.S. Department of the Interior, Bureau of Reclamation, Technical Service Center, Sedimentation and River Hydraulics Group, Denver, CO, pp. 6–1 – 6–33.

Acknowledgements

First of all, I would like to thank Prof. Katrin Huhn-Frehers and Dr. Julia C. Mullarney for their supervision and continuous support during my PhD research at the University of Bremen and the University of Waikato. Thank you for the initial project ideas, the input, the feedback on my work, and the freedom to design the research objectives. Additional thanks to Prof. Conrad A. Pilditch for his effort and feedback as part of my thesis committee and for the support during the lab work in New Zealand.
Many thanks to Dr. Gerhard Bartzke for his invaluable input to the numerical model and the data analysis, for sharing his experiences, reading my manuscripts, and discussing my results.

Furthermore I want to thank Dean Sandwell, Annette Rodgers, Janine Ryburn, and Renat Radosinsky for their support in the Earth Science labs of the University of Waikato. Thanks to Warrick Powrie and Dudley Bell who always found the proper lab equipment for me and were available for a chat. Many thanks to Nicola Lovett for helping me in the sieving room, Chris Eager who always had the right tool (or knew where to find it), and Dr. Rachel Harris for her support in the Benthic Flow Lab.

Many thanks to my other colleagues of the working group Huhn – Modelling of Sedimentary Systems at the Center for Marine Environmental Sciences: Lina Podszun, Dr. Jannis Kuhlmann, Lars Lindner, Marine Le Minor, Hadar Elyashiv, Nicole Bammann, Dr. Bryna Reinmold, Dr. Linda Wenk, and Dr. Lutz Torbahn.

Special thanks to the INTERCOAST “family”, PhD students, PostDocs, and associates in Germany and New Zealand, for the support during my research, the friendship, the good times in Hamilton, Bremen, Tauranga, Fehmarn, and beyond. Very special thanks to the INTERCOAST PostDocs Bryna, Bevis, Seth, and Gerhard for their guidance and support.

Zu guter Letzt möchte ich mich bei meiner Familie und meinem Freund für die Unterstützung (und die Geduld) in den letzten drei Jahren bedanken.

Erklärung

Name: Franziska Staudt
Adresse: Kulenkampffallee 101, 28213 Bremen, Deutschland

Ich, Franziska Staudt, erkläre hiermit, dass ich

1. diese Arbeit selbstständig und ohne unerlaubte fremde Hilfe angefertigt habe,
2. keine anderen als die von mir angegebenen Quellen und Hilfsmittel benutzt habe und
3. die den benutzten Werken wörtlich oder inhaltlich entnommenen Stellen als solche kenntlich gemacht habe.

_____

Franziska Staudt
Bremen, 29. Januar 2016